

Cathode innovations for enhanced H₂ production through microbial electrolysis

Adriaan W. Jeremiasse

Thesis committee**Thesis supervisor**

Prof. dr. ir. C.J.N. Buisman

Professor of Biological Recycling Technology

Thesis co-supervisors

Dr. ir. H.V.M. Hamelers

Associate professor, sub-department of Environmental Technology

Dr. ir. J. M. Kleijn

Assistant professor, Laboratory of Physical Chemistry and Colloid Science

Other members

Prof. dr. M. Koper, Leiden University

Prof. dr. G.J. Kramer, Leiden University

Prof. dr. ir. G. van Straten, Wageningen University

Dr. F. Barrière, University of Rennes, France

This research was conducted under the auspices of the Netherlands Research School for the Socio-Economic and Natural Sciences of the Environment (SENSE).

Cathode innovations for enhanced H₂ production through microbial electrolysis

Adriaan W. Jeremiasse

Thesis

submitted in fulfillment of the requirements for the degree of doctor
at Wageningen University
by the authority of the Rector Magnificus
Prof. dr. M.J. Kropff,
in the presence of the
Thesis Committee appointed by the Academic Board
to be defended in public
on Friday 30 September 2011
at 4 p.m. in the Frisian Museum, Leeuwarden

Adriaan W. Jeremiasse

Cathode innovations for enhanced H₂ production through microbial electrolysis

168 pages

Thesis Wageningen University, Wageningen, NL (2011)

With references, with summaries in Dutch and English

ISBN 978-90-8585-989-5

For My Parents

Table of Contents

1.	Introduction	9
2.	Use of biocompatible buffers to reduce the concentration overpotential for hydrogen evolution	33
3.	Microbial electrolysis cell with a microbial biocathode	53
4.	Acetate enhances development of a H ₂ -producing microbial biocathode	67
5.	Ni foam cathode enables high volumetric H ₂ production in a microbial electrolysis cell	83
6.	Performance of metal alloys as hydrogen evolution reaction catalysts in a microbial electrolysis cell	101
7.	General discussion and outlook	119
	Summary	141
	Samenvatting	147
	Appendix – Chapter 2	154
	Appendix – Chapter 4	155
	Appendix – Chapter 5	158
	Appendix – Chapter 6	159
	Publications	161
	Dankwoord	163
	Curriculum Vitae	166

1. Introduction

Microbial electrolysis is a recently developed, sustainable technology for H₂ production from waste streams. It combines the removal of organic material with the production of a valuable product. However, microbial electrolysis is still in its infancy. This thesis deals with improving the performance of microbial electrolysis cells (MECs), with the ultimate goal to come to a cost-effective H₂ production process.

In this introductory chapter a general background is given, starting with the challenge to produce H₂ for the world's steadily growing needs, and, via the production of H₂ from biomass with microbial electrolysis, narrowing down to the focus of this thesis, i.e. the development of a low-cost cathode capable of producing H₂ at high rate and low overpotential.

1. Introduction

1.1 The challenge of future H₂ supply

1.1.1 Importance of H₂

Hydrogen gas, H₂, is a valuable compound that is nowadays often associated with its use as fuel. However, it has many other applications. With respect to its use, H₂ is commonly divided into 1) captive H₂, 2) fuel H₂, and 3) merchant H₂.

Captive H₂ is produced and used on-site as chemical. At present, this is the main use of H₂. Of all produced H₂, about 50 % is used for ammonia production, 37 % for petroleum processing (e.g. desulphurization and hydro cracking), and 8 % for methanol production (percentages date from 1998 [1]).

Fuel H₂ is used in rockets, automotive, heating and power production. This application is still limited, but may increase to substitute our fossil based transportation fuels.

Merchant H₂ is produced at one location and transported to another location for various applications [2], such as hydrogenation of oils and fats and production of pharmaceuticals. Less than 1 % of all produced H₂ is sold as merchant H₂ [2].

In 2005, total H₂ use was about 5 EJ (exajoule, 10¹⁸ J) worldwide [3], corresponding to 5·10¹¹ m³ hydrogen gas at standard temperature and pressure (STP). According to one of the scenarios of the International Energy Agency (IEA) [3], total H₂ use may increase to 22 EJ in 2050, from which 12 EJ is fuel H₂. In this scenario, H₂ would become important for transportation, fuelling 30 % of the passenger cars in 2050. Although a large share of H₂ in the transportation sector is uncertain, the H₂ needs of fast growing economies (e.g. China) make it inevitable that future H₂ demands largely exceed 5 EJ.

1.1.2 H₂ production

Hydrogen is the most abundant element in the universe. However, gaseous hydrogen, H₂, is not naturally present in considerable quantities on earth. Therefore, it needs to be

produced, which requires an energy and H-source. Most H_2 is produced through partial oxidation of fossil fuels (Table 1), which are both energy and H-source.

Table 1 The share of H_2 production processes in 2005 [4].

H_2 production process	Share (%)
Steam reforming of natural gas	48
Recovery of refinery/chemical industry off-gasses	30
Coal gasification	18
Water electrolysis	3.9
Other	0.1

However, fossil fuels are a finite resource [5]. For example, crude oil production in the North Sea (Figure 1) seems to have peaked already [6]. Because our own fossil fuel resources are limited [7], supply largely depends from other countries, which may be politically unstable. For example, protests against governments, started at the end of 2010 in North-Africa and the Middle East, have raised oil prices to the highest levels in years (e.g. 13th of March 2011: over 100 USD per barrel WTI). Moreover, fossil fuel combustion causes air pollution through emissions of NO_x, SO₂ [8] and particulate matter [9], and seems to contribute to global warming [10] through emissions of greenhouse gasses such as CO₂ [6].

These issues raise the need for green H_2 without emissions. Thus, H_2 production technologies must be explored that do not require energy input from fossil fuels, but can use energy input from renewable sources. Examples of such technologies are water electrolysis, thermochemical water splitting, photoelectrolysis, and various biomass technologies [11]. This thesis is about the production of H_2 from biomass.

1.2 Biomass feedstocks for H_2 production

Biomass feedstocks can be divided into dedicated crops, and organic waste [12]. The use of arable land to grow crops for chemical and fuel production competes with use of land for food and feed production, and therefore, may threaten food supply [13]. Organic waste however, does not have this drawback. Two types of organic waste can be

1. Introduction

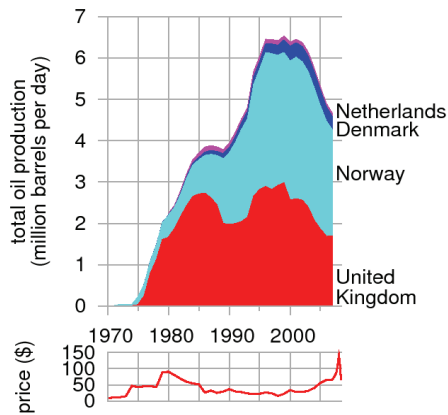


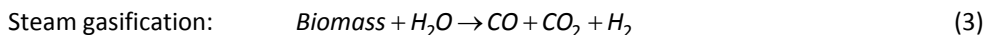
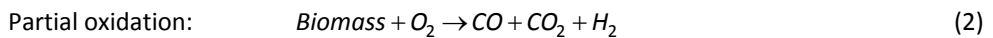
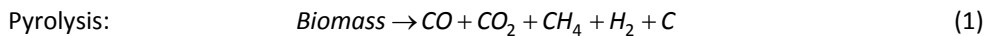
Figure 1 Total crude oil production in the North Sea and the oil price over the period 1970 – 2006 in USD per barrel (Reproduced with permission from [6]).

distinguished: solid organic waste such as crop residues, animal and municipal waste, and liquid organic waste such as industrial and municipal wastewaters.

Biomass can be converted into H_2 through thermal processes, fermentative processes, and microbial electrolysis. Thermal processes are mainly suitable for solid organic waste, and are less suitable for liquid organic waste because the high water content results in a low thermal efficiency [11,14]. Fermentative processes and microbial electrolysis are suitable for solid organic waste and liquid organic waste.

1.3 Thermal conversion of biomass into H_2

Thermal processes convert biomass through pyrolysis, partial oxidation and gasification [11,14] at high temperatures (600-1000 °C) into H_2 [15]:



Thermal conversion of biomass results in a mixture of CO, H₂, CO₂, CH₄ and N₂. The H₂ concentration of the gas can be increased through the water gas shift reaction:

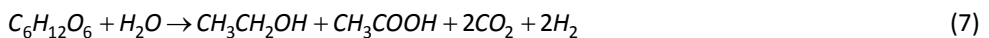


A subsequent separation process is required to produce pure H₂ and remove tars [11,15]. Large reactors for the thermal conversion of biomass into H₂ could achieve efficiencies of 35-50 % based on the lower heating value [11]. Production rates of 250 kg H₂/day (2800 m³ H₂ day⁻¹) have been reported for pilot plants [14]. A disadvantage of thermal processes is the loss of valuable nutrients in the ashes, which cannot be recycled back to the agricultural fields [16].

1.4 Fermentative H₂ production

Fermentative processes for conversion of biomass into H₂ are commonly divided in dark fermentation and photo fermentation.

In dark fermentation, bacteria (e.g. *Clostridium* species) anaerobically convert sugars into H₂. Complete stoichiometric conversion of 1 mol hexose (C₆ sugar) would produce 12 moles H₂. However, fermentative H₂ production is thermodynamically limited, i.e. complete conversion requires an energy input. Therefore, oxidation of 1 mol hexose yields maximally 4 moles of H₂ with acetic acid as by-product (eq. 1), 2 moles of H₂ with butyric acid as by-product (eq. 2), or 2 moles of H₂ with ethanol as by-product (eq. 3) [17]:



Practical H₂ yields are below these maximum yields [11]. Attempts have been made to

1. Introduction

increase the yield by optimizing reactor conditions, such as pH, hydraulic retention time and partial H₂ pressure [18]. Nevertheless, optimization of dark fermentation will at best produce 4 moles of H₂ per mole hexose, resulting in a conversion efficiency of 33%. The produced gas is a mixture of mainly H₂ and CO₂, but may also contain other components, such as CH₄ [19]. Therefore, gas purification is required. Production rates up to 29 m³ H₂ m⁻³ reactor day⁻¹ for synthetic wastewaters and up to 8.9 m³ H₂ m⁻³ reactor day⁻¹ for real wastewaters have been measured [17].

Photo-fermentation is the conversion of small-chain organic acids into H₂ by photosynthetic bacteria (e.g. *Rhodospseudomonas* species) with input of light energy to overcome the thermodynamical barrier [20]. Theoretically, 4 moles of hydrogen can be produced per mol acetate converted (eq. 4).



Practical yields are below the maximal yield, and can be maximized by optimizing reactor conditions and illumination. Yields of H₂ on substrate of 84 % have been obtained. However, efficiencies of the conversion of solar energy into H₂ energy were usually below 10 % [21]. To produce pure H₂, carbon dioxide must be removed from the produced gas. H₂ production rates of photo-fermentation are generally lower than of dark fermentation, and so far have been below 1 m³ H₂ m⁻³ reactor day⁻¹. Photo-fermentation can be coupled to dark fermentation in a 2-step process to increase the overall yield of H₂ on hexose [22].

1.5 H₂ production through microbial electrolysis

1.5.1 The microbial electrolysis cell

The conversion of biomass into H₂ through microbial electrolysis is the subject of this thesis. Microbial electrolysis was invented in 2003 [23] and is thus a relatively new process for production of H₂ from biomass. Electrochemically active microorganisms play a key role in this process. These microorganisms have a distinctive feature: they can transfer

electrons to a solid electron acceptor, such as an electrode. The electron transfer from microorganism to an electrode can occur directly or indirectly. *Geobacter sulfurreducens* is an important model organism for direct electron transfer. This species is believed to transfer electrons to the electrode via a path of electrically conductive pili and a c-type cytochrome. *Shewanella oneidensis* is a model organism for indirect electron transfer. It has been demonstrated that *S. oneidensis* can transfer electrons to the electrode via flavins that serve as electron shuttles [24].

In a microbial electrolysis cell (MEC) (Figure 2) electrochemically active microorganisms oxidize a substrate (e.g. acetate) into bicarbonate, protons and electrons, and transfer the electrons to the anode, the so-called bioanode. From the bioanode, the electrons travel through an electrical circuit with power supply, to the cathode. At the cathode, the electrons reduce protons or water to H₂. To compensate for the negative electrical charge transport through the external circuit, ionic charge is transported between the electrodes inside the cell. To avoid H₂ losses through re-oxidation at the anode, and a decrease in H₂ purity through mixing with CO₂, a membrane can be used to separate anode and cathode. Often, an anion or cation exchange membrane is used [25-26].

The Gibbs free energy for the overall conversion of acetate into H₂ (equation 5) under typical MEC conditions ($\Delta G'$, pH 7, p_{H_2} = 1 atm, 298 K, and 5 mM activities of CH₃COO⁻ and HCO₃⁻) is +91.1 kJ mol⁻¹ acetate [27]. The positive value of the Gibbs free energy implies that the conversion requires an input of energy.



From the Gibbs free energy, the electromotive force (E_{emf}) can be calculated:

$$E_{emf} = -\frac{\Delta G'}{nF} \quad (10)$$

1. Introduction

With n , the number of electrons involved in the conversion of acetate to H_2 ($n = 8$), and F , the Faraday constant ($96,485 \text{ C mol}^{-1}$). Under typical MEC conditions, the E_{emf} equals - 0.118 V [25].

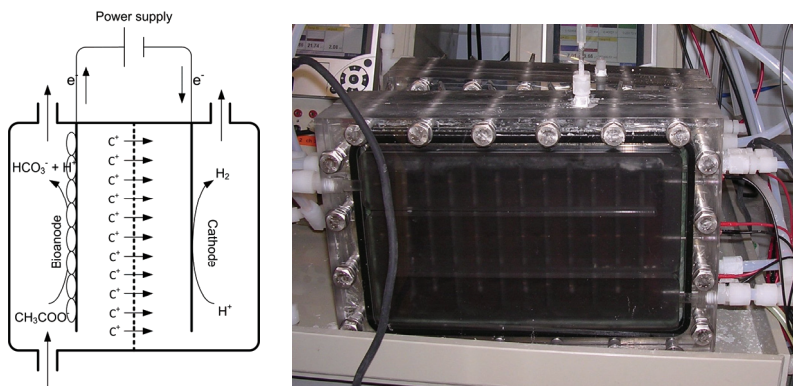


Figure 2 Schematics and photograph of a laboratory microbial electrolysis cell (MEC). At the bioanode, electrochemically active microorganisms oxidize a substrate (here acetate) into bicarbonate, protons and electrons. The electrons are transported through an electrical circuit with power supply, to the cathode. At the cathode, the electrons reduce protons or water to H_2 . To compensate for negative electrical charge transported outside the cell, ionic charge is transported inside the cell. Ionic charge transport is here represented by cation (C^+) transport through a cation exchange membrane, but can also occur by anion transport through an anion exchange membrane, or without a membrane [28]. The power source supplies the voltage for this process.

1.5.2 MEC electrode reactions

The microbial electrolysis of substrate to H_2 occurs in two electrode reactions. At the bioanode, substrate (e.g. acetate) is oxidized into bicarbonate, protons and electrons. At the cathode, protons are reduced to H_2 in the so-called hydrogen evolution reaction (HER) (Table 2).

In electrochemistry, it is common practice to express the energy level of an electrode as a potential (unit: $V = J C^{-1}$). The equilibrium potential (E') of an electrode reaction can be calculated with the Nernst equation:



$$E' = E^0 - \frac{RT}{nF} \ln \frac{(a_X)^x (a_Y)^y}{(a_P)^p (a_Q)^q} \quad (12)$$

with E^0 the standard electrode potential, R the universal gas constant ($8.314 \text{ J mol}^{-1} \text{ K}^{-1}$), T the absolute temperature (298 K at standard conditions) and a the activities of the reactants and products.

Assuming that the activities equal the concentrations of the substances (i.e. activity coefficients equal 1), the Nernst equation for an acetate-oxidizing bioanode becomes:

$$E'_{an} = E^0_{an} - \frac{RT}{8F} \ln \left(\frac{[\text{CH}_3\text{COO}^-]}{[\text{HCO}_3^-]^2 [\text{H}^+]^9} \right) \quad (13)$$

with E^0_{an} , the standard potential of acetate/bicarbonate at the anode (Table 2). Accordingly, The Nernst equation for the HER at the cathode becomes:

$$E'_{cat} = E^0_{cat} - \frac{RT}{2F} \ln \left(\frac{p_{\text{H}_2}}{[\text{H}^+]^2} \right) \quad (14)$$

with E^0_{cat} , the standard potential of H^+/H_2 at the cathode (Table 2). From the potential difference (i.e. voltage) between anode and cathode, the E_{emf} can be calculated again:

$$E_{emf} = E_{cat} - E_{an} \quad (15)$$

The E_{emf} equals -0.118 V under typical MEC conditions (Table 2), and thus at least 0.118 V must be applied between anode and cathode to produce H_2 from acetate.

1. Introduction

Table 2 Electrode potentials under standard conditions (E^0 ; 298 K, 1 M activity for all reactants, $p_{H_2} = 1 \text{ atm}$) and for MEC relevant conditions (E' ; 5 mM activities for CH_3COO^- and HCO_3^-).

Reaction	Equation	$E^0 \text{ (V)}$	$E' \text{ (V)}$
Anode	$CH_3COO^- + 4H_2O \rightarrow 2HCO_3^- + 9H^+ + 8e^-$	0.187	-0.296
Cathode	$2H^+ + 2e^- \rightarrow H_2$	0.00	-0.414

In practice, more than 0.118 V needs to be applied to produce H_2 from acetate. Part of this additional voltage is used at the cathode (i.e. cathode overpotential) to drive the HER. Previous studies showed that this part can be a few hundred millivolts in an MEC [26,29]. The voltage is, at constant coulombic efficiency, proportional to the electrical energy input ($\text{kWh m}^{-3} H_2$). To decrease the electrical energy input, it is thus relevant to decrease the voltage that is used for the cathode.

1.6 HER overpotential

1.6.1 Definition of overpotential

The HER overpotential is the extra potential, beyond the thermodynamical potential, required to drive the HER at a certain rate (i.e. current density) [30]. The total overpotential can be defined as the sum of concentration (η_c) and activation (η_a) overpotential [31]:

$$\eta = \eta_c + \eta_a \quad (16)$$

Although the overpotential can be defined more specifically [32], we stick to this expression because we did not go into the details of specific reactions. The concentration overpotential expresses the energy associated with the concentration difference of reactants and products between bulk and surface (1.6.2). The activation overpotential expresses the energy associated with the actual (electro)chemical reaction at the electrode interface (1.6.3). Division of the overpotential in an activation and a

concentration overpotential helps to identify which part of the overall cathode reaction consumes most of the applied voltage (i.e. energy).

1.6.2 HER concentration overpotential

If H_2 is produced (net cathodic current), reactants (e.g. H^+) must be transported from the bulk solution to the cathode surface, and products (e.g. OH^-) must be transported from surface to bulk. In case of a fast charge transfer reaction, transport cannot “catch up” with the reaction at the cathode surface. Consequently, the surface concentrations of reactants and products differ from the bulk concentrations. The difference between the potential (Nernst equation, equation 10) at surface concentrations and the potential at bulk concentrations is the concentration overpotential.

The concentration overpotential can be decreased through improving mass transport. Mass transport is the sum of transport through diffusion, migration (transport under influence of an electric field) and convection, which can be mathematically expressed with the Nernst-Planck equation [30]:

$$J_i(x) = -D_i \frac{\partial C_i(x)}{\partial x} - \frac{z_i F}{RT} D_i C_i \frac{\partial \phi(x)}{\partial x} + C_i v(x) \quad (17)$$

with $J_i(x)$ the flux of species i at distance x from the surface ($\text{mol m}^{-2} \text{s}^{-1}$), D_i the diffusion coefficient of species i ($\text{m}^2 \text{s}^{-1}$), $\partial C_i(x)/\partial x$ the concentration gradient at distance x , z_i the charge of species i , C_i the concentration of species i (mol m^{-3}), $\partial \phi(x)/\partial x$ the potential gradient at distance x , and $v(x)$ the linear flow speed of the electrolyte (m s^{-1}).

In some cases, transport can be limited to 1 or 2 transport terms. For example, migration can be decreased through the use of a supporting electrolyte. The effect of convective transport can be taken into account in the diffusion layer thickness [30].

1.6.3 HER activation overpotential for metal cathodes

If mass transport is not limiting, the current density (i.e. speed of electron transfer) at an

1. Introduction

electrode interface can be expressed with the Butler-Volmer equation [31]:

$$j = j_0 (e^{-\alpha \eta F / RT} - e^{(1-\alpha) \eta F / RT}) \quad (18)$$

with j , the current density, j_0 , the exchange current density, α , the transfer coefficient, and η , the overpotential. The left exponential expresses the cathodic reaction ($\eta < 0$, $j > 0$), whereas the right exponential expresses the anodic reaction ($\eta > 0$, $j < 0$) at the electrode.

The exchange current density is an important parameter in electrode kinetics. At thermodynamic equilibrium ($\eta = 0$) the rates of the electrochemical oxidation and reduction reaction are the same (dynamic equilibrium), and each equals the exchange current density. Any deviation from equilibrium (i.e. application of an overpotential) will result in a net oxidation or reduction reaction. Thus, the larger the value of the exchange current density, the larger the rate of the electrode reaction at any overpotential [31].

The transfer coefficient is another important parameter in electrode kinetics, because it determines *how* the overpotential affects the rate of the electrode reaction [31]. The transfer coefficient is related to the symmetry of the energy barrier of the electrode reaction. A transfer coefficient of 0.5 implies a symmetrical energy barrier, which results in a symmetrical anodic and cathodic part of the η - j curve. A transfer coefficient > 0.5 results in a steeper increase of the cathodic part, whereas a transfer coefficient < 0.5 results in a steeper increase of the anodic part of the η - j curve. The transfer coefficient is typically between 0.3 and 0.7, and often a value of 0.5 can be assumed [30].

For the HER, another term plays a role: the surface coverage (θ) [31-32]. The surface coverage factor plays a role in the individual HER reaction steps as described in 1.7.1. On the one hand, adsorbed H-atoms decrease the first electrochemical reaction rate (equation 21), because the number of free sites on the surface is decreased. On the other hand, adsorbed H-atoms increase the second reaction rate as follows from equations 22 and 23. The surface coverage factor should be taken into account in the rate expressions of the individual reaction steps [32].

The exchange current density, transfer coefficient and coverage factor determine the activation overpotential of the HER, which in their turn depend on many factors, such as cathode material, cathode structure, electrolyte composition and temperature. In this thesis, metal and microbial biocathodes were explored to decrease the HER activation overpotential of an MEC, while enhancing the HER rate (Figure 3). The activation overpotential theory is established for metal cathodes. However, it is still unexplored for microbial biocathodes in which bioelectrochemical kinetics and electrode kinetics are coupled.

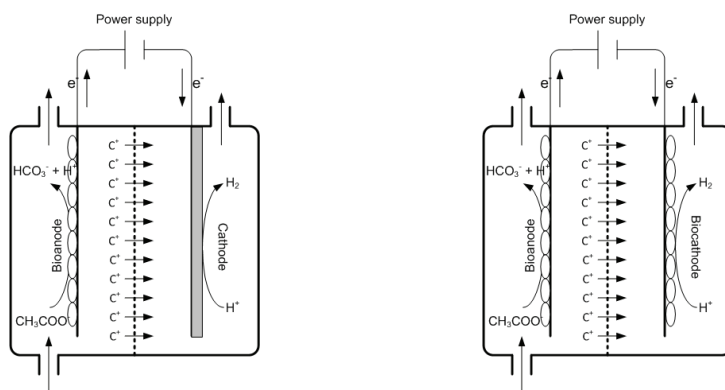


Figure 3 Left: MEC with a metal cathode. Right: MEC with a microbial biocathode.

1.7 HER metal cathodes

1.7.1 Hydrogen evolution reaction mechanism

The hydrogen evolution reaction (HER) is one of the most studied electrode reactions. The theory of electrode kinetics has been largely developed on the basis of measurements with the hydrogen electrode [32]. The overall reaction for the HER at low pH can be written as [32]:



1. Introduction

The overall reaction at high pH can be written as [32]:



The HER is a multistep reaction. In the first step, protons in solution are reduced to atomic hydrogen on the metal surface (M) [31]:



This step is also known as the Volmer reaction, which is an electrochemical reaction [32]. The second step can proceed according 2 different reactions: as a chemical or as an electrochemical reaction. The chemical reaction, also known as the Tafel reaction, can be written as:



The alternative, electrochemical reaction, also known as the Heyrovsky reaction, can be written as:



All these reactions can also be written for alkaline conditions with water molecules instead of protons as the reactant.

Which of the 2 different reactions in the second step takes place depends on the cathode material and experimental conditions [32]. Even for the same metal and same experimental conditions, the mechanism can be different. For example, Marković et al. [33] found that the HER under acidic conditions on Pt(110) follows an electrochemical-chemical mechanism, whereas the HER on Pt(100) follows an electrochemical-

electrochemical mechanism. The HER is thus also dependent on the metal surface structure [34]. Identification of the reaction mechanism and of the rate-limiting reaction step is not only relevant for fundamental understanding, but also for practical applications. For example, in case the rate-limiting reaction is the first electrochemical reaction, adsorbed H may diffuse into the bulk metal, which can cause mechanical instability of the metal [35].

1.7.2 Metals from the d-block of the periodic table

The HER activation overpotential varies considerably among metal cathodes (Figure 4). For example, the metals Pb, Hg, Cd and Cu require large overpotentials for the HER and therefore are not appropriate as cathode materials in an MEC. d-Block metals from group 8, 9 and 10 of the periodic table however, have low overpotentials for the HER [36]. The metals of these groups can be found close to, or at the optimum of “volcano” curves, which are plots of the catalytic activity of metals versus the metal-H bond strength [34] (Figure 4). At the optimum of the volcano curve, the metal-H bond is not too weak, so that the metal can be sufficiently covered with H, and not too strong, so that the adsorbed H is not immobilized on the surface [34,37].

Especially Pt group metals (Ru, Rh, Pd, Os, Ir, Pt) have a high catalytic activity, and thus a low overpotential for the HER. Unfortunately however, Pt group metals are very expensive. For example, Pt has a price of 43 €/g (3rd of March 2011, metalprices.com). To decrease the costs while maintaining catalytic activity, the amount of Pt can be decreased by designing nanostructured catalysts [38].

Instead of Pt group metals, non-noble d-block metals could be used [32,36]. For example, Ni- and Fe-based cathodes are often employed in commercial alkaline water electrolyzers [39]. Generally, there are 2 strategies to decrease the overpotential of such metals: i) alloying metals, and ii) increasing the specific surface area of the metal.

1.7.3 Alloys of the d-block metals

Through alloying d-block metals, it is possible to obtain a higher catalytic activity than that

1. Introduction

of each individual metal. To reach such a synergistic catalytic effect, it has been suggested

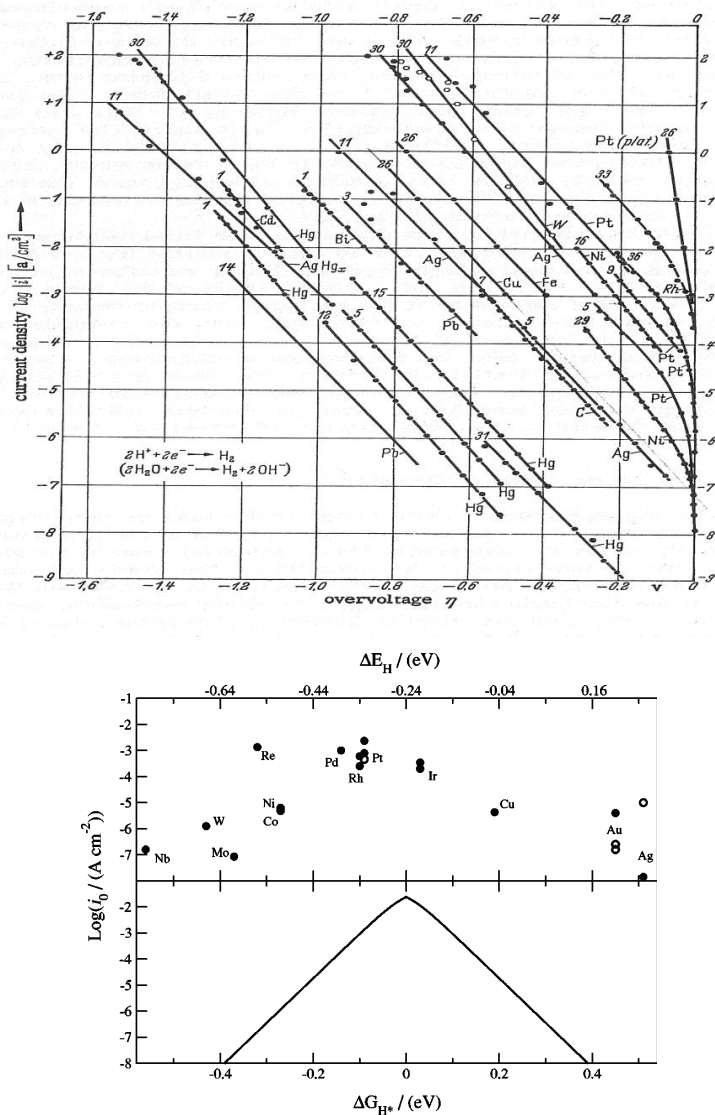


Figure 4 Top: Tafel curves for hydrogen evolution reaction on different metals (Reproduced from [32] by permission of Elsevier). Bottom: A “volcano” plot. The upper part shows the measured exchange current density as a function of the calculated hydrogen chemisorption energy ΔE_{H^*} whereas the lower part shows the calculated exchange current density as a function of the Gibbs free energy of hydrogen adsorption ΔG_{H^*} (Reproduced from [45] by permission of The Electrochemical Society).

to alloy metals from the right side of the d-block (e.g. Fe, Co, Ni) with metals of the left side (e.g. W, Mo) [40-43]. Various researchers attempted to predict the catalytic activity of alloys [40-44]. However, other authors [37] showed inconsistencies between predicted and experimentally measured catalytic activities.

1.7.4 Increase of specific surface area

Through increasing the specific surface area of a metal cathode, a higher H₂ production rate can be achieved at a given overpotential. However, the intrinsic catalytic activity of the metal is not increased by such a modification (except in case of a nanostructured catalyst [38]). Essentially, an increase in specific surface area increases the apparent current density (current density based on projected cathode area), while maintaining the true current density (current density based on true surface area). High specific surface areas can be obtained through the use of metallic felts and foams [46], sintered metals or Raney nickel coatings [47].

1.8 HER biocathodes

1.8.1 Hydrogenases

Biological H₂ production is usually based on the action of hydrogenases, although H₂ can also be produced by nitrogenases. Hydrogenases are enzymes that catalyze the reaction of hydrogen evolution and oxidation. They are present in bacteria, archaea, rhizobia, protozoa, fungi and algae [48]. There are 2 main classes of hydrogenases: [NiFe]-hydrogenases and [FeFe]-hydrogenases. Their names describe the bimetallic active center of the enzymes [49].

The [NiFe]-hydrogenases represent the majority of the hydrogenases present in microorganisms [50]. They are usually associated with hydrogen oxidation and therefore called 'uptake hydrogenases'. Hydrogen is taken up for sulfate, nitrate or carbon dioxide reduction, coupled to energy generation [51].

[FeFe]-hydrogenases are less abundant in micro-organisms. They are often

1. Introduction

described as ‘bidirectional’ or ‘reversible’ hydrogenases. The catalytic activity of [FeFe]-hydrogenases is one to two orders of magnitude higher than that of [NiFe]-hydrogenases [52]. The [FeFe]-hydrogenase from *Desulfovibrio vulgaris* Hildenborough is one of the most active hydrogenases described so far.

1.8.2 Enzymatic biocathodes

The catalytic activity of hydrogenases can be exploited by immobilizing them on an electrode [49,53]. Various studies have demonstrated HER catalysis by immobilized [NiFe]- and [FeFe]-hydrogenases cathodes [54-56]. As stated before, the catalytic activity towards the HER for [FeFe]-hydrogenases is one to two orders higher than for [NiFe]-hydrogenases [52]. However, the higher sensitivity of [FeFe]-hydrogenases towards oxygen make them less stable [49]. [NiFe]-hydrogenases on the contrary, seem more sensitive to (biochemically) reversible inhibition by H₂ than [FeFe]-hydrogenases, and therefore, H₂ must be continuously removed [54]. So far, current densities for the HER with hydrogenase-immobilized cathodes seem not to have exceeded 1 A m⁻² at overpotentials of a few hundred millivolts [49,57]. A disadvantage of a hydrogenase-immobilized cathode is the poor stability [58-59]. Furthermore, isolation, purification and production of hydrogenases may be time-consuming and costly [59].

1.8.3 Microbial biocathodes

Next to enzymatic biocathodes, microbial biocathodes have been studied [60] (Figure 3). The first microbial biocathodes for the HER were based on immobilized whole cells of *Desulfovibrio vulgaris* Hildenborough. However, these microbial biocathodes only produced H₂ if methyl viologen was present as electron shuttling compound. Moreover, the HER current density of these microbial biocathodes was below 1 A m⁻² at overpotentials of a few hundred millivolts [61-62].

Recently, Rozendal et al [63] demonstrated H₂ production by a microbial biocathode that consisted of a mixed consortium of electrochemically active microorganisms. The microbial biocathode could be obtained through polarity reversal of

a H₂-oxidizing microbial bioanode so that it turned into a H₂-producing biocathode. The microbial biocathode could also be obtained through direct inoculation of a cathode that was controlled at a potential more negative than the equilibrium potential of H⁺/H₂ (-0.42 V at pH 7). H₂ production by the microbial biocathode was stable for over 1000 h. Moreover, it did not require addition of an electron shuttling compound. The HER current density was 1.2 A m⁻² at a cathode overpotential of -0.28 V (pH 7). The microbial biocathode however, has only been studied in an electrochemical cell with chemical anode, not in an MEC. Furthermore, to become a viable alternative for metal cathodes, the development time of the microbial biocathode must be decreased, and H₂ production must be increased.

1.9 Objective and outline

Previous MEC studies demonstrated overpotentials for Pt-based cathodes of a few hundred millivolts at H₂ production rates below 10 m³ H₂ m⁻³ MEC day⁻¹ (at standard temperature and pressure (STP)). The aim was to decrease this overpotential, while to increase the volumetric H₂ production rate of the MEC (i.e. m³ H₂ m⁻³ MEC day⁻¹). Furthermore, the cathode must be made of a low cost material, which decreases costs per m³ MEC, while an increased volumetric H₂ production rate decreases MEC size and thus total MEC costs. The objective of this PhD project therefore was:

To develop a low-cost cathode, capable of producing H₂ at high rate and low overpotential

The research was divided in different topics that are subsequently discussed in various chapters.

Chapter 2 discusses the effect of mass transport on cathode overpotential under typical MEC cathode conditions. The effect of mass transport is best studied if the activation losses due to charge transfer at the cathode are low. Therefore, a Pt-catalyzed cathode was used in this chapter.

1. Introduction

Chapter 3 demonstrates the proof-of-principle of an MEC, in which both anode and cathode reactions are catalyzed by microorganisms. Furthermore, key issues that occurred during operation of an MEC with microbial bioanode and biocathode are identified in this chapter.

Chapter 4 discusses how the development and performance of a microbial biocathode can be improved. The effect of carbon source on microbial biocathode development is discussed. Furthermore, the flow-through operation to increase H₂ production rate of a microbial biocathode is presented.

Chapter 5 demonstrates the achievement of a high H₂ production rate with a high surface area, Ni foam cathode in an MEC. The chapter also identifies the main energy losses of an MEC with Ni foam cathode.

Chapter 6 compares the catalytic performance of various metal alloys for the HER. The chapter demonstrates that with non-noble, but highly active metal alloys, high H₂ production rates may be achieved in an MEC.

Finally, **Chapter 7** compares the various cathodes studied in this thesis. It shows how the improvements in MEC design during the past years can be employed to develop a H₂ production technology that is cost competitive with other H₂ production technologies.

References

- [1] Ramachandran R, Menon R K. An overview of industrial uses of hydrogen. *Int J Hydrogen Energy* 1998; 23: 593-8
- [2] Eklund G, Von Krusenstierna O. Storage and transportation of merchant hydrogen. *Int J Hydrogen Energy* 1983; 8: 463-70
- [3] International Energy Agency. Prospects for hydrogen and fuel cells. 2005;
- [4] Ewan B C R, Allen R W K. A figure of merit assessment of the routes to hydrogen. *Int J Hydrogen Energy* 2005; 30: 809-19
- [5] Shafiee S, Topal E. When will fossil fuel reserves be diminished? *Energy Policy* 2009; 37: 181-9
- [6] MacKay D J C. Sustainable Energy- without the hot air. ed. Cambridge: UIT; 2008.
- [7] Central Intelligence Agency. The World Factbook. 2011;
- [8] Kato N, Akimoto H. Anthropogenic emissions of SO₂ and NO_x in Asia: emission inventories. *Atmos Environ A-Gen* 1992; 26: 2997-3017

- [9] Bond T C, Streets D G, Yarber K F, Nelson S M, Woo J H, Klimont Z. A technology-based global inventory of black and organic carbon emissions from combustion. *J Geophys Res D: Atmos* 2004; 109:
- [10] IPCC, 2007. *Climate Change 2007: The Physical Science Basis, Summary for Policymakers*, Paris.
- [11] Holladay J D, Hu J, King D L, Wang Y. An overview of hydrogen production technologies. *Catal Today* 2009; 139: 244-60
- [12] Balat M, Balat M. Political, economic and environmental impacts of biomass-based hydrogen. *Int J Hydrogen Energy* 2009; 34: 3589-603
- [13] Field C B, Campbell J E, Lobell D B. Biomass energy: the scale of the potential resource. *Trends Ecol Evol* 2008; 23: 65-72
- [14] Ni M, Leung D Y C, Leung M K H, Sumathy K. An overview of hydrogen production from biomass. *Fuel Process Technol* 2006; 87: 461-72
- [15] Huber G W, Iborra S, Corma A. Synthesis of Transportation Fuels from Biomass: Chemistry, Catalysts, and Engineering. *Chem Rev* 2006; 106: 4044-98
- [16] Ostergard H, Markussen M V, Jensen E S, Challenges for sustainable development, in: Langeveld, H., Sanders, J., Meeusen, M. (Eds.), *The biobased economy: biofuels, materials and chemicals in the post-oil era*. Earthscan, London, 2010, pp. 33-48.
- [17] Li C L, Fang H H P. Fermentative hydrogen production from wastewater and solid wastes by mixed cultures. *Crit Rev Environ Sci Technol* 2007; 37: 1-39
- [18] Angenent L T, Karim K, Al-Dahhan M H, Wrenn B A, Domiguez-Espinosa R. Production of bioenergy and biochemicals from industrial and agricultural wastewater. *Trends in Biotechnology* 2004; 22: 477-85
- [19] Levin D B, Pitt L, Love M. Biohydrogen production: prospects and limitations to practical application. *Int J Hydrogen Energy* 2004; 29: 173-85
- [20] Barbosa M J, Rocha J M S, Tramper J, Wijffels R H. Acetate as a carbon source for hydrogen production by photosynthetic bacteria. *J Biotechnol* 2001; 85: 25-33
- [21] Reith J H, Wijffels R H, Barten H, 2003. *Bio-methane & bio-hydrogen, status and perspectives of biological methane and hydrogen production*. Dutch Biological Hydrogen Foundation, The Hague.
- [22] Kapdan I K, Kargi F. Bio-hydrogen production from waste materials. *Enzyme Microb Technol* 2006; 38: 569-82
- [23] Rozendal R A, Buisman C J N. Process for producing hydrogen. 2005; Patent WO2005005981:
- [24] Lovley D R, Nevin K P. A shift in the current: New applications and concepts for microbe-electrode electron exchange. *Curr Opin Biotechnol* In Press, Corrected Proof:
- [25] Logan B E, Call D, Cheng S, Hamelers H V M, Sleutels T H J A, Jeremiasse A W, et al. Microbial electrolysis cells for high yield hydrogen gas production from organic matter. *Environ Sci Technol* 2008; 42: 8630-40
- [26] Sleutels T H J A, Hamelers H V M, Rozendal R A, Buisman C J N. Ion transport resistance in microbial electrolysis cells with anion and cation exchange membranes *Int J Hydrogen Energy* 2009; 34: 3612-20
- [27] Thauer R K, Jungermann K, Decker K. Energy conservation in chemotrophic anaerobic bacteria. *Bacteriol Rev* 1977; 41: 100-80

1. Introduction

- [28] Call D, Logan B E. Hydrogen production in a single chamber microbial electrolysis cell lacking a membrane. *Environ Sci Technol* 2008; 42: 3401-6
- [29] Rozendal R A, Hamelers H V M, Euverink G J W, Metz S J, Buisman C J N. Principle and perspectives of hydrogen production through biocatalyzed electrolysis. *Int J Hydrogen Energy* 2006; 31: 1632-40
- [30] Bard A J, Faulkner L R. *Electrochemical methods: fundamentals and applications*. 2nd ed. New York: John Wiley & Sons; 2001.
- [31] Bockris J O M, Reddy A K N, Gamboa-Aldeco M. *Modern Electrochemistry 2A: Fundamentals of Electrodics*. ed. New York: Kluwer Academic; 2000.
- [32] Vetter K J. *Electrochemical kinetics: theoretical and experimental aspects*. ed. New York: Academic press; 1967.
- [33] Markovic N M, Grgur B N, Ross P N. Temperature-Dependent Hydrogen Electrochemistry on Platinum Low-Index Single-Crystal Surfaces in Acid Solutions. *J Phys Chem B* 1997; 101: 5405-13
- [34] Kibler L A. Hydrogen Electrocatalysis. *ChemPhysChem* 2006; 7: 985-91
- [35] Tilak B V, Ramamurthy A C, Conway B E. High performance electrode materials for the hydrogen evolution reaction from alkaline media. *Proc Indian Acad Sci (Chem Sci)* 1986; 97: 359-93
- [36] Miles M H. Evaluation of electrocatalysts for water electrolysis in alkaline solutions. *J Electroanal Chem Interfacial Electrochem* 1975; 60: 89-96
- [37] Petrii O A, Tsirlina G A. Electrocatalytic activity prediction for hydrogen electrode reaction: intuition, art, science. *Electrochim Acta* 1994; 39: 1739-47
- [38] Rolison D R. Catalytic Nanoarchitectures-the Importance of Nothing and the Unimportance of Periodicity. *Science* 2003; 299: 1698-701
- [39] Kinoshita K. *Electrochemical oxygen technology*. ed. New York: John Wiley & Sons, Inc.; 1992.
- [40] Jaksic J M, Vojnovic M V, Krstajic N V. Kinetic analysis of hydrogen evolution at Ni-Mo alloy electrodes. *Electrochim Acta* 2000; 45: 4151-8
- [41] Jaksic M M. Electrocatalysis of hydrogen evolution in the light of the brewer-engel theory for bonding in metals and intermetallic phases. *Electrochim Acta* 1984; 29: 1539-50
- [42] Jaksic M M. Hypo-hyper-d-electronic interactive nature of interionic synergism in catalysis and electrocatalysis for hydrogen reactions. *Int J Hydrogen Energy* 2001; 26: 559-78
- [43] Jaksic M M. Advances in electrocatalysis for hydrogen evolution in the light of the Brewer-Engel valence-bond theory. *Int J Hydrogen Energy* 1987; 12: 727-52
- [44] Ezaki H, Morinaga M, Watanabe S. Hydrogen overpotential for transition metals and alloys, and its interpretation using an electronic model. *Electrochim Acta* 1993; 38: 557-64
- [45] Norskov J K, Bligaard T, Logadottir A, Kitchin J R, Chen J G, Pandalov S, et al. Trends in the Exchange Current for Hydrogen Evolution. *J Electrochem Soc* 2005; 152: J23-J6
- [46] Marracino J M, Coeuret F, Langlois S. A first investigation of flow-through porous electrodes made of metallic felts or foams. *Electrochim Acta* 1987; 32: 1303-9
- [47] Rausch S, Wendt H. Morphology and utilization of smooth hydrogen-evolving raney nickel cathode coatings and porous sintered-nickel cathodes. *J Electrochem Soc* 1996; 143: 2852-62

- [48] Evans D J, Pickett C J. Chemistry and the hydrogenases. *Chem Soc Rev* 2003; 32: 268-75
- [49] Vincent K A, Parkin A, Armstrong F A. Investigating and Exploiting the Electrocatalytic Properties of Hydrogenases. *Chem Rev* 2007; 107: 4366-413
- [50] Darensbourg M Y, Lyon E J, Smee J J. The bio-organometallic chemistry of active site iron in hydrogenases. *Coordination Chemistry Reviews* 2000; 206-207: 533-61
- [51] Adams M W W. The structure and mechanism of iron-hydrogenases. *Biochimica et Biophysica Acta* 1990; 1020: 115-45
- [52] Frey M. Hydrogenases: Hydrogen-Activating Enzymes. *ChemBioChem* 2002; 3: 153-60
- [53] Mertens R, Liese A. Biotechnological applications of hydrogenases. *Curr Opin Biotechnol* 2004; 15: 343-8
- [54] Goldet G, Wait A F, Cracknell J A, Vincent K A, Ludwig M, Lenz O, et al. Hydrogen Production under Aerobic Conditions by Membrane-Bound Hydrogenases from *Ralstonia* Species. *J Am Chem Soc* 2008; 130: 11106-13
- [55] Guiral-Brugna M, Giudici-Ortoconi M-T, Bruschi M, Bianco P. Electrocatalysis of the hydrogen production by [Fe] hydrogenase from *Desulfovibrio vulgaris* Hildenborough. *J Electroanal Chem* 2001; 510: 136-43
- [56] Morozov S V, Karyakina E E, Zorin N A, Varfolomeyev S D, Cosnier S, Karyakin A A. Direct and electrically wired bioelectrocatalysis by hydrogenase from *Thiocapsa roseopersicina*. *Bioelectrochemistry* 2002; 55: 169-71
- [57] Guiral-Brugna M, Giudici-Ortoconi M-T, Bruschi M, Bianco P. Electrocatalysis of the hydrogen production by [Fe] hydrogenase from *Desulfovibrio vulgaris* Hildenborough. *Journal of Electroanalytical Chemistry* 2001; 510: 136-43
- [58] Morozov S V, Vignais P M, Cournac L, Zorin N A, Karyakina E E, Karyakin A A, et al. Bioelectrocatalytic hydrogen production by hydrogenase electrodes. *International Journal of Hydrogen Energy* 2002; 27: 1501-5
- [59] Cracknell J, Vincent K, Armstrong F. Enzymes as Working or Inspirational Electrocatalysts for Fuel Cells and Electrolysis. *Chem Rev* 2008; 108: 2439-61
- [60] He Z, Angenent L T. Application of bacterial biocathodes in microbial fuel cells. *Electroanalysis* 2006; 18: 2009-15
- [61] Lojou E, Bianco P. Electrocatalytic reactions at hydrogenase-modified electrodes and their applications to biosensors: From the isolated enzymes to the whole cells. *Electroanalysis* 2004; 16: 1093-100
- [62] Lojou E, Durand M C, Dolla A, Bianco P. Hydrogenase activity control at *Desulfovibrio vulgaris* cell-coated carbon electrodes: Biochemical and chemical factors influencing the mediated bioelectrocatalysis. *Electroanalysis* 2002; 14: 913-22
- [63] Rozendal R A, Jeremiasse A W, Hamelers H V M, Buisman C J N. Hydrogen production with a microbial biocathode. *Environ Sci Technol* 2008; 42: 629-34

2. Use of biocompatible buffers to reduce the concentration overpotential for hydrogen evolution

The hydrogen evolution reaction (HER) at Pt-cathodes of microbial electrolysis cells (MEC) has been associated with overpotentials of several hundred millivolts. The high overpotentials challenge the sustainability of an MEC. This chapter shows that the HER overpotential at MEC relevant pH values is reduced if buffer is present. At 15 A/m² and 50 mM buffer, the lowest overpotential for phosphate was -0.05 V at pH 6.2, for ammonia was -0.05 V at pH 9.0, for carbonate was -0.09 V at pH 9.3, for Tris(hydroxymethyl)aminomethane was -0.07 V at pH 7.8 and for N-2-Hydroxyethylpiperazine-N'-2-ethanesulfonic acid was -0.08 V at pH 7.2. It was shown that the effect of buffer on the overpotential is strongly pH dependent. Furthermore, experimental data and a mass transport equation showed that by increasing the buffer concentration or linear flow speed (i.e. pump speed), or decreasing the current density (i) the overpotential reduces and (ii) the minimum overpotential is reached at a pH that approaches the buffer dissociation constant (pK_a). Thus, to reduce the HER overpotential of an MEC, buffer (i.e. pK_a), buffer concentration, linear flow speed and current density must be well balanced with the expected operational pH.

This chapter has been published as:

Jeremiasse A W, Hamelers H V M, Kleijn J M, Buisman C J N. Use of biocompatible buffers to reduce the concentration overpotential for hydrogen evolution. *Environ Sci Technol* 2009; 43: 6882-7

2. Concentration overpotential

2.1 Introduction

Hydrogen can be sustainably produced from organic matter through microbial electrolysis [1]. In a microbial electrolysis cell (MEC), electrochemically active microorganisms convert organic matter into carbon dioxide, protons and electrons, and transfer the electrons to an anode. The so-called bioanode is connected to an anaerobic cathode via a power supply. By means of the power supply, a voltage is applied (typically 0.2-1.0 V) so that at the cathode the hydrogen evolution reaction (HER) proceeds via protons (eq 1) or water (eq 2) [2-3]:



The HER is one of the most studied electrode reactions. The HER has mainly been studied under conditions of extremely low pH (e.g. polymer electrolyte water electrolysis, eq 1), or extremely high pH (alkaline water electrolysis, eq 2). In an MEC however, the cathode is ionically connected to a bioanode, which operates near pH 7. Therefore, the HER at the cathode proceeds at MEC relevant pH values, typically pH 7 or higher [1]. At these pH values, HER potentials have been observed [4-6] of a few hundred millivolts more negative than the equilibrium potential that follows from the Nernst equation. The extra potential, beyond the equilibrium potential, required to drive the HER at a certain rate, is called the overpotential (negative for cathodic overpotentials) [7]. For each -0.1 V overpotential, an extra electricity input of 0.22 kWh/Nm³ H₂ is required. Assuming an energy recovery of 2.66 kWh/Nm³ H₂ based on Gibbs free energy [1], the extra electricity input means an overall electrical efficiency loss of 8% per -0.1 V overpotential. Overpotentials, such as observed by Rozendal et al. (-0.28 V) [4], thus strongly challenge the overall sustainability of an MEC.

The overpotential can be divided in activation and concentration overpotential [7-8]. Activation overpotential is determined by the nature of the electron transfer

reaction, type of electrode material, electrode surface area and operating temperature. Concentration overpotential is caused by limited transport of reactants (protons) and products (hydroxide, hydrogen) between electrode surface and bulk. It can be expected that for MECs, the HER overpotential on Pt-catalyzed cathodes mainly consists of concentration overpotential. An MEC that operates at neutral pH has a low difference in proton concentration (maximally 10^{-7} M) between bulk and cathode surface, compared to a polymer electrolyte water electrolyzer that operates at a pH below 0 (proton concentration in the polymer electrolyte $\sim 10^1$ M, similar to a 20 wt% sulphuric acid solution [9]). Consequently, for an MEC the proton gradient near the cathode surface is small and therefore, proton transport is limited, resulting in a high concentration overpotential.

From literature it is known that transport of protons from bulk to cathode surface is improved if a weak acid or buffer is added to the catholyte. Daniele et al. [10-11] found that the limiting current for the HER increased if the buffer concentration was increased while the pH of the buffer solution stayed constant. Honda et al. [12] demonstrated that the surface pH of a copper cathode, poised at -1.0 V vs. NHE, was decreased from 11 to 2.5 (bulk pH 2) when 0.2 M glycine buffer was added, resulting in higher current densities. Linter and Burstein [13] showed that at pH 4.0, the current density on stainless steel increased if the catholyte contained dissolved CO_2 . Very recently, Merrill and Logan [14] found that an increased concentration of weak acids could improve MEC performance. At a pH below pK_a (acid dissociation constant) of the weak acid, this was attributed to a decreased HER overpotential, whereas at a pH above pK_a , this was attributed to an increased conductivity.

In this study, we systematically investigated how different buffers, buffer concentrations, linear flow speeds (i.e. pump speeds) and current densities affect the HER overpotential at different pH values, and under conditions of controlled mass transport. Furthermore, we present a mass transport equation that relates all studied factors (buffer pK_a , buffer concentration, linear flow speed, current density and pH) to the HER concentration overpotential. Both the measurements and mass transport equation will

2. Concentration overpotential

make it possible for specific situations to identify conditions that minimize the HER overpotential, and thus improve the sustainability of an MEC. Buffers were chosen that are relevant for MEC applications, i.e. they (i) are biocompatible, considering that future MECs may lack a membrane [15-16] and/or use a biocathode [17-18] and (ii) buffer best between pH 7 and 10, considering that at higher pH hydroxide transport from surface to bulk determines the HER concentration overpotential [3].

2.2 Materials and Methods

2.2.1 Electrochemical cell and set-up

Experiments were performed with two identical electrochemical cells, similar to the one used by Ter Heijne et al. [19]. Both electrochemical cells consisted of two Plexiglas plates with flow channel, two electrodes, and two Plexiglas support plates. The flow channel was 11 cm long, 2 cm high and 1.5 cm wide. One plate with flow channel was the anode chamber, and the other plate with flow channel was the cathode chamber. The two chambers were separated by a cation exchange membrane (Qianqiu, Zhejiang, China). Anode and cathode were made of titanium coated with 0.5 mg/cm^2 Pt/Ir mixed metal oxide (Magneto Special Anodes, Schiedam, The Netherlands) with a geometric surface area of 22 cm^2 that was in contact with the liquid. Anolyte consisted of 5 mM KH_2PO_4 , 5 mM K_2HPO_4 and 0.1 M NaNO_3 background electrolyte, and was continuously recycled (380 mL/min) over a stock vessel of 1 L. Catholyte consisted of buffer, and 1 M KCl background electrolyte to minimize the solution iR drop. Also, the high concentration of background electrolyte excludes migration and conductivity effects. Phosphate buffer was prepared from KH_2PO_4 , carbonate buffer from NaHCO_3 and ammonia buffer from NH_4Cl (Boom B.V., Meppel, The Netherlands). Good's buffers [20] Tris(hydroxymethyl)aminomethane (trivial name: Tris) and N-2-Hydroxyethylpiperazine-N'-2-ethanesulfonic acid (trivial name: Hepes) were obtained from Sigma-Aldrich (Schnelldorf, Germany). Catholyte was recycled (pump speed was varied) over a flow cell containing a pH electrode (Liquisys M CPM 253, Endress + Hauser, Naarden, The Netherlands). The total volume of cathode chamber, flow

cell and tubing was 220 mL. The temperature of catholyte was controlled at 30°C (±1°C). H₂ that was supplied to, or produced in the cathode chamber could leave the system via a water lock. A glass tube filled with 3 M KCl was placed on 5 mm distance of the cathode and connected to an Ag/AgCl 3 M KCl reference electrode (QM 710X, ProSense B.V., Oosterhout, The Netherlands).

2.2.2 Methods

Each experiment was performed with both electrochemical cells (duplicates). The current between anode and cathode was controlled at a constant value using a Wenking Potentiostat/Galvanostat (KP5V3A, Bank IC, Pohlheim, Germany), and the cathode potential was measured relative to the reference electrode. The catholyte was replaced each experiment. Before start of an experiment, the catholyte was adjusted to pH 2.4 using concentrated HCl, flushed with H₂, and the cathode pre-treated at 15 A/m² (33 mA) for 15 minutes to remove oxides. During the experiment, the pH of the catholyte gradually increased due to proton consumption by the HER. Cathode potential and pH were recorded every minute using a data logger (Ecograph T, Endress+Hauser, Naarden, The Netherlands) until pH 11.5 was reached. Measured cathode potentials vs Ag/AgCl 3 M KCl were converted to cathode potentials vs NHE. Cathodic currents are expressed with a positive sign, whereas cathode overpotentials are expressed with a negative sign [7].

2.2.3 Calculations

The equilibrium potential was calculated for each measured pH and a partial hydrogen pressure of 1 atm, using the Nernst equation:

$$E_{eq} = E^0 + \frac{RT}{nF} \ln \frac{[H^+]_{bulk}^2}{p_{H_2}} \quad (3)$$

2. Concentration overpotential

where E^0 is the equilibrium potential at standard conditions ($T=298$ K, $p_{H_2}=10^5$ Pa, and $[H^+] = 1$ M) which equals 0.00 V (by definition), R (8.314 J/K mol) is the ideal gas law constant, T is the absolute temperature, n is the amount of electrons involved in the reaction ($n=2$ for the HER), and F is the Faraday constant (96485 C/mol e^-). At 30 °C (303 K), and assuming a constant hydrogen pressure of 1 atm, the Nernst equation reduces to:

$$E_{eq} = -0.060pH \quad (4)$$

The overpotential (η) was calculated by subtracting the equilibrium potential from the measured potential (vs NHE):

$$\eta = E_{meas} - E_{eq} = E_{meas} + 0.060pH \quad (5)$$

In Table 1, the dissociation constants (pK_a values) of the buffers are listed. The pK_a values of phosphate, carbonate and ammonia buffer under experimental conditions (1 M KCl, 30 °C) were predicted using OLI StreamAnalyzer (version 2.0; OLI systems, Morris Plains, NJ, USA).

Table 1 Dissociation constants (pK_a) of the buffers investigated in this study

Buffer	Buffer Species	pK_a
Phosphate ¹	$H_3PO_4 \leftrightarrow H^+ + H_2PO_4^-$	$pK_{a1} = 1.8$
	$H_2PO_4^- \leftrightarrow H^+ + HPO_4^{2-}$	$pK_{a2} = 6.6$
	$HPO_4^{2-} \leftrightarrow H^+ + PO_4^{3-}$	$pK_{a3} = 11.6$
Carbonate ¹	$H_2CO_3 \leftrightarrow H^+ + HCO_3^-$	$pK_{a1} = 6.0$
	$HCO_3^- \leftrightarrow H^+ + CO_3^{2-}$	$pK_{a2} = 9.7$
Ammonia ¹	$NH_4^+ \leftrightarrow H^+ + NH_3$	$pK_a = 9.4$
Tris ²	$Tris^+ \leftrightarrow H^+ + Tris$	$pK_a = 8.1$
Hepes ²	$Hepes^+ \leftrightarrow H^+ + Hepes$	$pK_{a1} \sim 3$
	$Hepes \leftrightarrow H^+ + Hepes^-$	$pK_{a2} = 7.6$

¹Values were predicted using OLI StreamAnalyzer for 1 M KCl and 30°C.

² Values were taken from [21] for zero ionic strength and 25°C.

Tris and Hepes are not in the database of OLI StreamAnalyzer and therefore their pK_a 's at standard conditions (zero ionic strength and 25°C) were taken from literature [21]. However, it must be noted that the pK_a is dependent on temperature and ionic strength [21], and that especially increasing ionic strength may lower the pK_a with a few tenths of a unit.

2.3 Results and discussion

2.3.1 Overpotential optimum depends on buffer pK_a

The HER overpotential (η) between pH 2.5 and pH 11.5 was measured for catholytes containing 50 mM phosphate, carbonate, ammonia, Tris, or Hepes buffer, and 1 M KCl background electrolyte, at a linear flow speed of 2.8 cm/s and a current density of 15 A/m² (Figure 1). Also, the HER overpotential was measured for catholyte that only contained 1 M KCl background electrolyte (non-buffered catholyte).

For non-buffered catholyte, the overpotential increased sharply from -0.05 V at pH 2.5 to -0.50 V at pH 3, and decreased between pH 3 and 11.5 with about 60 mV per pH unit. From pH 2.5 to 3, the flux of protons to the cathode surface drops sharply because more protons are reduced than can be supplied from the bulk. Consequently, the flux of hydroxide moving away from the cathode surface increases correspondingly to sustain the current density [3]. This implicates that the hydroxide concentration at the cathode surface increases sharply, which results in high concentration overpotentials at low pH (low bulk hydroxide concentrations). If the pH increases however, the overpotential decreases with 60 mV per pH unit because the surface pH hardly changes.

For buffered catholyte between pH 3 and 10, the overpotential was reduced compared to non-buffered catholyte. For all buffered catholytes, the overpotential reached an optimum at a pH near the buffer pK_a . The optimum of phosphate buffer was -0.05 V at pH 6.2, near its pK_{a2} . The optimum of ammonia buffer was -0.05 V at pH 9.0, near its pK_a . Carbonate buffer had two optima between pH 3 and 10. The first optimum was less pronounced, but was about -0.25 V at a pH between pH 5 and 6, near its pK_{a1} .

2. Concentration overpotential

The second optimum was -0.09 V at pH 9.3, near its pK_{a2} . It is not clear what caused the higher overpotential of carbonate buffer at its optima compared to phosphate and ammonia buffer. Likely part of the carbonate buffer was stripped as CO_2 , as a consequence of adjusting the pH to 2.4 and flushing the headspace with H_2 prior to an experiment. The optimum of Tris buffer was -0.07 V at pH 7.8, near its pK_a . Hepes buffer had two optima. The first optimum was about -0.04 V at pH 3.0 ($\sim pK_{a1}$), and the second optimum was -0.08 V at pH 7.2, near its pK_{a2} . Tris and Hepes buffer show a higher overpotential than phosphate and ammonia buffer. Tris and Hepes buffer species however, are larger in size and therefore have a lower diffusion coefficient than phosphate, ammonia or carbonate buffer species. Consequently, the diffusional flux of protonated Tris and Hepes species to the cathode surface is lower than dihydrogen phosphate or ammonium, resulting in a higher concentration overpotential.

Thus, buffered catholyte shows a reduced overpotential for the HER compared to non-buffered catholyte. Furthermore, the reduction in overpotential depends on pH and buffer pK_a , with an optimum at a pH near the pK_a .

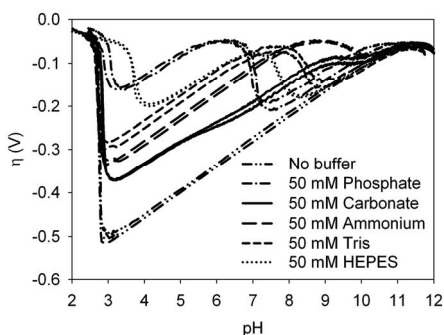


Figure 1 HER overpotential (η) between pH 2.5 and 11.5 measured for catholytes containing different biocompatible buffers, and 1 M KCl background electrolyte, at a linear flow speed of 2.8 cm/s and a current density of 15 A/m². All buffers were tested in duplicate.

2.3.2 Overpotential optimum depends on buffer concentration

The HER overpotential for $pK_{a2} - 2 \leq \text{pH} \leq pK_{a2} + 2$ was investigated for catholytes

containing 5, 10, 20 or 50 mM phosphate buffer, and 1 M KCl background electrolyte, at a linear flow speed of 2.8 cm/s and a current density of 15 A/m² (Figure 2). The overpotential for the entire range from pH 2.5 to 11.5 can be found in Figure S1 of Appendix - Chapter 2. A concentration of 5 mM phosphate buffer did not affect the overpotential. An increase in concentration to 10 mM or higher however, did reduce the overpotential. This can be explained by an increased diffusional flux of protonated buffer species to the cathode surface, thereby reducing the concentration overpotential. A reduced overpotential for increased phosphate concentrations was also found by Merrill and Logan [14].

The largest change in overpotential reduction was obtained between 5 and 20 mM buffer. At 10 mM phosphate buffer, the duplicates show different curves. Apparently, around this phosphate buffer concentration the overpotential is much more sensitive to the concentration than at lower or higher concentrations. For an increased concentration of phosphate buffer, the position of the optimum moved to higher pH values, approaching the pK_{a2} (pH- pK_{a2} = 0) of phosphate.

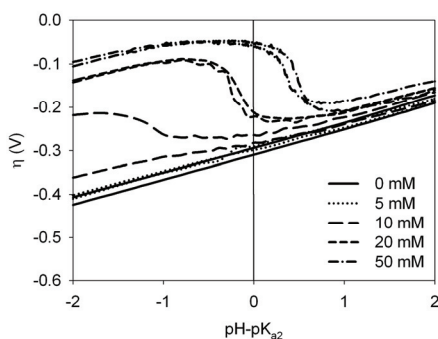


Figure 2 HER overpotential (η) at $pK_{a2} - 2 \leq \text{pH} \leq pK_{a2} + 2$ for catholytes containing different concentrations of phosphate buffer, with 1 M KCl background electrolyte, at a linear flow speed of 2.8 cm/s and a current density of 15 A/m². All concentrations were tested in duplicate.

2.3.3 Overpotential optimum depends on linear flow speed

The HER overpotential for $pK_{a2} - 2 \leq \text{pH} \leq pK_{a2} + 2$ was investigated for catholyte containing 20 mM phosphate buffer and 1 M KCl background electrolyte, at a current density of 15

2. Concentration overpotential

A/m^2 and a linear flow speed of 1, 1.5, 2, 3, or 4 cm/s (Figure 3). The overpotential for the entire range from pH 2.5 to 11.5 can be found in Figure S2 of Appendix – Chapter 2. The effect of increasing the flow speed was the same as of increasing the buffer concentration. An increase in flow speed from 1 to 3 cm/s led to a reduction in overpotential. This can be explained by a decreased diffusion layer thickness, which results in an increased diffusional flux of protonated buffer species. Consequently, the concentration overpotential is reduced. A change in flow speed from 3 to 4 cm/s however, did not further reduce the overpotential. Also for increased linear flow speeds, the position of the optimum moved to higher pH, approaching the pK_{a2} of phosphate.

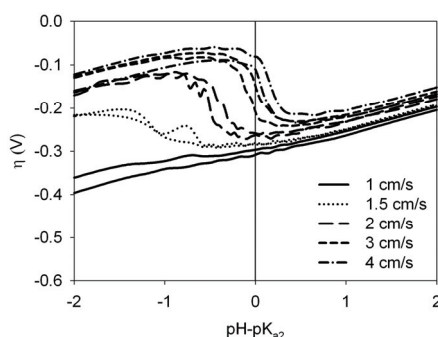


Figure 3 HER overpotential (η) at $pK_{a2} - 2 \leq \text{pH} \leq pK_{a2} + 2$ for 20 mM phosphate buffer with 1 M KCl background electrolyte, at a current density of $15 A/m^2$ and different linear flow speeds. All linear flow speeds were tested in duplicate.

2.3.4 Overpotential optimum depends on current density

The HER overpotential for $pK_{a2} - 2 \leq \text{pH} \leq pK_{a2} + 2$ was investigated for catholyte containing 20 mM phosphate buffer and 1 M KCl background electrolyte, at a linear flow speed of 2.8 cm/s and a current density of 2, 5, 10, 15 or $30 A/m^2$ (Figure 4). The overpotential for the entire range from pH 2.5 to 11.5 can be found in Figure S3 of Appendix – Chapter 2. An increase in current density resulted in an increase in overpotential, which is due to both an increase in concentration overpotential and activation overpotential for the HER. A comparison of $30 A/m^2$ (20 mM phosphate buffer, Figure 4) with $15 A/m^2$ (no buffer, Figure 2) shows that at $30 A/m^2$, 20 mM phosphate buffer still reduced the concentration

overpotential, though to a low extent. The concentration overpotential may be further decreased by increasing the buffer concentration and/or linear flow speed. Also for decreased current densities, the optimum moved to a higher pH, approaching the pK_{a2} of phosphate.

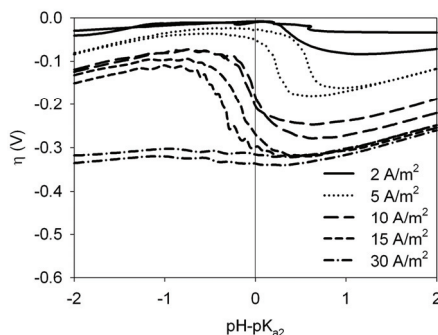


Figure 4 HER overpotential (η) at $pK_{a2} - 2 \leq pH \leq pK_{a2} + 2$ for 20 mM phosphate buffer with 1 M KCl background electrolyte, at a linear flow speed of 2.8 cm/s and different current densities. All current densities were tested in duplicate.

2.3.5 A simple mass transport equation relates buffer transport to the concentration overpotential

The experimental data showed that from pH 3 to 10, a large part of the HER overpotential on Pt/Ir is concentration overpotential, caused by poor mass transport. The concentration overpotential could be reduced through addition of buffer, which transports protons to the cathode surface. The reduction in concentration overpotential at a certain pH depended on buffer pK_a , buffer concentration, linear flow speed and operating current density. To relate buffer transport to the concentration overpotential, first the concentration overpotential is written in terms of the ratio of proton concentration at the surface and at the bulk

$$\eta_{conc.} = 0.060 \log \frac{[H^+]_{surface}}{[H^+]_{bulk}} \quad (6)$$

2. Concentration overpotential

If the proton concentration at the surface approaches the proton concentration in the bulk, the concentration overpotential approaches zero. It is assumed that the protonated buffer species only transports protons from bulk to surface, it does not react itself at the cathode surface. The transport of protonated buffer species from bulk to surface can be described with a flux equation

$$J = \frac{DC_T}{\delta} (X_{HYb} - X_{HYs}) \quad (7)$$

where J is the flux of protonated buffer species ($\text{mol}/\text{m}^2\text{ s}^{-1}$), D is the diffusion coefficient of the protonated buffer species (m^2/s), C_T is the buffer concentration (sum of protonated and dissociated buffer species), δ is the thickness of the diffusion layer (m) that depends on the linear flow speed, X_{HYb} is the fraction of protonated buffer species in the bulk, and X_{HYs} is the fraction of protonated buffer species at the surface. Given the small difference in diffusion coefficients of the dissociated and protonated buffer species, there is no gradient in buffer concentration between surface and bulk. Migrational transport can be safely neglected, because a high concentration of background electrolyte was applied. The fraction of protonated buffer (in the bulk or at the surface) depends on the acid dissociation constant K_a (mol/l) according

$$X_{HY} = \frac{[H^+]}{K_a + [H^+]} \quad (8)$$

Substituting eq 8 in eq 7 results in

$$J = \frac{DC_T}{\delta} \left(\frac{[H^+]_{bulk}}{K_a + [H^+]_{bulk}} - \frac{[H^+]_{surface}}{K_a + [H^+]_{surface}} \right) \quad (9)$$

2. Concentration overpotential

The concentration overpotential (eq 6) follows from the ratio of the proton concentrations at the surface and in the bulk, which can now be written as

$$\frac{[H^+]_{surface}}{[H^+]_{bulk}} = \frac{\frac{J\delta([H^+]_{bulk} + K_a)}{D[H^+]_{bulk}C_T} - 1}{\frac{J\delta([H^+]_{bulk} + K_a)}{DK_aC_T} + 1} \quad (10)$$

The diffusion coefficient (D), thickness of the diffusion layer (δ) and buffer concentration (C_T) are the mass transport factors that determine the maximal possible flux. The maximal possible flux is in fact the limiting current density, i.e. the current density when the concentration of reactants is zero at the electrode surface. Depending on the actual current density, which determines J (dividing the current density by the Faraday constant) and the mass transport factors, the fraction λ can be calculated as follows

$$\lambda = \frac{J}{\left(\frac{DC_T}{\delta}\right)} \quad (11)$$

This fraction can be calculated for every combination of the mass transport factors (D , C_T , δ) at a certain current density. For example, at a current density of 15 A/m^2 , $D = 9.7 \cdot 10^{-10} \text{ m}^2/\text{s}$ for dihydrogen phosphate at 30°C (corrected for temperature [22]), $\delta = 150 \text{ }\mu\text{m}$ [19], and $C_T = 50 \text{ mM}$, λ equals about 0.48. The difference between pH and pK_a of the buffer can be expressed as

$$pH - pK_a = \log\left(\frac{K_a}{[H^+]_{bulk}}\right) \quad (12)$$

Combining eq 10, 11 and 12 results in eq 13, which describes the effects of pH, buffer pK_a , buffer concentration, linear flow speed and current density on the concentration

2. Concentration overpotential

overpotential, with only 3 master variables: pH, pK_a and λ

$$\eta_{conc} = 0.060 \log \left(- \frac{10^{(pH-pK_a)} (\lambda + 10^{(pH-pK_a)} \lambda - 1)}{\lambda + 10^{(pH-pK_a)} \lambda + 10^{(pH-pK_a)}} \right) \quad (13)$$

In Figure 5, the estimated concentration overpotential is plotted versus the pH- pK_a for different values of λ . Only the concentration overpotential at $pK_a - 2 \leq \text{pH} \leq pK_a + 2$ is plotted, because at lower pH, transport of other species (e.g. protons or other protonated buffer species) contribute considerably to the proton concentration at the cathode surface and at higher pH, hydroxide transport from cathode surface to bulk determines the proton concentration at the surface [3].

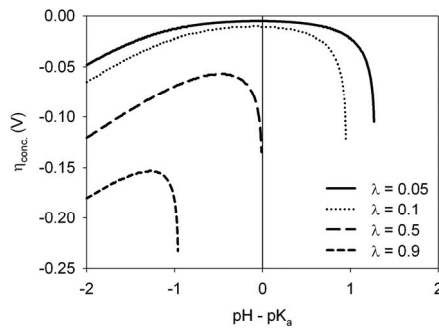


Figure 5 Estimation of the HER concentration overpotential (η_{conc}) at $pK_a - 2 \leq \text{pH} \leq pK_a + 2$, for different values of λ .

From Figure 5 it can be seen that (i) by decreasing λ , the concentration overpotential reduces over the entire range $pK_{a2} - 2 \leq \text{pH} \leq pK_{a2} + 2$, (ii) by decreasing λ , the optimum of the concentration overpotential moves to higher pH values, approaching the pK_a , and (iii) all concentration overpotential curves are not symmetrical.

The 3 characteristics can be understood from eq 7. If λ is decreased, because e.g. C_T is increased, or δ or J is decreased, the difference in bulk and surface fractions of protonated buffer species ($X_{HYb} - X_{HYS}$ in eq 7) is decreased. This implies that the pH difference between bulk and surface decreases and consequently the concentration

overpotential decreases. If λ approaches zero, the optimum of the concentration overpotential is reached for a pH (bulk and surface pH) approaching the pK_a , because the protonated buffer gradient (dX_{HY}/dpH) is largest at the pK_a . If λ is increased, because e.g. C_T is decreased or δ or J is increased, the difference in bulk and surface fractions of protonated buffer species ($X_{HYb}-X_{HYs}$ in eq 7) is increased. This has two implications: (i) the pH difference between bulk and surface increases and consequently, the concentration overpotential increases, and (ii) the optimum of the concentration overpotential is reached at a pH below pK_a (and a surface pH above pK_a). For certain, critical pH above the optimum of the concentration overpotential, the difference in bulk and surface fractions of protonated buffer is not sufficiently high to sustain the required flux of protons. Above this critical pH, the flux of hydroxide moving away from the cathode surface increases correspondingly to sustain the current density [3]. This results in a sharp increase in concentration overpotential, and consequently, a non-symmetrical shape of the overpotential curves. The transport of hydroxide is not included in the mass transport equation, which explains the abrupt ending of the concentration overpotential curves.

The mass transport equation (eq 13) consists of only 3 master variables to relate all studied factors to the concentration overpotential. It can be qualitatively summarized that with decreasing λ the overpotential decreases and the pH of the optimum approaches the buffer pK_a . This prediction of the mass transport equation is consistent with experimental observations on the effect of buffer pK_a , buffer concentration, linear flow speed and current density. Indeed, for the selected buffers, the optimum was found close to the buffer pK_a . An increased buffer concentration means a decrease in λ . And indeed, if the concentration of phosphate buffer was increased the overpotential decreased and the pH of the optimum approached the pK_a . This also accounts for an increase in linear flow speed, which results in a decrease in λ , and for an increase in current density, which results in an increase in λ . The mass transport equation is thus able to explain the effects of all studied factors on the concentration overpotential at different pH.

2.4 Implications

2.4.1 HER overpotential in an MEC can be reduced by optimizing buffer transport

This study with flat Pt/Ir cathodes shows that the HER overpotential in MECs can be reduced through the use of buffer, but this effect is strongly pH dependent. Therefore, the choice of buffer (i.e. pK_a) must be well balanced with the expected operational pH of the cathode. In this respect, the asymmetric performance of the buffer needs to be considered; a choice of buffer with a pK_a above operating pH is preferred. Furthermore, it is important to realize that the pH at which the concentration overpotential reaches a minimum is not simply the buffer pK_a , but depends on buffer concentration, linear flow speed of the catholyte and operating current density. Only if buffer concentration and linear flow speed are adapted to the current density, the overpotential optimum is reached at a pH approaching the buffer pK_a . It should be considered that the buffer pK_a under experimental conditions may vary from the pK_a under standard conditions, reported in literature (different temperature and solution ionic strength).

The choice of buffer is also limited by other constraints, such as its precipitation tendency with divalent cations. For instance, for phosphate buffer it was shown that precipitation of calcium phosphate on a microbial biocathode slowly deteriorated cathode performance [17]. In this respect, Good's buffers such as Tris and Hepes may be a viable replacement because they have a pK_a close to pH 7, are biocompatible but not likely biodegradable in an MEC, and have a low precipitation tendency [20].

2.4.2 Optimized buffer transport results in reduced energy input of an MEC

The reduction in overpotential for the HER under neutral conditions is relevant for improving MEC performance. Experimental data show that on Pt/Ir, the overpotential of the HER at 15 A/m^2 and pH 7 can be reduced from -0.28 V in non-buffered (or poorly buffered) catholyte to, for example, -0.08 V in catholyte containing 50 mM Tris buffer. If it is assumed that the same reduction in overpotential (0.2V) is obtained in an MEC, this implies a decrease in energy input of more than 0.4 kWh/Nm^3 hydrogen gas. For each

specific situation, the use of buffer for the HER in an MEC must be evaluated. In an MEC with membrane, the buffer could be retained in the catholyte, but it will be a challenge to maintain the pH around 7. Membrane-less MECs can be maintained around pH 7, but addition of buffer to the electrolyte will not be cost-effective and therefore, membrane-less MECs will likely be depended on optimizing the use of buffer naturally present in the feed stream. Optimization may then be achieved by lowering the diffusion layer thickness at the cathode through, e.g. an increase in pump speed, the use of a turbulence promoter or the use of a flow through cathode.

2.4.3 Mass transport equation as interesting tool to quantify concentration overpotential

The mass transport equation (eq 13) could relate the effects of pH, buffer pK_a , buffer concentration, linear flow speed and current density to the concentration overpotential. There was no need for including the HER mechanism to explain our results. Further development of this simple model would result in an interesting tool to quantify the concentration overpotential and to develop strategies for optimized use of buffer for the HER in an MEC.

2.5 Acknowledgements

This work was performed in the TTIW-cooperation framework of Wetsus, centre of excellence for sustainable water technology (www.wetsus.nl). Wetsus is funded by the Dutch Ministry of Economic Affairs, the European Union Regional Development Fund, the Province of Fryslân, the City of Leeuwarden and the EZ/Kompas program of the “Samenwerkingsverband Noord-Nederland”. The authors like to thank Tom Sleutels and Michel Saakes for critically reading the manuscript, and Shell, Paques bv and Magneto Special Anodes bv of the research theme “Hydrogen” for the fruitful discussions and their financial support.

2.6 References

- [1] Logan B E, Call D, Cheng S, Hamelers H V M, Sleutels T H J A, Jeremiasse A W, et al. Microbial electrolysis cells for high yield hydrogen gas production from organic matter. *Environ Sci Technol* 2008; 42: 8630-40
- [2] Vetter K J. *Electrochemical kinetics: theoretical and experimental aspects*. ed. New York: Academic press; 1967.
- [3] Harris L B. Change in pH near the cathode during the electrodeposition of a bivalent metal. *Analysis. J Electrochem Soc* 1973; 120: 1034-40
- [4] Rozendal R A, Hamelers H V M, Euverink G J W, Metz S J, Buisman C J N. Principle and perspectives of hydrogen production through biocatalyzed electrolysis. *Int J Hydrogen Energy* 2006; 31: 1632-40
- [5] Rozendal R A, Hamelers H V M, Molenkamp R J, Buisman C J N. Performance of single chamber biocatalyzed electrolysis with different types of ion exchange membranes. *Water Res* 2007; 41: 1984-94
- [6] Sleutels T H J A, Hamelers H V M, Rozendal R A, Buisman C J N. Ion transport resistance in microbial electrolysis cells with anion and cation exchange membranes *Int J Hydrogen Energy* 2009; 34: 3612-20
- [7] Bard A J, Faulkner L R. *Electrochemical methods: fundamentals and applications*. 2nd ed. New York: John Wiley & Sons; 2001.
- [8] Clauwaert P, Aelterman P, Pham T H, De Schamphelaire L, Carballa M, Rabaey K, et al. Minimizing losses in bio-electrochemical systems: the road to applications. *Appl Microbiol Biotechnol* 2008; 79: 901-13
- [9] Millet P, Andolfatto F, Durand R. Design and performance of a solid polymer electrolyte water electrolyzer. *Int J Hydrogen Energy* 1996; 21: 87-93
- [10] Daniele S, Lavagnini I, Baldo M A, Magno F. Steady state voltammetry at microelectrodes for the hydrogen evolution from strong and weak acids under pseudo-first and second order kinetic conditions. *J Electroanal Chem* 1996; 404: 105-11
- [11] Daniele S, Baldo M A, Bragato C, Lavagnini I. Steady state voltammetry in the process of hydrogen evolution in buffer solutions. *Anal Chim Acta* 1998; 361: 141-50
- [12] Honda T, Murase K, Hirato T, Awakura Y. pH measurement in the vicinity of a cathode evolving hydrogen gas using an antimony microelectrode. *J Appl Electrochem* 1998; 28: 617-22
- [13] Linter B R, Burstein G T. Reactions of pipeline steels in carbon dioxide solutions. *Corros Sc* 1999; 41: 117-39
- [14] Merrill M D, Logan B E. Electrolyte effects on hydrogen evolution and solution resistance in microbial electrolysis cells. *J Power Sources* 2009; 191: 203-8
- [15] Call D, Logan B E. Hydrogen production in a single chamber microbial electrolysis cell lacking a membrane. *Environ Sci Technol* 2008; 42: 3401-6
- [16] Tartakovsky B, Manuel M-F, Wang H, Guiot S R. High rate membrane-less microbial electrolysis cell for continuous hydrogen production. *Int J Hydrogen Energy* 2009; 34: 672-7
- [17] Jeremiasse A W, Hamelers H V M, Buisman C J N. Microbial electrolysis cell with a microbial biocathode. *Bioelectrochemistry* 2009; doi:10.1016/j.bioelechem.2009.05.005:

- [18] Rozendal R A, Jeremiasse A W, Hamelers H V M, Buisman C J N. Hydrogen production with a microbial biocathode. *Environ Sci Technol* 2008; 42: 629-34
- [19] Ter Heijne A, Hamelers H V M, Saakes M, Buisman C J N. Performance of non-porous graphite and titanium-based anodes in microbial fuel cells. *Electrochim Acta* 2008; 53: 5697-703
- [20] Good N E, Winget G D, Winter W, Conolly T N. Hydrogen Ion Buffers for Biological Research. *Biochemistry* 1966; 5: 467-77
- [21] Goldberg R N, Kishore N, Lennen R M. Thermodynamic quantities for the ionization reactions of buffers. *J Phys Chem Ref Data* 2002; 31: 231-370
- [22] Lide R L, 2004-2005. *CRC Handbook of Chemistry and Physics*, 85th ed. CRC Press, Boca Raton.

3. Microbial Electrolysis Cell with a Microbial Biocathode

This study demonstrates, for the first time, the proof-of-principle of an MEC in which both the anodic and cathodic reaction are catalyzed by microorganisms. No expensive chemical catalysts, such as platinum, are needed. Two of these MECs were simultaneously operated and reached a maximum of 1.4 A/m^2 at an applied cell voltage of 0.5 V. At a cathode potential of -0.7 V, the biocathode in the MECs had a higher current density (MEC 1: 1.9 A/m^2 , MEC 2: 3.3 A/m^2) than a control cathode (0.3 A/m^2 , graphite felt without biofilm) in an electrochemical half cell. This indicates that hydrogen production is catalyzed at the biocathode, likely by electrochemically active microorganisms. The cathodic hydrogen recovery was 17% for MEC 1 and 21% for MEC 2. Hydrogen losses were ascribed to diffusion through membrane and tubing, and methane formation. After 1600 h of operation, the current density of the MECs had decreased to 0.6 A/m^2 , probably caused by precipitation of calcium phosphate on the biocathode. The slow deteriorating effect of calcium phosphate and the production of methane show the importance of studying the combination of bioanode and biocathode in one electrochemical cell, and of studying long term performance of such an MEC.

This chapter has been published as:

Jeremiasse A W, Hamelers H V M, Buisman C J N. Microbial electrolysis cell with a microbial biocathode. *Bioelectrochemistry* 2010; 78: 39-43

3.1 Introduction

Microbial electrolysis is a process for the production of green hydrogen from organic matter [1-3]. In a microbial electrolysis cell (MEC), organic material is converted by electrochemically active microorganisms into CO_2 , H^+ , and electrons. These electrons are transferred to the anode and flow from the anode, via an electrical circuit containing a power supply, to the cathode. At the cathode, hydrogen is produced via reduction of protons or water. The flow of negative charge outside the cell is compensated by cation transport from anode to cathode inside the cell. To drive hydrogen production under biological conditions, theoretically 0.14 V has to be applied [3]. In practice however, more than 0.14 V has to be applied, partly due to the cathode overpotential.

So far in microbial electrolysis, mainly cathodes have been used that apply platinum as catalyst. The choice for platinum originates from its excellent performance in water electrolyzers and fuel cells. Platinum however, is an expensive catalyst. Besides, platinum performance can be negatively affected by components often present in waste streams [4]. Therefore, there is need for an alternative catalyst at the cathode.

In 2008, Rozendal et al. developed a microbial biocathode as a potential alternative for platinum [5]. This biocathode was obtained by enriching a biofilm of hydrogen oxidizing, electrochemically active microorganisms on a graphite felt anode (bioanode). Next, the polarity of this bioanode was reversed, turning it into a hydrogen producing biocathode. At a controlled potential of -0.7 V vs normal hydrogen electrode (NHE), the biocathode had a current density of 1.1 A/m^2 , whereas the control cathode (graphite felt without biofilm) had a current density of only 0.3 A/m^2 . Subsequently, effluent of the biocathode was used to inoculate the control cathode, which then also turned into a biocathode that reached a current density of 1.1 A/m^2 . This biocathode did not require a mediator for hydrogen production, which is an advantage compared to other reported hydrogen producing biocathodes [6-8]. The biocathode however, was only tested in an electrochemical half cell (Figure 1A), in which ferrocyanide was oxidized at the anode.

The objective of this study was to give a proof-of-principle of an MEC in which both the anodic and cathodic reaction are catalyzed by microorganisms, i.e. a full

biological MEC (Figure 1B). Such a study is needed because the performance of a full biological MEC can be different from the performance predicted from half cell studies, because the bioanode and biocathode in a full MEC influence each other via transport of materials through the membrane. For this purpose, anode and cathode chamber of an MEC were inoculated with electrochemically active microorganisms, and the MEC was operated at an applied cell voltage of 0.5 V.

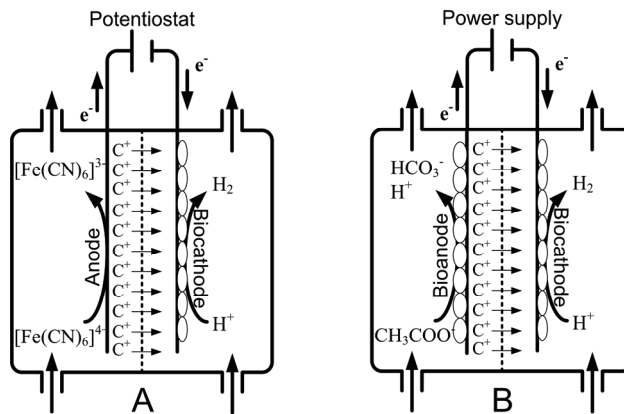


Figure 1 A) The biocathode controlled at a potential of -0.7 V (vs NHE) in an electrochemical half cell [5], and B) the biocathode coupled to a bioanode in an MEC (this study, C^+ = cations).

3.2 Materials and Methods

3.2.1 Experimental set-up

Experiments were performed with 2 identical electrochemical cells (MEC 1 and MEC 2) with graphite felt electrodes in the same experimental set-up that was used by Rozendal et al. [5]. Anode and cathode chamber (each with a volume of 0.25 L) were continuously fed with medium (1.3 mL/min) from separate supply tanks (volume 25 L). Both anode and cathode medium consisted of 0.74 g/L KCl, 0.58 g/L NaCl, 0.68 g/L KH_2PO_4 , 0.87 g/L K_2HPO_4 , 0.28 g/L NH_4Cl , 0.1 g/L $MgSO_4 \cdot 7H_2O$, 0.1 g/L $CaCl_2 \cdot 2H_2O$ and 1 mL/L of a trace element mixture [9]. In addition, the anode influent medium contained 1.36 g/L $NaCH_3COO \cdot 3H_2O$,

3. MEC with microbial biocathode

and the cathode influent medium contained 0.84 g/L NaHCO_3 , unless stated otherwise. The pH of the anode chamber was controlled at pH 7 by dosing with 1 M NaOH, and the pH of the cathode chamber was controlled at pH 7 by dosing with 1 M HCl (Liquisys M CPM 253, Endress + Hauser). The temperature of the MECs was controlled at 303 K. All potentials are reported vs NHE.

3.2.2 Start-up and operation

The applied cell voltage of both MECs was controlled at 0.5 V using a potentiostat (Wenking Potentiostat/Galvanostat KP5V3A, Bank IC) operated as a 2-electrode setup. MEC 2 was started up 96 h later than MEC 1. At time zero, the anode chamber of both MECs was inoculated with effluent from a bioanode of a previous MEC [10]. To first establish a bioanode, and subsequently a biocathode, the cathode chamber of both MECs was inoculated after 600 h. The cathode chamber inoculum was effluent from a previous set-up with a biocathode [5]. Both MECs were operated for 1600 h.

3.2.3 Polarization curves

Polarization curves were recorded for both MECs on the same day, i.e. 1025 h after start-up for MEC 1, and 929 h after start-up for MEC 2. The current and cathode potential were measured at applied cell voltages of 0.2, 0.3, 0.4, 0.5, 0.6, 0.7 and 0.8 V. For each applied cell voltage, measurements were recorded every 5 min for 1 h. The last 5 measurements for each applied cell voltage were averaged. Two polarization plots were made: One plot of the average current density versus the applied cell voltage and one plot of the average current density versus the cathode potential. Cathodic current densities are expressed with a positive sign.

3.2.4 Hydrogen yield test

A hydrogen yield test of 52 h was performed for both MECs on the same day, i.e. 1313 h after start-up for MEC 1, and 1217 h after start-up for MEC 2 (applied cell voltage: 0.5 V). Before the hydrogen yield test, the biocathode was fed with medium that was not

supplemented with 10 mM NaHCO_3 to reduce methanogenesis, and the biocathode chamber was flushed with nitrogen gas. During the yield test, the biocathode was operated in batch mode. The headspace of the biocathode was sampled after 0, 4, 6, 24, 28, 30, 48 and 52 h and the gas samples were analyzed for hydrogen and methane with a gas chromatograph (Shimadzu GC-2010 with a thermal conductivity detector and a Varian molsieve 5A column). Hydrogen production was calculated from the total gas production, measured with a gas flow meter (Milligascounter®, Ritter), and the measured hydrogen fractions using the mass balance equation described by Rozendal et al. [11].

3.2.5 Scanning Electron Microscopy (SEM) and element analysis

After 1600 h of operation, one MEC was disassembled and precipitates on the graphite felt biocathode were collected. SEM photos were taken with a JEOL JSM-6480LV SEM (acceleration voltage 15 kV, LV mode, BES detector). A NORAN System SIX Model 300 X-ray microanalysis system (Thermo Electron Corporation) was used for element analysis of the precipitates.

3.3 Results and Discussion

3.3.1 Start-up and operation at an applied cell voltage of 0.5V

Two MECs with graphite felt electrodes were started up by applying a cell voltage of 0.5 V and inoculating the anode chamber with electrochemically active microorganisms. After start-up, the current density of both MECs increased (Figure 2). The current density of the MECs showed more fluctuations than that of the biocathode in the electrochemical half cell [5]. After 300 h for MEC 1, and after 200 and 400 h for MEC 2, a drop and subsequent increase in current density was observed. As will be discussed further on, it is hypothesized that this could be the result of calcium phosphate precipitation on the biocathode. Both MECs reached a maximum of 1.4 A/m^2 . This is higher than the current density of the continuous flow MEC with platinum coated (50 g/m^2) aqueous cathode used by Rozendal et al. [2], which had an average current density of 0.47 A/m^2 at an applied cell

3. MEC with microbial biocathode

voltage of 0.5 V.

Inoculation of the cathode chamber after 600 h of operation did not have a clear effect on development of the current density. The same electrochemical cells were used in previous experiments with the biocathode [5], and were not sterilized afterwards. It is therefore likely that electrochemically active microorganisms were already present in the biocathode chamber since start-up, and the biocathode was already developing since start-up. This could explain why further inoculation did not have a clear effect on development of the current density.

The increase in current density since start-up is likely limited by the growth of electrochemically active microorganisms on the biocathode. Rozendal et al. [5] showed that growth of microorganisms on the biocathode was slower than on the bioanode. The biocathode reached a maximum current density 500 h after inoculation, whereas the bioanode reached a maximum current density 130 h after inoculation [5]. The MECs in our study also needed more time to reach a maximum current density than an MEC with bioanode alone. MEC 1 reached its maximum current density 650 h after start-up, and MEC 2 reached its maximum current density 850 h after start-up.

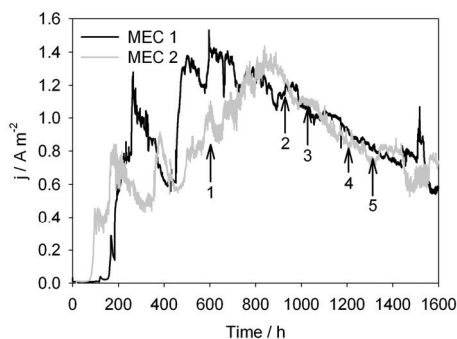


Figure 2 Development of the current density of both MECs at an applied cell voltage of 0.5 V. (1) Inoculation of biocathodes of both MECs, (2) polarization curve of MEC 2 (Figure 3), (3) polarization curve of MEC 1 (Figure 3), (4) hydrogen yield test MEC 2 (Figure 4), and (5) hydrogen yield test of MEC 1 (Figure 4).

The differences in time before reaching maximum current density for the two MECs in this study may be explained by different amounts of electrochemically active microorganisms

present at start-up in both MECs.

3.3.2 Polarization curves

After 1025 h of operation for MEC 1 and 929 h of operation for MEC 2, polarization curves were recorded (Figure 3). At an applied cell voltage of 0.8 V, both MECs had a current density of 3.3 A/m². This current density is comparable to the current density of a continuous flow MEC without membrane [12], which had a current density of 3.2 A/m² at an applied cell voltage of 0.85V. The MEC without membrane however, used a gas diffusion cathode with 5 g/m² platinum. The current density found in our study is lower than the current density of a batch-type MEC lacking a membrane, reported by Call and Logan [13]. This batch-type MEC had a current density of about 11.7 A/m² cathode at an applied cell voltage of 0.8 V. However, also in this study a platinum coated (5 g/m²) cathode was used.

In Figure 3B, the current densities at different cathode potentials for the biocathodes in the MECs are shown, together with those for the biocathode and control cathode (graphite felt without biofilm) tested in the electrochemical half cell by Rozendal et al. [5]. The biocathodes in the MECs had higher current densities than the control cathode. At a cathode potential of -0.7 V, the biocathode in MEC 1 had a current density of 1.9 A/m² and in MEC 2 a current density of 3.3 A/m², whereas the control cathode in the electrochemical half cell had a current density of 0.3 A/m². This indicates that hydrogen production is catalyzed by the biocathodes in the MECs, likely due to the presence of electrochemically active micro-organisms. Furthermore, the biocathodes in the MECs showed higher current densities than the biocathode in the electrochemical half cell. The biocathode chambers of the MECs contained electrochemically active microorganisms that originated from previous experiments (section 3.1) [5]. Consequently, the right microorganisms were probably further enriched in the MECs.

At a measured cathode potential of -0.7 V, and a theoretical potential of -0.42 V (Nernst equation, pH 7), the cathode overpotential was -0.28 V. To design a system with a cathode overpotential of maximum -0.1 V at a current density of 10 A/m² [14], the

3. MEC with microbial biocathode

biocathode overpotential has to be reduced further, while the current density has to be increased.

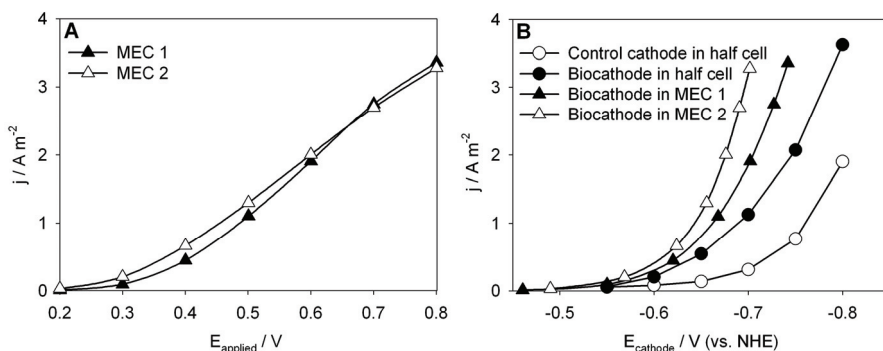


Figure 3 A) Current density versus applied cell voltage, and B) current density versus cathode potential of the biocathodes in the MECs, current density versus cathode potential of the biocathode in the electrochemical half cell [5] (Figure 1A), and current density versus cathode potential of the control cathode in the electrochemical half cell (graphite felt without biofilm) [5]. MEC graphs were recorded 1025 h after start-up of MEC 1 and 929 h after start-up of MEC 2.

3.3.3 Hydrogen yield test

During the 52-h yield test, MEC 1 had an average current density of 0.79 A m^{-2} and produced 0.08 L of hydrogen, and MEC 2 had an average current density of 0.84 A m^{-2} and produced 0.11 L of hydrogen (Figure 4). After 52 h, the cathodic hydrogen recovery for MEC 1 was 17% and for MEC 2 was 21%. Hydrogen is easily lost by diffusion through membrane [2] and tubing [3]. In our study, the same set-up (with Fumasep® FKE membrane) was used as by Rozendal et al. [5]. They estimated that most of the hydrogen loss was due to diffusion through the membrane, and it can be expected that the same occurred in our study. Diffusional losses of hydrogen become relatively smaller at higher current densities, which results in higher hydrogen recoveries [2].

Although the biocathode of the MEC was operated under carbon-limited conditions during the yield test, methane was found in the headspace. At the end of the yield test, the headspace of MEC 1 contained 2.4% methane, and that of MEC 2 contained 8.3% methane. This methane might have been produced by methanogens at the bioanode,

and subsequently diffused through the membrane to the biocathode. It might also have been produced by methanogens at the biocathode from hydrogen and carbon dioxide (e.g. originating from the bioanode), which would also explain part of the hydrogen loss [15].

The cathodic hydrogen recoveries found in our study resulted in lower hydrogen production rates compared to other studies [3]. MEC 1 produced hydrogen at a rate of $0.03 \text{ Nm}^3/\text{m}^3$ reactor liquid/day and MEC 2 produced hydrogen at a rate of $0.04 \text{ Nm}^3/\text{m}^3$ reactor liquid/day.

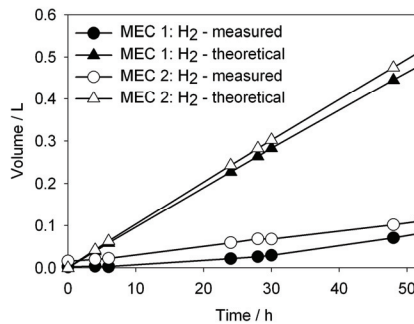


Figure 4 Measured hydrogen production and theoretical hydrogen production (based on charge) for both MECs during 52 h at an applied cell voltage of 0.5 V.

3.3.4 Precipitates on biocathode

After the maximum current density was reached, the current density decreased to 0.6 A/m^2 in both MECs (Figure 2). Both MECs were disassembled after 1600 h of operation. The membrane that was in direct contact with the graphite felt biocathode was removed. A precipitation layer was visible on both sides (membrane side and chamber side) of both graphite felt biocathodes. Precipitate was collected from the chamber side and analyzed with SEM (Figure 5), and for elemental composition. The crystalline structure of the precipitate and the high atomic fractions of oxygen, calcium and phosphor indicate that the precipitate was calcium phosphate. The precipitation was caused by cations, including divalent cations such as Ca^{2+} , which were continuously transported from anode to cathode through the cation exchange membrane. Moreover, divalent cations and phosphate buffer were continuously supplied with the cathode medium. Continuous supply of Ca^{2+} and

3. MEC with microbial biocathode

phosphate, and the high local pH at the cathode due to hydrogen production, locally led to saturated conditions for calcium phosphate. As a result, calcium phosphate precipitates on the biocathode. The precipitate shields the biocathode from hydrogen production, which probably caused the decrease in current density, a phenomenon that also has been demonstrated by Gabrielli et al. [16]. They explained fluctuations in current density, which were also observed in our study, by detachment of precipitate under the influence of produced hydrogen gas bubbles. Furthermore, the lower current densities for MEC 1 compared to MEC 2 during the polarization and yield tests were probably due to a longer operating time of MEC 1, which resulted in more precipitation.

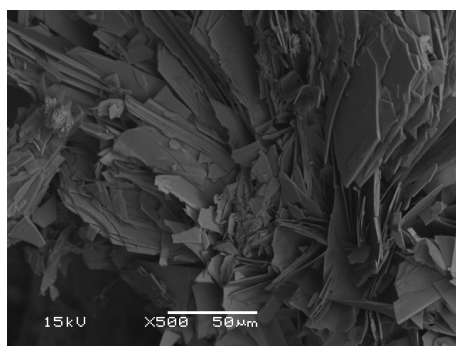


Figure 5 SEM image of the precipitation layer present on the chamber side of the biocathode.

3.4 Conclusions and implications

This study demonstrated for the first time that it is possible to operate a full biological MEC, i.e. no expensive chemical catalysts such as platinum are needed. Start-up of the full biological MEC was slow compared to an MEC with platinum cathode. However, it can be expected that further enrichment of microorganisms on the biocathode will decrease the start-up time of the full biological MEC, and increase the current densities up to bioanode level. Current densities in this study were already higher than in the previous study with the biocathode [5].

The full biological MEC was operated for a prolonged period (1600 h). This allowed us to observe the slow deteriorating effect of precipitate on the biocathode.

Although the cathode chamber pH was controlled at pH 7, calcium phosphate precipitated on the biocathode. This is explained by local concentration differences, resulting from the high pH near the biocathode surface, and from transport of divalent cations such as Ca^{2+} through the membrane. Transport of Ca^{2+} through the membrane is a disadvantage of cation exchange membranes, because they are more selective for multivalent cations than monovalent cations.

In this study, methane was produced by both MECs. As a consequence, the produced hydrogen gas is not pure. Therefore, it is important to find out whether the methane is produced in the bioanode or in the biocathode chamber, and how methane production can be prevented. The choice of membrane is critical for MEC performance: The use of a cation exchange membrane results in precipitation on the biocathode, whereas the use of an anion exchange membrane would lead to precipitation on the bioanode due to transport of phosphate from cathode to anode. If no membrane is used, bicarbonate produced at the anode is easily transported to the cathode, creating favorable conditions for methanogens to produce methane [17].

The slow deteriorating effect of calcium phosphate, and the production of methane show the importance of studying the combination of bioanode and biocathode in one electrochemical cell, and of studying the long term performance of such a full biological MEC.

3.5 Acknowledgements

This work was performed in the TTIW-cooperation framework of Wetsus, centre of excellence for sustainable water technology (www.wetsus.nl). Wetsus is funded by the Dutch Ministry of Economic Affairs, the European Union Regional Development Fund, the Province of Fryslân, the City of Leeuwarden and the EZ/Kompas program of the “Samenwerkingsverband Noord-Nederland”. The authors like to thank Tom Sleutels for critically reading the manuscript, and Shell, Paques bv and Magneto Special Anodes bv of the research theme “Hydrogen” for the fruitful discussions and their financial support.

3.6 References

- [1] Liu H, Grot S, Logan B E. Electrochemically assisted microbial production of hydrogen from acetate. *Environ Sci Technol* 2005; 39: 4317-20
- [2] Rozendal R A, Hamelers H V M, Euverink G J W, Metz S J, Buisman C J N. Principle and perspectives of hydrogen production through biocatalyzed electrolysis. *Int J Hydrogen Energy* 2006; 31: 1632-40
- [3] Logan B E, Call D, Cheng S, Hamelers H V M, Sleutels T H J A, Jeremiasse A W, et al. Microbial electrolysis cells for high yield hydrogen gas production from organic matter. *Environ Sci Technol* 2008; 42: 8630-40
- [4] Selembo P A, Merrill M D, Logan B E. The use of stainless steel and nickel alloys as low-cost cathodes in microbial electrolysis cells. *J Power Sources* 2009; 190: 271-8
- [5] Rozendal R A, Jeremiasse A W, Hamelers H V M, Buisman C J N. Hydrogen production with a microbial biocathode. *Environ Sci Technol* 2008; 42: 629-34
- [6] Tatsumi H, Takagi K, Fujita M, Kano K, Ikeda T. Electrochemical study of reversible hydrogenase reaction of *Desulfovibrio vulgaris* cells with methyl viologen as an electron carrier. *Anal Chem* 1999; 71: 1753-9
- [7] Lojou E, Durand M C, Dolla A, Bianco P. Hydrogenase activity control at *Desulfovibrio vulgaris* cell-coated carbon electrodes: Biochemical and chemical factors influencing the mediated bioelectrocatalysis. *Electroanalysis* 2002; 14: 913-22
- [8] Aulenta F, Canosa A, Majone M, Panero S, Reale P, Rossetti S. Trichlorethene dechlorination and H₂ evolution are alternative biological pathways of electric charge utilization by a dechlorinating culture in a bioelectrochemical system. *Environ Sci Technol* 2008; 42: 6185-90
- [9] Zehnder A J B, Huser B A, Brock T D, Wuhrmann K. Characterization of an acetate-decarboxylating, non-hydrogen-oxidizing methane bacterium. *Arch Microbiol* 1980; 124: 1-11
- [10] Rozendal R A, Sleutels T H J A, Hamelers H V M, Buisman C J N. Effect of the type of ion exchange membrane on performance, ion transport, and pH in biocatalyzed electrolysis of wastewater. *Water Sci Technol* 2008; 57: 1757-62
- [11] Rozendal R A, Hamelers H V M, Molenkamp R J, Buisman C J N. Performance of single chamber biocatalyzed electrolysis with different types of ion exchange membranes. *Water Res* 2007; 41: 1984-94
- [12] Tartakovsky B, Manuel M-F, Wang H, Guiot S R. High rate membrane-less microbial electrolysis cell for continuous hydrogen production. *Int J Hydrogen Energy* 2008; doi:10.1016/j.ijhydene.2008.11.003
- [13] Call D, Logan B E. Hydrogen production in a single chamber microbial electrolysis cell lacking a membrane. *Environ Sci Technol* 2008; 42: 3401-6
- [14] Rozendal R A, 2007. Hydrogen Production through Biocatalyzed Electrolysis, Department of Environmental Technology. Wageningen University, Wageningen.
- [15] Wang A, Liu W, Cheng S, Xing D, Zhou J, Logan B E. Source of methane and methods to control its formation in single chamber microbial electrolysis cells. *Int J Hydrogen Energy* 2009; 34: 3653-8

- [16] Gabrielli C, Maurin G, Francy-Chausson H, Thery P, Tran T T M, Tlili M. Electrochemical water softening: principle and application. *Desalination* 2006; 201: 150-63
- [17] Clauwaert P, Verstraete W. Methanogenesis in membraneless microbial electrolysis cells. *Appl Microbiol Biotechnol* 2008; doi:10.1007/s00253-008-1796-4

4. Acetate enhances development of a H₂-producing microbial biocathode

H₂ can be produced from organic matter with a microbial electrolysis cell (MEC). To decrease MEC capital costs, a cathode is needed that is made of low-cost material and produces H₂ at high rate. A microbial biocathode is a low-cost candidate, but suffers from long development times and a low H₂ production rate. In this study, > 2 times faster development was observed for biocathodes fed with acetate than with bicarbonate as carbon source. The faster development was likely caused by a higher biomass yield for acetate than for bicarbonate, which was supported by thermodynamic calculations. To increase the H₂ production rate, a flow through biocathode fed with acetate was investigated. This biocathode produced 2.2 m³ H₂ m⁻³ reactor day⁻¹ at -0.7 V vs NHE, which was 7 times higher than of a parallel flow biocathode.

This chapter has been submitted as:

Jeremiasse A W, Hamelers H V M, Croese E, Buisman C J N, Acetate enhances development of a H₂-producing microbial biocathode.

4. Acetate enhances biocathode development

4.1 Introduction

Valuable H_2 can be produced from organic matter through a bioelectrochemical process called microbial electrolysis. In a microbial electrolysis cell (MEC), electrochemically active microorganisms convert organic matter and transfer the liberated electrons to the anode (i.e. bioanode). From the bioanode, the electrons are transported through an external circuit containing a power supply, to the cathode where the H_2 evolution reaction (HER) proceeds. To maintain electroneutrality, an ionic current must flow through the MEC. The power supply delivers a voltage to overcome the thermodynamical barrier of the production of H_2 from organic matter. This thermodynamical barrier is 0.14 V for the production of H_2 from acetate under biological conditions [1].

In practice, more than 0.14 V is applied to produce H_2 from acetate. Part of this additional voltage is consumed at the cathode as cathode overpotential, i.e. the extra potential beyond the thermodynamical potential (Nernst equation) required to drive the HER at a certain rate. To decrease the cathode overpotential, a catalyst can be used that is composed of a noble metal such as Pt, or non-noble metals such as Fe and Ni [2-4]. Alternatively, a biological cathode based on living microbial cells (i.e. a microbial biocathode) can be used [5]. A microbial biocathode is advantageous compared to metal based cathodes because the catalyst is cheap, continuously regenerated, and not susceptible to corrosion [6-7].

Previous studies demonstrated the development of a H_2 -producing biocathode based on *Geobacter sulfurreducens* [8], *Desulfitobacterium*- and *Dehalococcoides*-enriched cultures [9], and on a naturally selected mixed culture fed with bicarbonate [10]. Furthermore, microbial biocathodes were successfully applied in an MEC [8,11]. However, the main limitations of these MECs were a long development time (i.e. slow startup) and low H_2 production rate at high overpotential of the microbial biocathode. These limitations need to be resolved before the microbial biocathode can be a viable alternative for metal catalyzed cathodes.

We hypothesize that the long development time of the microbial biocathode reflects a low growth yield of biomass. Assuming that analogously to bioanodes [12],

microorganisms grow from an energy gain of electron transfer at the cathode, the energy gain must be increased to increase the growth yield, and thus to decrease the development time. It is expected that the energy gain can be increased through application of a more negative cathode potential. Furthermore, microorganisms need to invest less energy for growth on a heterotrophic instead of an autotrophic carbon source [13]. Consequently, a heterotrophic carbon source would increase the growth yield and thus decrease the development time.

The objective of this study was to decrease the development time and to increase the H₂ production rate of a H₂-producing microbial biocathode. First, the effects of cathode potential, and an autotrophic (bicarbonate) and heterotrophic (acetate) carbon source on biocathode development were predicted with a thermodynamic analysis [13]. Subsequently, the effects of cathode potential and carbon source were experimentally investigated. Finally, the carbon source and cathode potential that resulted in the fastest development were chosen for development of a biocathode on a porous electrode with flow through configuration to increase the H₂ production rate [14]. To minimize effects of scaling and possible limitation by a bioanode [11], the biocathodes were studied in electrochemical cells with a chemical counter electrode (hexacyanoferrate).

4.2 Materials and Methods

4.2.1 Electrochemical cells and setup

The effect of carbon source and cathode potential on biocathode development was investigated with 2 identical setups. Each setup contained 4 electrochemical cells (total: 8 cathodes), similar to the cells used in a previous study [15]. However, the anode (22 cm²) consisted of graphite (MR200, gas tight impregnated, Müller & Rössner GmbH & Co., Troisdorf, Germany), and the cathode (22 cm²) of graphite paper (Cixi Sealing Spacer Material Factory, Ningbo City, China) pressed against a graphite current collector (MR200). The graphite paper was cleaned by submerging it for 15 min in 0.1 M HCl and subsequently 15 min in MilliQ water. The anode and cathode chamber were separated by

4. Acetate enhances biocathode development

a cation exchange membrane (Ralex CMH-PES, Mega A.S., Prague, Czech Republic). For each setup, the anolyte (0.1 M $K_4[Fe(CN)_6]$) was continuously recycled (50 mL/min) over the 4 anodes in series and a 5 L stock vessel. The catholyte (microbial growth medium) was recycled (50 mL/min) over the 3 cathodes and 2 flow cells (30 mL each) in series. One flow cell contained a pH electrode, and the other flow cell contained a liquid/gas outlet, connected via a water lock to a liquid/gas separator with gas sampling port. A dosing pump was connected to the catholyte recycle to control the pH at 7.0 ± 0.1 by dosing 1 M HCl (Liquisys M CPM 253, Endress + Hauser, Naarden, The Netherlands). Liquid samples were taken via a sampling port in the catholyte recycle. The temperature of anolyte and catholyte was controlled at $30\text{ }^{\circ}\text{C}$ ($\pm 1\text{ }^{\circ}\text{C}$).

The catholyte was continuously replenished (0.6 mL/min) with fresh microbial growth medium from stock vessels. The standard medium contained (in demineralized water): 0.68 g/L KH_2PO_4 , 0.87 g/L K_2HPO_4 , 0.74 g/L KCl, 0.58 g/L NaCl, 0.28 g/L NH_4Cl , 0.1 g/L $CaCl_2 \cdot 2H_2O$, 0.01 g/L $MgSO_4 \cdot 7H_2O$ and 0.1 mL/L of a trace element mixture [16]. For setup 1, the standard medium was initially supplemented with 0.17 g/L (2 mM) $NaHCO_3$, and from day 34 with 0.84 g/L (10 mM) $NaHCO_3$. For setup 2, the standard medium was supplemented with 0.136 g/L (1 mM) $NaCH_3COO \cdot 3H_2O$. To prevent microbial growth in the stock vessels, the carbon source and standard medium were stored in different vessels that were continuously flushed with nitrogen (>99.9 %).

At the inlet of each cathode chamber, a capillary with glass frit, filled with 3 M KCl was placed, and connected via a 3 M KCl bridge to an Ag/AgCl 3 M KCl reference electrode (+0.200 V vs NHE. ProSense QiS, Oosterhout, The Netherlands). Each cathode and its reference electrode were connected to a high impedance ($>10^{12}$ Ohm) potential meter (PPM-3C, Bank IC, Pohlheim, Germany) to measure the cathode potential. Each cathode was controlled at a fixed potential (± 0.005 V) by daily adjusting the voltage between anode and cathode using a power supply (EST-150, Delta Elektronika BV, Zierikzee, The Netherlands). Current was measured using a 10 Ohm resistor that was included in the leads of the power supply.

After the effect of carbon source and cathode potential were investigated, the 4

electrochemical cells of setup 2 were replaced by 1 large electrochemical cell (100 cm² electrodes) with flow through cathode to increase the H₂ production rate. The large electrochemical cell was the same as used in a previous study [17], except for that the cathode was made of graphite felt (thickness: 0.25 cm, National Electrical Carbon BV, Hoorn, The Netherlands) and that the membrane was a Ralex cation exchange membrane. The anolyte and catholyte recycle were adjusted to 60 mL/min, and the catholyte was continuously replenished with fresh microbial growth medium (2.6 mL/min), unless stated otherwise.

A data logger (Memograph M, Endress + Hauser, Naarden, The Netherlands) recorded each 5 minutes for each electrochemical cell the current, cathode potential, and cathode pH. Measured potentials in V vs Ag/AgCl were converted to potentials vs the normal hydrogen electrode (NHE). Cathodic overpotentials are expressed with a negative sign and cathodic currents are expressed with a positive sign [18].

4.2.2 Startup and operation

To start up the biocathodes, the catholyte of setup 1 and setup 2 were each inoculated with 10 mL of a mixture of effluents of previously operated biocathodes fed with bicarbonate or acetate. The 4 cathodes in each setup were controlled at -0.5, -0.6, -0.7 and -0.8 V (vs NHE). During the development period, the catholyte was analyzed for acetate, propionate and butyrate using ion chromatography (Metrohm 761 Compact IC equipped with a conductivity detector and a Metrosep Organic Acids 6.1005.200 ion exclusion column). The sulfate concentration was measured using ion chromatography (Metrohm 761 Compact IC equipped with a conductivity detector and a Metrosep A Supp 5 6.1006.520 column) and the bicarbonate concentration was measured using a total organic carbon analyzer (Shimadzu TOC-VCPh).

4.2.3 Polarization

The activities of the biocathodes in setup 1 and 2 were compared through polarization curves. To prevent disruption of the biocathodes during development, polarization curves

4. Acetate enhances biocathode development

were only recorded after their development. The polarization curves were made by measuring each 5 minutes, current, and cathode pH at cathode potentials of -0.50, -0.55, -0.60, -0.65, -0.70, -0.75, -0.80 V. Each cathode potential was applied for 1 h. For each cathode potential, the last 5 measurements were averaged.

4.2.4 H₂ yield tests

A 48 h H₂ yield test of the large biocathode of setup 2 was performed in duplicate (without MgSO₄·7H₂O in the growth medium). During H₂ yield tests, the biocathode was operated in batch mode. The liquid/gas outlet of the catholyte recycle was connected via a 1 L flask to a gas flow meter (Milligascounter®, Ritter, Bochum, Germany). Gas samples were taken after 0, 3, 6, 24, 27, 30 and 48 h via a septum in the 1 L flask. The gas samples were analyzed for H₂ and CH₄ using gas chromatography (Varian CP-4900 microGC, TCD detector, MS5 and PPU columns in parallel). The H₂ production was calculated using the mass balance equation described in [19]. The calculated H₂ production volumes were corrected for water vapor, and converted to volumes at standard temperature and pressure (STP, 273.15 K and 10⁵ Pa).

4.3 Results and Discussion

4.3.1 A more negative cathode potential and acetate were predicted to enhance development

Previous studies [8,10,20] suggested that microorganisms gain energy from electron transfer at the cathode. The energy gain results in biomass growth, which is reflected in an increase of current density in time [8,10]. Through increasing the energy gain, for example through applying a more negative cathode potential or a heterotrophic instead of autotrophic carbon source, the biomass yield and thus biocathode development could be enhanced.

The effect of cathode potential and carbon source on biomass yield was predicted using a thermodynamic analysis. This analysis requires identification of the stoichiometry

of the catabolic and anabolic reaction, and subsequent bioenergetic coupling of the catabolic and anabolic reaction. The methodology described by Kleerebezem and Van Loosdrecht was used for this analysis [13] (calculations in Appendix – Chapter 4).

For the catabolic reaction, it is assumed that microorganisms gain energy from the reduction of protons with electrons donated by the cathode:

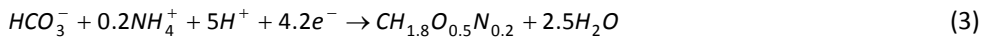


The difference between the Gibbs energy levels of electron donor (i.e. cathode) and acceptor (i.e. protons) represents the maximum catabolic energy available to biocathode microorganisms if a local concentration overpotential [15], which likely exists in the biofilm, is neglected. The catabolic energy is related to the cathode overpotential according:

$$\Delta G_{cat} = -n \cdot F \cdot |\eta_{cat}| \quad (2)$$

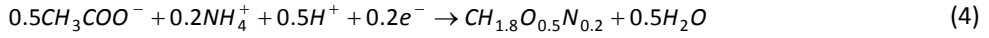
with n the amount of electrons involved in the reaction ($n=1$), F the Faraday constant (96485 C mol^{-1}) and η_{cat} the cathode overpotential (V). For example, a cathode potential of -0.70 V , and an equilibrium potential of -0.41 V ($\text{pH } 7, p_{H_2}=1$) results in an overpotential of -0.29 V . At this overpotential, the catabolic energy is $-28 \text{ kJ mol}^{-1} e^{-}$.

In the anabolic reaction, biomass, which can be represented with a simplified composition $CH_{1.8}O_{0.5}N_{0.2}$, is synthesized. The synthesis of biomass requires a nitrogen and carbon source. The nitrogen source is ammonium. If bicarbonate is the carbon source, the anabolic reaction for the production of biomass can be expressed as:



If acetate is the carbon source, the anabolic reaction for the production of biomass can be expressed as:

4. Acetate enhances biocathode development



Both anabolic reactions require an electron donor to supply the required electrons. Like for the catabolic reaction, we assume the cathode donates the required electrons in the anabolic reaction.

To couple the catabolic reaction to the anabolic reaction and calculate the biomass yield, the Gibbs energy dissipation method was used. This method was chosen, because other yield estimation methods either require biochemical knowledge of biocathode microorganisms ("ATP method"), which is not available for the mixed culture of the biocathode, or assume that the Gibbs energy dissipated during microbial growth (ΔG_{dis}) is independent of carbon source ("TEEM method") [13]. The Gibbs energy dissipation method is based on an energy balance in which the sum of catabolic (ΔG_{cat}), anabolic (ΔG_{an}) and dissipated Gibbs energy (ΔG_{dis}) in the overall metabolism equals zero. The ΔG_{cat} , ΔG_{an} , and ΔG_{dis} were calculated for experimental concentrations (calculations in Appendix - Chapter 4), and the yield of microbial biomass on electrons (Y_{xe}) was estimated [13].

Based on this thermodynamic analysis, the biomass yield is expected to be higher at more negative cathode potentials (i.e. higher overpotentials) (Figure 1). If assumed that the colonization of microorganisms per unit cathode area is initially low and equal at all cathode potentials, a higher biomass yield results faster in a maximum colonization of the cathode surface area. Consequently, this would enhance biocathode development, which is defined here as the time required before a stable current density is reached. Furthermore, the biomass yield is expected to be > 2 times higher for acetate than for bicarbonate as carbon source (Figure 1), and thus biocathode development would be enhanced if acetate instead of bicarbonate is used as carbon source.

4. Acetate enhances biocathode development

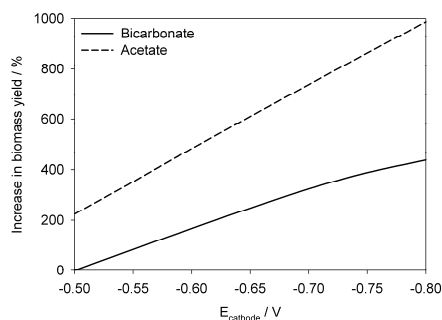


Figure 1 The effect of cathode potential (expressed vs NHE) and carbon source on the relative increase in biomass yield (relative to $E_{\text{cat}} = -0.5 \text{ V}$ and bicarbonate as carbon source) as predicted with a thermodynamic analysis.

4.3.2 More negative cathode potential did not enhance development

Based on thermodynamic analysis, it was expected that a more negative cathode potential would enhance biocathode development. This was experimentally studied through measuring current density development at -0.5, -0.7 and -0.8 V, for biocathodes fed with bicarbonate or acetate as carbon source. The cathodes controlled at -0.6 V are not further discussed because of a malfunctioning, which was apparently caused by poor electrical contact between the graphite paper and the graphite current collector.

A more negative cathode potential (i.e. a higher cathode overpotential) did not enhance development of biocathodes fed with bicarbonate nor with acetate as carbon source (Figure 2). This suggests that a more negative cathode potential hampers a higher biomass yield, for example through an increased chemical HER. An increased chemical HER decreases the local proton concentration and thus decreases the energy gain, and increases the partial H_2 pressure and limits colonization on the cathode surface. Studies with mixed culture bioanodes similarly demonstrated that a more positive anode potential (i.e. a higher anode overpotential) did not necessarily result in a faster bioanode development [21-22].

To establish if there is a direct relation between cathode potential and biomass yield, the amount of biomass attached to the cathode should be measured in real-time. The set-up used in this study however, did not allow for such measurements. Future

4. Acetate enhances biocathode development

studies with an electrochemical quartz crystal microbalance [23] or a fluorescent microscope coupled to electric current measurements [24], could provide insight in the effect of cathode potential on biomass yield.

A more negative cathode potential (i.e. a higher overpotential) did result in higher current densities for biocathodes fed with bicarbonate or acetate as carbon source. Although from electrochemical point of view this seems trivial, from bioelectrochemical point of view this is not. For example, Torres et al. [21] demonstrated that for mixed culture bioanodes, development at a higher anode potential (i.e. a higher overpotential) resulted in a lower current density, and ascribed this to selection of less efficient microorganisms at higher potentials.

The maximum current density (1.0 A m^{-2}) was below that measured in previous studies ($>1.2 \text{ A m}^{-2}$) [10-11], because of the use of graphite paper instead of graphite felt as cathode. The low specific surface area of graphite paper compared to graphite felt results in a lower colonization per m^2 projected cathode, and consequently, a lower current density [25]. H_2 production by the biocathodes was confirmed through the presence of H_2 (not quantified) in the headspace of both setups. No CH_4 was detected in the headspace of both setups.

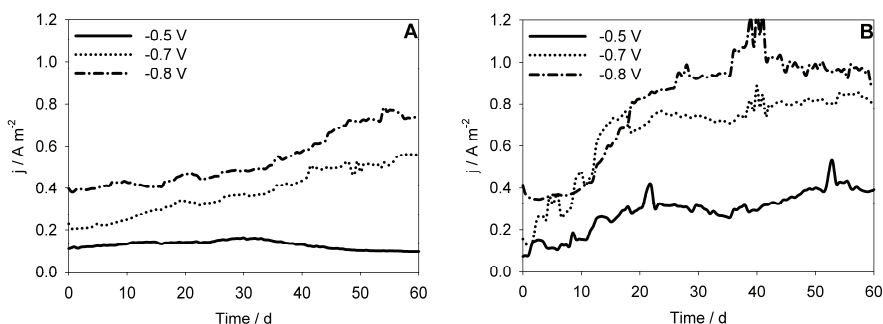


Figure 2 Development of biocathodes at 3 different potentials (vs NHE), with A) bicarbonate, 2 mM for days 0-34 and 10 mM for days 34-63, and B) 1 mM acetate as carbon source. The increase in current density around day 40 for biocathodes fed with acetate was caused by a drop from pH 7 to pH 6.5.

4.3.3 Acetate instead of bicarbonate as carbon source did enhance development

Based on thermodynamic analysis, it was expected that acetate instead of bicarbonate as carbon source enhances biocathode development. This was experimentally investigated through feeding the biocathodes of setup 1 with 2 mM bicarbonate, and of setup 2 with 1 mM acetate. The biocathodes fed with acetate developed >2 times faster, and generated higher currents than the biocathodes fed with bicarbonate (Figure 2). After 30 days at -0.8 V, the biocathode fed with acetate had stabilized at 1.0 A m^{-2} , whereas the biocathode fed with bicarbonate reached 0.5 A m^{-2} and its current density was still increasing. An increase from 2 mM to 10 mM bicarbonate from day 34 did slightly increase the current density rise in time of the biocathode controlled at -0.8 V. After 60 days at -0.8 V, the current density of the biocathode fed with acetate was still 1.0 A m^{-2} , whereas that of the biocathode fed with bicarbonate had further increased to 0.8 A m^{-2} . Thus, the experimental data support the predicted enhanced startup with acetate instead of bicarbonate as carbon source.

4.3.4 No observable relation between potential during development and final catalytic activity

After 62 days, polarization curves were made for the 6 biocathodes to compare their catalytic activity (Figure 3). At -0.8 V in the polarization curve, biocathodes fed with acetate reached 1.0 to 1.4 A m^{-2} , whereas biocathodes fed with bicarbonate reached 0.9 to 1.1 A m^{-2} . The catalytic activity of the biocathodes was substantially higher than measured previously (0.4 A m^{-2}) for an uninoculated control cathode in the same type of electrochemical cell [8]. The higher catalytic activity of biocathodes fed with acetate compared to biocathodes fed with bicarbonate is consistent with the development curves (Figure 2). The order in catalytic activity (e.g. for acetate -0.8<-0.5<-0.7 V) was inconsistent with the order in current density during biocathode development (e.g. for acetate -0.5<-0.7<-0.8 V). Hence, there was no observable relation between the potential at which the biocathodes were developed, and the final catalytic activity, which suggests that the microbial pathways for HER catalysis were not dependent from cathode potential.

4. Acetate enhances biocathode development

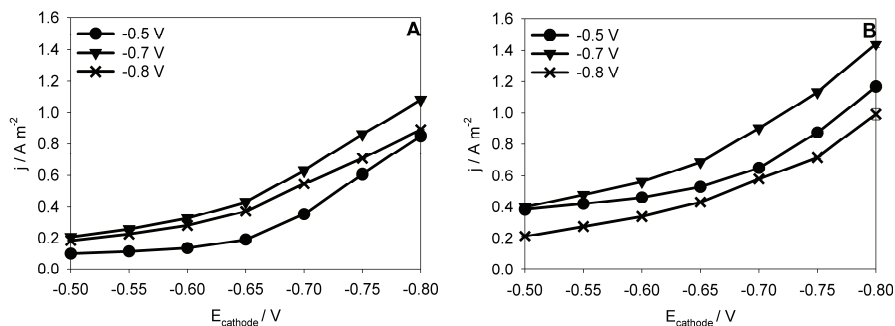


Figure 3 Polarization curves of biocathodes with A) bicarbonate, and B) acetate as carbon source after 62 days of operation. Legends indicate cathode potentials (vs NHE) during biocathode development. All standard deviations were below 0.3 A m^{-2} .

4.3.5 Enhanced H_2 production for biocathode with flow through configuration

The biocathode fed with 1 mM acetate and controlled at -0.7 V demonstrated the fastest development and highest catalytic activity. These conditions were chosen to develop a biocathode in a larger electrochemical cell with graphite felt cathode (100 cm^2 instead of 22 cm^2 projected cathode surface). The catholyte was forced to flow through the graphite felt cathode (“flow through biocathode”) to improve mass transfer and to make maximal use of the cathode surface area [14]. A cathode that was fed with standard medium without added carbon source served as control. Each time, the cathode was operated for 28 days. In 28 days, the biocathode had increased from 0.2 A m^{-2} to 2.7 A m^{-2} , whereas the control cathode had increased from 0.4 A m^{-2} to 0.8 A m^{-2} (Figure 4). The increase in current density of the control cathode was likely caused by growth of electrochemically active microorganisms, because the control cathode was operated directly after the biocathode in the same electrochemical cell without sterilization of the cathode chamber. The current density of the flow through biocathode was more than 3 times higher than that of the parallel flow biocathodes (0.8 A m^{-2} at -0.7 V, Figure 2), because of the larger surface area and improved mass transport of the flow through biocathode.

To measure H_2 production by the biocathode, 48h-yield tests were performed. To avoid growth of SO_4^{2-} reducing bacteria that consume H_2 , a biocathode was developed with 1 mM acetate, but without $\text{MgSO}_4 \cdot 7\text{H}_2\text{O}$ in the standard medium (Biocathode 2

Figure 4). The yield tests were performed in duplicate 47 days after inoculation, and the biocathode was operated in batch mode during the tests. The average cathodic recovery of H_2 on electrons of both yield tests was 50 % (standard deviation: ± 2.9 %), which is comparable to that of a biocathode in an electrochemical cell of a previous study [10]. A cathodic H_2 recovery of less than 100 % is mainly caused by diffusional losses of H_2 through membrane [10-11] and tubing [1]. It is unlikely that the cathodic H_2 recovery was affected by formation of reduced products other than H_2 , such as CH_4 [26] or acetate [27]. CH_4 was not detected in the produced gas. Furthermore, acetate was not detected in the catholyte at the end of the yield test.

The average H_2 production rate of the biocathode was $2.2 \text{ m}^3 \text{ H}_2 \text{ m}^{-3} \text{ reactor d}^{-1}$ (at STP), which is 7 times higher than measured in a previous study of a graphite felt biocathode in an electrochemical cell ($0.32 \text{ m}^3 \text{ m}^{-3} \text{ reactor d}^{-1}$) [10]. The higher H_2 production rate was largely caused by the high cathode surface to cathode volume ratio ($500 \text{ m}^2 \text{ m}^{-3}$ vs $100 \text{ m}^2 \text{ m}^{-3}$ in [10]), but was also caused by the flow-through configuration instead of the parallel flow configuration [10].

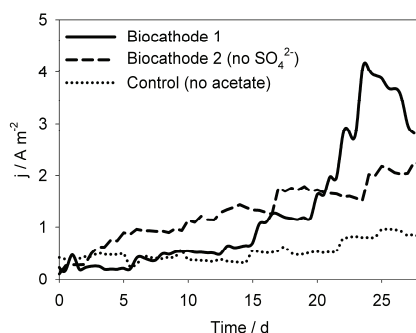


Figure 4 Development of flow-through biocathodes (100 cm^2) at -0.7 V with 1 mM acetate as carbon source in the growth medium. The biocathode was developed 2 times. The 2nd time, the standard medium did not contain SO_4^{2-} . The control cathode was fed with standard medium without any carbon source.

For both yield tests, the current decreased from 2.2 A m^{-2} at the start of the yield test, to 1.3 A m^{-2} at the end of the yield test. After the yield test, the biocathode was operated in continuous mode again, which restored the initial current density (2.2 A m^{-2}). The

4. Acetate enhances biocathode development

decrease in current density during batch operation may have been caused by a lack of trace nutrients, but this is still unclear.

4.4 Conclusions

Through feeding the H₂-producing microbial biocathode with medium containing a low concentration of acetate (1 mM), the development time of the biocathode could be decreased. Application of a more negative cathode potential however, did not decrease the development time of the microbial biocathode. Furthermore, a flow-through biocathode instead of a parallel flow biocathode increased the H₂ production rate. A decreased development time and an increased H₂ production rate are relevant for making the microbial biocathode a viable alternative for metal catalyzed HER cathodes.

4.5 Acknowledgements

This work was performed in the TTIW-cooperation framework of Wetsus, centre of excellence for sustainable water technology (www.wetsus.nl). Wetsus is funded by the Dutch Ministry of Economic Affairs, the European Union Regional Development Fund, the Province of Fryslân, the City of Leeuwarden and the EZ/Kompas program of the “Samenwerkingsverband Noord-Nederland”. The authors like to thank Annemiek ter Heijne for critically reading the manuscript, Ágnes Janoska for performing part of the experiments, and the participants of the Wetsus research theme “Bio-energy” for the fruitful discussions and their financial support.

4.6 References

- [1] Logan B E, Call D, Cheng S, Hamelers H V M, Sleutels T H J A, Jeremiasse A W, et al. Microbial electrolysis cells for high yield hydrogen gas production from organic matter. *Environ Sci Technol* 2008; 42: 8630-40
- [2] Hu H, Fan Y, Liu H. Hydrogen production in single-chamber tubular microbial electrolysis cells using non-precious-metal catalysts. *Int J Hydrogen Energy* 2009; 34: 8535-42
- [3] Selembo P A, Merril M D, Logan B E. Hydrogen production with nickel powder cathode catalysts in microbial electrolysis cells. *Int J Hydrogen Energy* 2009; 35: 428-37

- [4] Selembo P A, Merrill M D, Logan B E. The use of stainless steel and nickel alloys as low-cost cathodes in microbial electrolysis cells. *J Power Sources* 2009; 190: 271-8
- [5] Rosenbaum M, Aulenta F, Villano M, Angenent L T. Cathodes as electron donors for microbial metabolism: Which extracellular electron transfer mechanisms are involved? *Bioresour Technol* 2011; 102: 324-33
- [6] He Z, Angenent L T. Application of bacterial biocathodes in microbial fuel cells. *Electroanalysis* 2006; 18: 2009-15
- [7] Vetter K J. *Electrochemical kinetics: theoretical and experimental aspects*. ed. New York: Academic press; 1967.
- [8] Geelhoed J S, Stams A J M. Electricity-Assisted Biological Hydrogen Production from Acetate by *Geobacter sulfurreducens*. *Environ Sci Technol* 2010; 45: 815-20
- [9] Villano M, De Bonis L, Rossetti S, Aulenta F, Majone M. Bioelectrochemical hydrogen production with hydrogenophilic dechlorinating bacteria as electrocatalytic agents. *Bioresour Technol* 2011; 102: 3193-9
- [10] Rozendal R A, Jeremiasse A W, Hamelers H V M, Buisman C J N. Hydrogen production with a microbial biocathode. *Environ Sci Technol* 2008; 42: 629-34
- [11] Jeremiasse A W, Hamelers H V M, Buisman C J N. Microbial electrolysis cell with a microbial biocathode. *Bioelectrochemistry* 2010; 78: 39-43
- [12] Wei J, Liang P, Cao X, Huang X. A New Insight into Potential Regulation on Growth and Power Generation of *Geobacter sulfurreducens* in Microbial Fuel Cells Based on Energy Viewpoint. *Environ Sci Technol* 2010; 44: 3187-91
- [13] Kleerebezem R, Van Loosdrecht M C M. A Generalized Method for Thermodynamic State Analysis of Environmental Systems. *Crit Rev Env Sci Technol* 2010; 40: 1 - 54
- [14] Sleutels T H J A, Lodder R, Hamelers H V M, Buisman C J N. Improved performance of porous bio-anodes in microbial electrolysis cells by enhancing mass and charge transport. *Int J Hydrogen Energy* 2009; 34: 9655-61
- [15] Jeremiasse A W, Hamelers H V M, Kleijn J M, Buisman C J N. Use of biocompatible buffers to reduce the concentration overpotential for hydrogen evolution. *Environ Sci Technol* 2009; 43: 6882-7
- [16] Zehnder A J B, Huser B A, Brock T D, Wuhrmann K. Characterization of an acetate-decarboxylating, non-hydrogen-oxidizing methane bacterium. *Arch Microbiol* 1980; 124: 1-11
- [17] Jeremiasse A W, Hamelers H V M, Saakes M, Buisman C J N. Ni foam cathode enables high volumetric H₂ production in a microbial electrolysis cell. *Int J Hydrogen Energy* 2010; 35: 12716-23
- [18] Bard A J, Faulkner L R. *Electrochemical methods: fundamentals and applications*. 2nd ed. New York: John Wiley & Sons; 2001.
- [19] Rozendal R A, Hamelers H V M, Molenkamp R J, Buisman C J N. Performance of single chamber biocatalyzed electrolysis with different types of ion exchange membranes. *Water Res* 2007; 41: 1984-94
- [20] Strycharz S M, Glaven R H, Coppi M V, Gannon S M, Perpetua L A, Liu A, et al. Gene expression and deletion analysis of mechanisms for electron transfer from electrodes to *Geobacter sulfurreducens*. *Bioelectrochem* 2011; 80: 142-50

4. Acetate enhances biocathode development

- [21] Torres C I, Krajmalnik-Brown R, Parameswaran P, Marcus A K, Wanger G, Gorby Y A, et al. Selecting Anode-Respiring Bacteria Based on Anode Potential: Phylogenetic, Electrochemical, and Microscopic Characterization. *Environ Sci Technol* 2009; 43: 9519-24
- [22] Aelterman P, Freguia S, Keller J, Verstraete W, Rabaey K. The anode potential regulates bacterial activity in microbial fuel cells. *Appl Microbiol Biotechnol* 2008; 78: 409-18
- [23] Kleijn J M, Lhuillier Q, Jeremiasse A W. Monitoring the development of a microbial electrolysis cell bioanode using an electrochemical quartz crystal microbalance. *Bioelectrochem* 2010; 79: 272-5
- [24] McLean J S, Wanger G, Gorby Y A, Wainstein M, McQuaid J, Ishii S, et al. Quantification of electron transfer rates to a solid phase electron acceptor through the stages of biofilm formation from single cells to multicellular communities. *Environ Sci Technol* 2010; 44: 2721-7
- [25] Logan B E, Materials for BES, in: Rabaey, K., Angenent, L., Schroder, U., Keller, J. (Eds.), *Bioelectrochemical systems: from extracellular electron transfer to biotechnological application*. IWA Publishing, London, 2010, pp. 185-204.
- [26] Cheng S, Xing D, Call D F, Logan B E. Direct biological conversion of electrical current into methane by electromethanogenesis. *Environ Sci Technol* 2009; 43: 3953-8
- [27] Nevin K P, Woodard T L, Franks A E, Summers Z M, Lovley D R. Microbial electrosynthesis: Feeding microbes electricity to convert carbon dioxide and water to multicarbon extracellular organic compounds. *mBio* 2010; 1: 1-4

5. Ni foam cathode enables high volumetric H₂ production in a microbial electrolysis cell

Abstract

Valuable, “green” H₂ can be produced with a microbial electrolysis cell (MEC). To achieve a high volumetric production rate of high purity H₂, a continuous flow MEC with an anion exchange membrane, a flow through bioanode and a flow through Ni foam cathode was constructed. At an electrical energy input of 2.6 kWh m⁻³ H₂ (applied cell voltage: 1.00 V), this MEC was able to produce over 50 m³ H₂ m⁻³ MEC d⁻¹ (22.8 ± 0.1 A m⁻²). The MEC had a low cathode overpotential compared to an MEC with Pt-based cathode, because of the high specific surface area of Ni foam (128 m² m⁻² projected area). The MEC performance however, decreased during 32 days of operation due to an increase in anode and cathode overpotentials. Scaling likely caused the increase in anode overpotential, but it remained unclear what caused the increase in cathode overpotential.

This chapter has been published as:

Jeremiasse A W, Hamelers H V M, Saakes M, Buisman C J N. Ni foam cathode enables high volumetric H₂ production in a microbial electrolysis cell. *Int J Hydrogen Energy* 2010; 35: 12716-23

5.1 Introduction

Organic substrates can be converted into valuable, “green” H_2 through microbial electrolysis [1-3]. In a microbial electrolysis cell (MEC), electrochemically active microorganisms oxidize substrate and transfer the liberated electrons to the anode. Subsequently, the electrons are transported through an electrical circuit containing a power source, to the cathode. To compensate for the negative electrical current outside the cell, an ionic current flows inside the cell. At the cathode, the hydrogen evolution reaction (HER) proceeds. The HER does not proceed spontaneously under typical MEC conditions, but requires an applied voltage that is supplied by the power source [2]. Thermodynamically (Nernst equation), an applied voltage of 0.14 V is required under standard biological conditions. However, a higher applied voltage (e.g. 0.5-1.0 V) is required under operating conditions because of potential losses in the MEC [2].

To achieve a high volumetric H_2 production rate (i.e. $m^3 H_2 m^{-3} MEC d^{-1}$) at low electrical energy input (i.e. $kWh m^{-3} H_2$) the potential losses need to be minimized. The largest potential losses are caused by the presence of a membrane, anode overpotential, and cathode overpotential [4]. The membrane can be excluded [5], however, the H_2 gas produced by these so-called membrane-less MECs is not pure. The anode overpotential can be decreased by improvement of charge and mass transport of the anode, for example by using a flow through anode [6]. The cathode overpotential can be decreased by using a Pt-based cathode (to decrease the activation overpotential) and by improving mass transport (to decrease the concentration overpotential) [7]. However, the high price of Pt-based cathodes increases the capital costs of an MEC. Therefore, development of a non-noble metal cathode is highly desired.

Most investigated non-noble metal cathodes for MECs are based on Ni [8-13]. Ni has a lower HER overpotential and is more stable under alkaline conditions than most other non-noble metals, such as Fe [14-18]. Membrane-less MECs with Ni-based cathodes [8-13] reached current densities and volumetric H_2 production rates comparable to MECs with Pt. To increase the volumetric H_2 production rate, the HER overpotential of Ni-based cathodes must be decreased. To decrease the HER overpotential, the specific surface area

of the Ni-based catalyst can be increased. An increased specific surface area results in a decreased, true surface current density, and thus a lower activation overpotential [18]. Furthermore, a decreased, true surface current density results in a lower concentration overpotential [7].

The aim of our study was to achieve a high volumetric production rate of high purity H_2 , at an electrical energy input that is still below the thermodynamic input of water electrolysis. Therefore, we designed a continuous flow MEC with an anion exchange membrane, a flow through bioanode, and a flow through Ni foam cathode with high specific surface area. We chose Ni foam as cathode, because (i) Ni foam is a good HER catalyst under alkaline conditions [19-20], but has not been studied yet in an MEC, (ii) Ni foam also serves as current collector with low electrical resistivity compared to graphite or titanium [18], (iii) Ni foam is an already existing product that is being produced on large scale, for instance for the NiMH battery industry, and (iv) Ni has a low price (0.02 USD/g, metalprices.com) compared to previously used noble metal catalysts (e.g Pt: 50 USD/g, metalprices.com). To achieve a high volumetric H_2 production rate, the MEC was operated at an applied cell voltage of 1.00 V. This applied cell voltage is still below the thermodynamic input of 1.23 V for water electrolysis. Furthermore, the MEC was operated without pH control for a long period (32 days), which allowed us to observe changes in overpotentials. These changes typically occur during long term operation, as has been shown for water electrolyzers [21] and continuous flow MECs [22].

5.2 Materials and Methods

5.2.1 Microbial electrolysis cell and setup

The MEC consisted of 2 identical Plexiglas plates of 21 x 21 cm (Figure 1 A). One plate contained the anode chamber and the other the cathode chamber. Each chamber was 10 x 10 x 0.20 cm, had 9 channels at inlet and outlet over which the flow was distributed, and was sealed by a Viton[®] O-ring. Anode and cathode chamber were separated by an anion exchange membrane (AMX –Neosepta, Tokuyama Corp., Japan). The anode consisted of

5. MEC with Ni foam cathode

graphite felt of 10 x 10 x 0.25 cm (National Electrical Carbon BV, Hoorn, The Netherlands). The graphite felt was compressed in the anode chamber, where it was in contact with 4 Pt/Ir wires (Pt/Ir 80/20, 0.025 cm diameter, Advent Research Materials, Oxford, UK) that served as current collectors. The cathode consisted of Ni foam (10 x 10 x 0.2 cm, 1360 kg m⁻³, Metafoam, Brossard, Canada). The specific surface area of Ni foam was determined with nitrogen adsorption (Micromeritics Tristar 3000) using the 5-point BET method [23], and was found to be 128 m² m⁻² projected area (47.2 ± 0.9 m² kg⁻¹). The Ni foam was welded to a Ni current collector. To optimally use the electrode area, anolyte and catholyte were forced to flow through the electrodes.

The anolyte (microbial nutrient medium) was continuously recycled (120 mL min⁻¹) over the anode chamber and a flow cell (0.2 L) containing a pH electrode (Liquisys M CPM 253, Endress + Hauser, Naarden, The Netherlands) and a liquid outlet (Figure 1 B). Liquid samples were taken via a sample port in the anolyte recycle. The anolyte was continuously replenished (2.6 mL min⁻¹) with fresh microbial nutrient medium. The microbial nutrient medium contained (in demineralized water): 2.72 g/L NaCH₃COO·3H₂O, 0.68 g/L KH₂PO₄, 0.87 g/L K₂HPO₄, 0.74 g/L KCl, 0.58 g/L NaCl, 0.28 g/L NH₄Cl, 0.1 g/L CaCl₂·2H₂O, 0.01 g/L MgSO₄·7H₂O and 0.1 mL/L of a trace element mixture [24]. NaCH₃COO·3H₂O was stored in a different stock vessel than the other medium components to prevent its consumption prior to entering the anolyte recycle. The stock vessels were continuously flushed with nitrogen (>99.9 %). The catholyte consisted of 0.1 M KCl, which was continuously recycled (120 mL min⁻¹) over the cathode chamber and a flow cell containing a pH electrode and a gas outlet. The gas outlet was connected via a 1 L flask to a gas flow meter (Milligascounter®, Ritter, Bochum, Germany). The flask was filled with 0.2 L demineralized water and had a headspace of 0.8 L that served as buffer volume. Gas samples were taken via a septum in the flask. Liquid samples were taken via a sample port in the catholyte recycle. The temperature of anolyte and catholyte was controlled at 30 °C (±1 °C).

At the inlet of each chamber, a capillary filled with 3 M KCl was placed, and connected via a 3 M KCl bridge to an Ag/AgCl 3 M KCl reference electrode (+0.200 V vs NHE. ProSense QiS, Oosterhout, The Netherlands). A power supply (ES 030-5, Delta

Elektronika BV, Zierikzee, The Netherlands) was used to apply a voltage between anode and cathode. The current was measured using the monitor output of the power supply. The anode, cathode and their reference electrodes were connected to a high impedance ($>10^{12}$ Ohm) potential meter (PPM-3C, Bank IC, Pohlheim, Germany) to measure anode and cathode potential. A data logger (Memograph M, Endress + Hauser, Naarden, The Netherlands) recorded applied voltage, current, anode potential, cathode potential, anode pH and cathode pH every 5 minutes for all experiments. Measured potentials in V vs. Ag/AgCl were converted to potentials versus the normal hydrogen electrode (NHE). Cathodic overpotentials are expressed with a negative sign, unless stated otherwise.

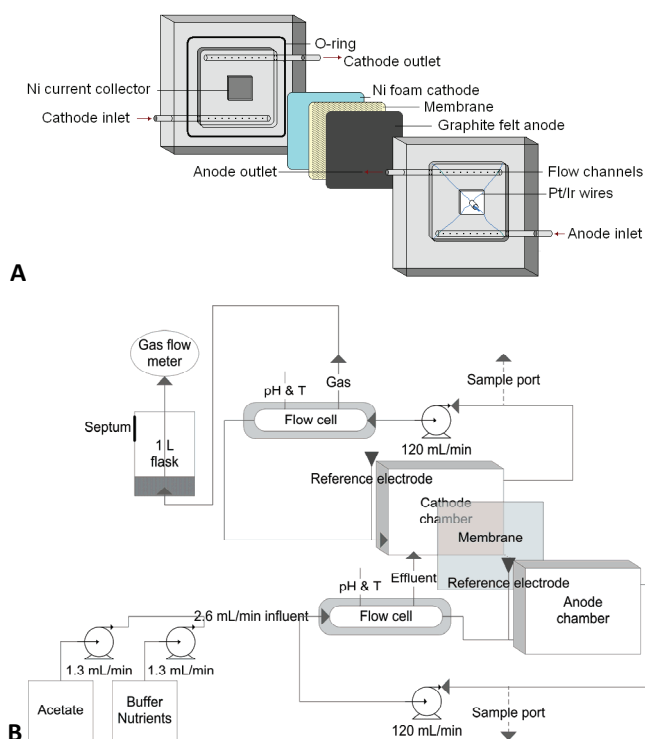


Figure 1 A: MEC used in this study, B: Experimental setup used in this study

5. MEC with Ni foam cathode

5.2.2 Start-up and operation

The MEC was started up at an applied cell voltage of 0.5 V. During startup, the cathode potential is still relatively high. Therefore, to prevent oxidation of the Ni foam cathode, the MEC was started up with a cathode of sintered Ti (10 x 10 x 0.2 cm) with 5 g m⁻² projected area Pt coating (Magnet Special Anodes BV, Schiedam, The Netherlands). The anode chamber was inoculated with 10 mL effluent of a previous MEC [6]. After a startup period of 3 weeks at an applied cell voltage of 0.5 V, the cathode potential had decreased to -0.91 V (pH 12.7), and the sintered Ti-Pt cathode was replaced by the Ni foam cathode. The MEC with Ni foam cathode was operated for 32 days

5.2.3 Polarization curves for MEC with Ni foam

The polarization curve of the MEC with Ni foam cathode was measured directly after the Ti-Pt cathode was replaced by the Ni foam cathode (days 1-14). Each 5 minutes, current, anode potential, cathode potential, anode pH and cathode pH were measured at applied cell voltages of 0.50, 0.53, 0.62, 0.70, 0.80, 0.85, 0.90, 0.95 and 1.00 V. Each cell voltage was applied for at least 24 h. For each applied cell voltage, the last 10 measurements were averaged. Average current densities are reported with \pm standard deviation. During the polarization, the H₂ concentration of the cathode was measured using gas chromatography (Varian CP-4900 microGC, TCD detector, MS5 and PPU columns in parallel). The acetate concentration of the anolyte was measured using ion chromatography (Metrohm 761 Compact IC equipped with a conductivity detector and a Metrosep Organic Acids 6.1005.200 ion exclusion column). The bicarbonate concentration of the anolyte was measured using a total organic carbon analyzer (Shimadzu TOC-VCPH).

5.2.4 Long term MEC performance

During days 14-32 the MEC was operated at an applied cell voltage of 1.00 V. The acetate concentration of the anolyte was measured each 4 days. The bicarbonate concentration was not measured during days 12-32. Therefore, a concentration of 5 mM bicarbonate was assumed for calculation of the anode overpotential in this period. From day 25, two

subsequent 48 h H₂ yield tests were performed (duplicates) for the MEC with Ni foam cathode at an applied cell voltage of 1.00 V. At 0, 4, 6, 24, 28, 30 and 48 h, the H₂ concentration in the gas was measured. The produced gas volume was measured with the gas flow meter. Measured gas volumes were corrected for water vapor, and converted to volumes at standard temperature and pressure (STP, 273.15 K and 10⁵ Pa). At the start and end of the yield tests, the concentration of Ni was measured in the catholyte with inductively coupled plasma-optical emission spectroscopy (ICP-OES, Perkin Elmer Optima 3000XL). On day 32, the concentration of phosphate in the catholyte was measured using ion chromatography (Metrohm 761 Compact IC equipped with a conductivity detector and a Metrosep A Supp 5 6.1006.520 column), and the concentration of cations (Mg²⁺, Ca²⁺) in the catholyte was measured with ICP-OES.

5.2.5 Calculations

The current density, expressed in A m⁻², was based on the projected electrode area (100·10⁻⁴ m², projected anode and cathode surface area were equal). The current density, expressed in A m⁻³ MEC, was based on the total MEC volume (40·10⁻⁶ m³).

Anode and cathode overpotential (η) were calculated with:

$$\eta = E_{meas} - E_{eq} \quad (1)$$

where E_{meas} is the measured anode or cathode potential (V vs NHE) and E_{eq} is the equilibrium anode or cathode potential (V vs NHE). The equilibrium cathode potential was calculated using the Nernst equation:

$$E_{eq,cath} = E_{cat}^0 - \frac{RT}{nF} \ln \left(\frac{p_{H_2}}{[H^+]^2} \right) \quad (2)$$

where E_{cat}^0 is the equilibrium cathode potential at standard conditions ($T = 298$ K, 10^5 Pa,

5. MEC with Ni foam cathode

and $[H^+] = 1 \text{ M}$; $E_{\text{cat}}^0 = 0.00 \text{ V}$ by definition), R (8.314 J/K mol) is the ideal gas law constant, T is the absolute temperature, n is the amount of electrons involved in the reaction ($n = 2$ for the HER), and F is the Faraday constant ($96485 \text{ C mol}^{-1} \text{ e}^-$). At unit partial H_2 pressure and 30°C (303 K), this reduces to:

$$E_{\text{eq,cat}} = -0.060 pH \quad (3)$$

The equilibrium anode potential was calculated with:

$$E_{\text{eq,an}} = E_{\text{an}}^0 - \frac{RT}{nF} \ln \left(\frac{[CH_3COO^-]}{[HCO_3^-]^2 [H^+]^8} \right) \quad (4)$$

where E_{an}^0 is the equilibrium anode potential at standard conditions ($E^0 = 0.187 \text{ V}$), and $n = 8$.

The electrical energy input in $\text{kWh m}^{-3} H_2$ at STP was calculated with:

$$E_{\text{electricity}} = 2F \cdot \frac{1}{3.6 \cdot 10^6} E_{\text{app}} \cdot \frac{P}{RT} \frac{1}{r_{\text{cat}}} \quad (5)$$

where 2 is the number of electrons per H_2 , $1/3.6 \cdot 10^6$ is a factor to convert Joules to kWh, E_{app} is the applied cell voltage (V), P is the pressure (10^5 Pa), and r_{cat} is the cathodic H_2 recovery as described in equation 6 of Sleutels et al. [4]. T is 273.15 K at STP. The electrical energy input was subdivided in (i) equilibrium input, (ii) anode input, (iii) cathode input, and (iv) membrane and electrolyte input. These inputs were calculated by substituting E_{app} in equation 5 by (i) the equilibrium voltage that was calculated as described in [4], (ii) the anode overpotential, (iii) the cathode overpotential, and (iv) the voltage that remains after subtracting (i), (ii) and (iii) from E_{app} .

5.3 Results and Discussion

5.3.1 MEC with Ni foam cathode enables high current densities and H₂ production rates

An MEC was constructed with anion exchange membrane, flow through bioanode, and flow through Ni foam cathode. The MEC was operated in continuous mode without pH control. Current production of this MEC was investigated for applied cell voltages between 0.50 and 1.00 V (Figure 2 A). At all applied cell voltages, the catholyte pH was above 12. At the maximum applied cell voltage (1.00 V), the MEC produced $22.8 \pm 0.1 \text{ A m}^{-2}$ ($5704 \pm 32 \text{ A m}^{-3} \text{ MEC}$). This current density is high compared to the current density reported by Sleutels et al. (16.4 A m^{-2}) [6].

Based on the measured current densities, the volumetric H₂ production rates can be calculated using equation 6 of [4]. A cathodic H₂ recovery of 90 % was assumed, which seems reasonable considering that the H₂ concentration in the headspace was always above 95 % (remaining fraction was N₂), and taking into account H₂ losses through membrane and tubing [3]. The calculated, volumetric H₂ production rate was plotted against the applied cell voltage (Figure 2 A). The MEC reached volumetric H₂ production rates over $50 \text{ m}^3 \text{ H}_2 \text{ m}^{-3} \text{ MEC d}^{-1}$ (at STP) at an applied cell voltage of 1.00 V.

The high volumetric H₂ production rate was the result of a combination of MEC design (high ratio of electrode surface area to MEC volume), flow through bioanode and flow through Ni foam cathode. An increase in MEC current density by the use of a flow through instead of a flow past bioanode was demonstrated before by Sleutels et al. Their MEC however, consisted of a Ti-Pt mesh cathode ($50 \text{ g m}^{-2} \text{ Pt}$) [6]. Here, a Ni foam cathode was used instead of a Pt-based cathode. The Ni foam cathode had a low overpotential compared to the Ti-Pt mesh cathode. At a current density of 5.3 A m^{-2} , the overpotential of the Ni foam cathode was -0.11 V (Figure 2 B), whereas that of the Ti-Pt mesh cathode was -0.17 V [4].

The difference in overpotential was mainly caused by a difference in activation overpotential, because the catholytes of the Ni foam cathode and the Ti-Pt mesh cathode

5. MEC with Ni foam cathode

were both pH 12 or higher. At such high pH, transport of hydroxide from cathode surface to bulk is not limiting, and therefore there is a negligible concentration overpotential [7,25]. From literature however, it is known that Ni has a higher activation overpotential than Pt for the HER [14-16]. Therefore, the low overpotential of Ni foam compared to Ti-Pt mesh can be attributed to the high specific surface area of Ni foam ($128 \text{ m}^2 \text{ m}^{-2}$ projected area) compared to Ti-Pt mesh ($1.7 \text{ m}^2 \text{ m}^{-2}$ projected area). The high surface area resulted in a decreased, true surface current density, and thus lower activation overpotential. The measured overpotential for Ni foam (-0.14 V at 10.5 A m^{-2}) was similar to the overpotential of sintered Ni with high specific surface area ($200 \text{ m}^2 \text{ m}^{-2}$ projected area) measured by Rausch and Wendt (-0.16 V at 10 A m^{-2}) [20].

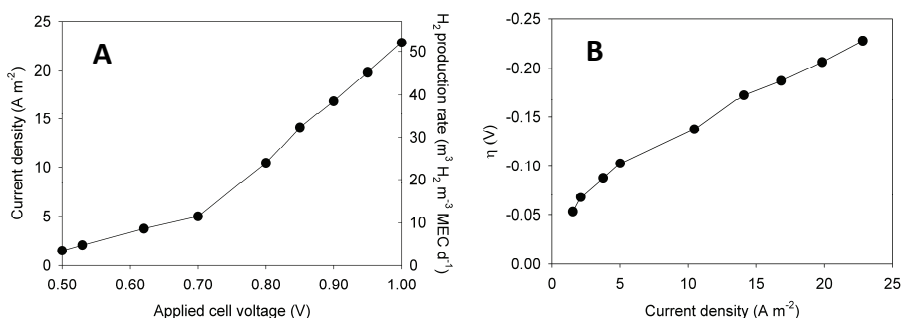


Figure 2 A: Current production (per m^2 projected electrode area) and volumetric H_2 production rate for MEC with Ni foam cathode. B: Overpotential (η) of the Ni foam cathode. The linear flow speed of the catholyte was 1 cm/s . Each data point was the average of 10 measurements (all standard deviations were below 0.15 A m^{-2}).

5.3.2 Largest part of electrical energy input is consumed by the membrane

To achieve a volumetric H_2 production rate of more than $50 \text{ m}^3 \text{ H}_2 \text{ m}^{-3} \text{ MEC d}^{-1}$, an electrical energy input of $2.6 \text{ kWh m}^{-3} \text{ H}_2$ was required (Figure 3). This is high compared to the $0.28 \text{ kWh m}^{-3} \text{ H}_2$ thermodynamically required for the complete conversion of acetate into H_2 , but still below the thermodynamic minimum of $2.9 \text{ kWh m}^{-3} \text{ H}_2$ for water electrolysis.

To identify which of the MEC components consumed most of the electrical energy input at different H_2 production rates, the electrical energy input was subdivided in equilibrium input, anode input, cathode input, and membrane and electrolyte input (Figure 3). The electrical energy consumption by the anode was low (below $0.3 \text{ kWh m}^{-3} H_2$), because of the use of a flow through anode. The consumption of the cathode was higher than that of the anode (up to $0.6 \text{ kWh m}^{-3} H_2$), but still much lower than that of the membrane and electrolyte (up to 1.5 kWh m^{-3}). For all H_2 production rates, the consumption by the membrane and electrolyte was highest. The consumption of the membrane and electrolyte includes the consumption due to the pH gradient that develops over the membrane, due to transport of ions through the membrane and due to transport of ions through the electrolytes (anolyte and catholyte) [4]. The consumption due to transport of ions through the electrolytes was not separately quantified, because the conductivity of anolyte and catholyte were not measured. Given the average distance (2 mm) between anode and cathode, and assuming an average electrolyte conductivity of 0.5 S m^{-1} , the consumption of the electrolyte was estimated to be maximally $0.24 \text{ kWh m}^{-3} H_2$ (at 22.8 A m^{-2}).

It is clear that an MEC with membrane consumes a large amount of extra electrical energy per m^3 produced H_2 compared to an MEC without membrane [26]. However, an MEC with membrane is able to continuously produce high purity H_2 gas, in contrast to an MEC without membrane [27]. The headspace contained more than 95 % H_2 . The remaining fraction was N_2 , which originated from the air that was initially present in the cathode headspace and is expected to be flushed out on the long term. Negligible concentrations of CH_4 (<0.3%) were found in the headspace. Such low and constant concentrations of CH_4 may have been caused by diffusion of CH_4 from anode to cathode chamber [28]. The production of high purity H_2 gas is advantageous if the H_2 is to be used for applications that require high purity H_2 gas, such as electricity production with a proton exchange membrane fuel cell [29].

5. MEC with Ni foam cathode

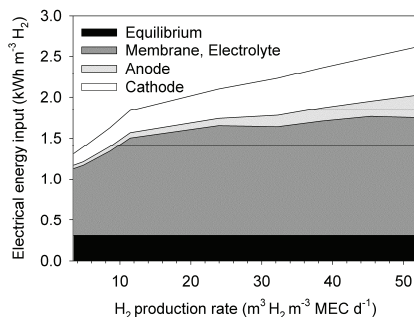


Figure 3 Subdivision of the electrical energy input (expressed as kWh m⁻³ H₂ at STP) over equilibrium input, membrane and electrolyte input, anode and cathode input, for different H₂ production rates. The H₂ production rates were based on the measured current density, and a cathodic H₂ recovery of 90%.

5.3.3 H₂ production decreased during long term operation at 1.00 V

During days 14-32 the current decreased from 22.8 (5704 A m⁻³ MEC) to 13.8 A m⁻² (3438 A m⁻³ MEC) (Figure 4). A decrease in current density implies a decrease in volumetric H₂ production rate. This was confirmed during two subsequent 48 h H₂ yield tests (see Appendix – Chapter 5). The H₂ yield tests were performed from day 25. The average current of the MEC was 15.4 ± 1.2 A m⁻² (3850 ± 290 A m⁻³ MEC) during test 1 and 15.7 ± 0.55 A/m² (3925 ± 138 A m⁻³ MEC) during test 2. The cathodic H₂ recovery was 92 % for test 1 and 93 % for test 2. This resulted in a volumetric production rate of 36 m³ H₂ m⁻³ MEC d⁻¹ for test 1 and 37 m³ H₂ m⁻³ MEC d⁻¹ for test 2 (MEC volume: 40 · 10⁻⁶ m³).

While the current decreased during days 14-32, the anode overpotential increased from 0.12 V to 0.15 V and the cathode overpotential increased from -0.23 to -0.24 V. The increase in anode potential was likely caused by scaling, which was observed on the membrane side of the graphite felt anode (Figure 5). In previous studies, scaling has been found on the cathode of an MFC [30] and MEC [22] during long term operation with a cation exchange membrane. The MEC with Ni foam cathode had an anion exchange membrane through which hydroxide was continuously transported from cathode to anode chamber. The high local pH at the membrane side of the bioanode resulted in scaling, for example of calcium phosphate. Scaling shields the bioanode, which results in a decrease in active surface area, a decrease in mass transport of reactants (i.e. acetate) and products

(i.e. carbonate buffer species and protons), and an increase in ohmic resistance. Consequently, the current decreases and the anode overpotential increases. Spontaneous detachment of scaling from the bioanode may explain the sudden changes in current density and overpotential at days 22, 25 and 29 [22,31]. Continuous flow MECs with membrane that run on synthetic wastewater inherently suffer from scaling because of the presence of buffer, such as phosphate or carbonate, and divalent cations, such as Ca^{2+} and Mg^{2+} . The presence of these components in real wastewater should be more considered for an MEC than for a normal wastewater plant, due to the high local pH that is created in an MEC.

So far, it remains unclear what caused the increase in cathode overpotential. Various possible explanations can be found in literature, such as (i) blanketing of active surface area by H_2 gas bubbles in the pores [20,32], (ii) poisoning of the active surface area [14,33], and (iii) formation of Ni-hydride that decreases electrocatalytic activity [14,34-36]

Scaling may be another cause for the increase in cathode overpotential. Scaling on the cathode was not visually observed, and is unlikely, because concentrations of divalent cations (Ca^{2+} and $\text{Mg}^{2+} < 50 \mu\text{g L}^{-1}$ (detection limit ICP)) and anions (phosphate species = 343 mg L^{-1} , carbonate species not analyzed) did not exceed the solubility product at the catholyte pH (> 12). However, scaling on the anode shielded part of the anode, which resulted in uneven current distribution. Given the parallel electrode configuration of the MEC, also part of the cathode was thus shielded.

Selembo et al. [9] also found an increase in overpotential of a cathode made of Ni catalyzed carbon cloth after 12 batch cycles of MEC operation. They ascribed this to Ni corrosion during exposure to air between each cycle. This was supported by higher Ni concentrations in electrolyte that was replaced in air compared to electrolyte that was replaced in an anaerobic glove box. Corrosion could not explain the increase in cathode overpotential for Ni foam. Ni foam was continuously operated as cathode and the concentration of Ni in the catholyte (maximum: $16 \mu\text{g L}^{-1}$) did not change during the 48 h yield tests.

To keep MEC performance stable, scaling has to be avoided. This may be

5. MEC with Ni foam cathode

achieved by the use of a turbulence promoter between bioanode and membrane, such as a spacer [6]. The increase in cathode overpotential should be further investigated.

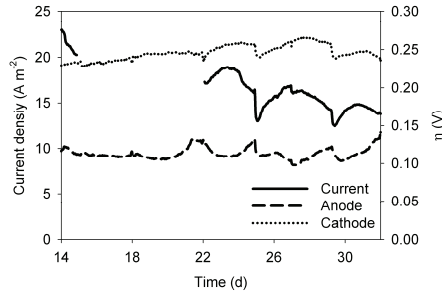


Figure 4 Current density, anode and cathode overpotential (η) of the MEC with Ni foam cathode during 20 days operation at 1.00 V. The cathode overpotential is expressed with a positive sign for convenience. Current density was not recorded between day 15 and 22 because of failure of the monitor output of the power supply.



Figure 5 Unused graphite felt (left) and membrane side of the graphite felt bioanode after 32 days of operation (right).

5.4 Conclusions

The MEC with flow through bioanode and flow through Ni foam cathode with high specific surface area ($128 \text{ m}^2 \text{ m}^{-2}$ projected area) achieved a high H_2 production rate. The MEC produced more than $50 \text{ m}^3 \text{ H}_2 \text{ m}^{-3} \text{ MEC d}^{-1}$ (22.82 A m^{-2}) at an electrical energy input of $2.6 \text{ kWh m}^{-3} \text{ H}_2$ (applied cell voltage: 1.00 V). However, MEC performance decreased during 32 days due to an increase in anode and cathode overpotentials. Scaling likely caused the increase in anode overpotential, but it remained unclear what caused the increase in cathode overpotential.

5.5 Acknowledgements

This work was performed in the TTIW-cooperation framework of Wetsus, centre of excellence for sustainable water technology (www.wetsus.nl). Wetsus is funded by the Dutch Ministry of Economic Affairs, the European Union Regional Development Fund, the Province of Fryslân, the City of Leeuwarden and the EZ/Kompas program of the “Samenwerkingsverband Noord-Nederland”. The authors like to thank Tom Sleutels for critically reading the manuscript, Oane Galama for preparing Figure 1, and the participants of the Wetsus research theme “Bio-energy” for the fruitful discussions and their financial support.

5.6 References

- [1] Liu H, Grot S, Logan B E. Electrochemically assisted microbial production of hydrogen from acetate. *Environ Sci Technol* 2005; 39: 4317-20
- [2] Logan B E, Call D, Cheng S, Hamelers H V M, Sleutels T H J A, Jeremiasse A W, et al. Microbial electrolysis cells for high yield hydrogen gas production from organic matter. *Environ Sci Technol* 2008; 42: 8630-40
- [3] Rozendal R A, Hamelers H V M, Euverink G J W, Metz S J, Buisman C J N. Principle and perspectives of hydrogen production through biocatalyzed electrolysis. *Int J Hydrogen Energy* 2006; 31: 1632-40
- [4] Sleutels T H J A, Hamelers H V M, Rozendal R A, Buisman C J N. Ion transport resistance in microbial electrolysis cells with anion and cation exchange membranes *Int J Hydrogen Energy* 2009; 34: 3612-20
- [5] Call D, Logan B E. Hydrogen production in a single chamber microbial electrolysis cell lacking a membrane. *Environ Sci Technol* 2008; 42: 3401-6
- [6] Sleutels T H J A, Lodder R, Hamelers H V M, Buisman C J N. Improved performance of porous bio-anodes in microbial electrolysis cells by enhancing mass and charge transport. *Int J Hydrogen Energy* 2009; 34: 9655-61
- [7] Jeremiasse A W, Hamelers H V M, Kleijn J M, Buisman C J N. Use of biocompatible buffers to reduce the concentration overpotential for hydrogen evolution. *Environ Sci Technol* 2009; 43: 6882-7
- [8] Hrapovic S, Manuel M F, Luong J H T, Guiot S R, Tartakovsky B. Electrodeposition of nickel particles on a gas diffusion cathode for hydrogen production in a microbial electrolysis cell. *Int J Hydrogen Energy* 35: 7313-20
- [9] Selembo P A, Merrill M D, Logan B E. Hydrogen production with nickel powder cathode catalysts in microbial electrolysis cells. *Int J Hydrogen Energy* 2009; 35: 428-37
- [10] Selembo P A, Merrill M D, Logan B E. The use of stainless steel and nickel alloys as low-cost cathodes in microbial electrolysis cells. *J Power Sources* 2009; 190: 271-8

- [11] Hu H, Fan Y, Liu H. Hydrogen production in single-chamber tubular microbial electrolysis cells using non-precious-metal catalysts. *Int J Hydrogen Energy* 2009; 34: 8535-42
- [12] Hu H, Fan Y, Liu H. Optimization of NiMo catalyst for hydrogen production in microbial electrolysis cells. *Int J Hydrogen Energy* 2010; 35: 3227-33
- [13] Manuel M F, Neburchilov V, Wang H, Guiot S R, Tartakovsky B. Hydrogen production in a microbial electrolysis cell with nickel-based gas diffusion cathodes. *J Power Sources* 2010; 195: 5514-9
- [14] Vetter K J. *Electrochemical kinetics: theoretical and experimental aspects*. ed. New York: Academic press; 1967.
- [15] Miles M H. Evaluation of electrocatalysts for water electrolysis in alkaline solutions. *J Electroanal Chem Interfacial Electrochem* 1975; 60: 89-96
- [16] Couper A M, Pletcher D, Walsh F C. *Electrode materials for electrosynthesis*. *Chem Rev* 1990; 90: 837-65
- [17] Kinoshita K. *Electrochemical oxygen technology*. ed. New York: John Wiley & Sons, Inc.; 1992.
- [18] Rozendal R A, Harnisch F, Jeremiasse A W, Schröder U, Chemically catalyzed cathodes in bioelectrochemical systems, in: Rabaey, K., Angenent, L., Schröder, U., Keller, J. (Eds.), *Bioelectrochemical systems: from extracellular electron transfer to biotechnological application*. IWA Publishing, London, 2010, pp. 263-84.
- [19] Marracino J M, Coeuret F, Langlois S. A first investigation of flow-through porous electrodes made of metallic felts or foams. *Electrochim Acta* 1987; 32: 1303-9
- [20] Rausch S, Wendt H. Morphology and utilization of smooth hydrogen-evolving raney nickel cathode coatings and porous sintered-nickel cathodes. *J Electrochem Soc* 1996; 143: 2852-62
- [21] LeRoy R L, Janjua M B I, Renaud R, Leuenberger U. Analysis of time-variation effects in water electrolyzers. *J Electrochem Soc* 1979; 126: 1674-82
- [22] Jeremiasse A W, Hamelers H V M, Buisman C J N. Microbial electrolysis cell with a microbial biocathode. *Bioelectrochemistry* 2009; 78: 39-43
- [23] Brunauer S, Emmett P H, Teller E. Adsorption of gases in multimolecular layers. *J Am Chem Soc* 1938; 60: 309-19
- [24] Zehnder A J B, Huser B A, Brock T D, Wuhrmann K. Characterization of an acetate-decarboxylating, non-hydrogen-oxidizing methane bacterium. *Arch Microbiol* 1980; 124: 1-11
- [25] Harris L B. Change in pH near the cathode during the electrodeposition of a bivalent metal. *Analysis. J Electrochem Soc* 1973; 120: 1034-40
- [26] Lee H-S, Rittmann B E. Characterization of energy losses in an upflow single-chamber microbial electrolysis cell. *Int J Hydrogen Energy* 2010; 35: 920-7
- [27] Clauwaert P, Verstraete W. Methanogenesis in membraneless microbial electrolysis cells. *Appl Microbiol Biotechnol* 2009; 82: 829-36
- [28] Chae K-J, Choi M-J, Lee J H, Ajayi F F, Kim I S. Biohydrogen production via biocatalyzed electrolysis in acetate-fed bioelectrochemical cells and microbial community analysis. *Int J Hydrogen Energy* 2008;

- [29] Besancon B M, Hasanov V, Imbault-Lastapis R, Benesch R, Barrio M, Molnvik M J. Hydrogen quality from decarbonized fossil fuels to fuel cells. *Int J Hydrogen Energy* 2009; 34: 2350-60
- [30] Di Lorenzo M, Curtis T P, Head I, Scott K. A single-chamber microbial fuel cell as a biosensor for wastewaters. *Water Res* 2009; 43: 3145-54
- [31] Gabrielli C, Maurin G, Francy-Chausson H, Thery P, Tran T T M, Tlili M. Electrochemical water softening: principle and application. *Desalination* 2006; 201: 150-63
- [32] Ateya B, El-Anadouli B E. Effects of gas bubbles on the polarization behavior of porous flow through electrodes. *J Electrochem Soc* 1991; 138: 1331-6
- [33] Nidola A, Schira R. Poisoning mechanisms and structural analyses on metallic contaminated cathode catalysts in chlor-alkali membrane cell technology. *J Electrochem Soc* 1986; 133: 1653-6
- [34] Rommal H E G, Moran P J. Time-dependent energy efficiency losses at nickel cathodes in alkaline water electrolysis systems. *J Electrochem Soc* 1985; 132: 325-9
- [35] Rommal H E G, Morgan P J. The role of absorbed hydrogen on the voltage-time behavior of nickel cathodes in hydrogen evolution. *J Electrochem Soc* 1988; 135: 343-6
- [36] Soares D M, Teschke O, Torriani I. Hydride effect on the kinetics of the hydrogen evolution reaction on nickel cathodes in alkaline media. *J Electrochem Soc* 1992; 139: 98-105

6. Performance of metal alloys as hydrogen evolution reaction catalysts in a microbial electrolysis cell

Abstract

H₂ can be produced from organic matter with a microbial electrolysis cell (MEC). To decrease the energy input and increase the H₂ production rate of an MEC, a catalyst is used at the cathode. Platinum is an effective catalyst, but its high costs stimulate searching for alternatives, such as non-noble metal alloys. This study demonstrates that copper sheet coated with nickel-molybdenum, nickel-iron-molybdenum or cobalt-molybdenum alloys have a higher catalytic activity for the hydrogen evolution reaction than nickel cathodes, measured near neutral pH. However, the catalytic activity cannot be fully exploited near neutral pH because of mass transport limitation. The catalytic activity is best exploited at alkaline pH where mass transport is not limiting. This was demonstrated in an MEC with a cobalt-molybdenum coated cathode and anion exchange membrane, which produced 50 m³ H₂ m⁻³ MEC d⁻¹ (at standard temperature and pressure) at an electricity input of 2.5 kWh m⁻³ H₂.

This chapter has been published as:

Jeremiasse A W, Bergsma J, Kleijn J M, Saakes M, Buisman C J N, Cohen Stuart M, Hamelers HVM. Performance of metal alloys as hydrogen evolution reaction catalysts in a microbial electrolysis cell. Int J Hydrogen Energy 2011: doi:10.1016/j.ijhydene.2011.06.013

6.1 Introduction

H₂ is an energy carrier and chemical, which can be sustainably produced from organic matter with a microbial electrolysis cell (MEC). At the anode of an MEC, electrochemically active microorganisms convert organic matter (e.g. acetate) into bicarbonate, protons and electrons. The produced electrons move from the anode through an external electrical circuit with power supply to the cathode. At the cathode, the electrons combine with protons in a process called the hydrogen evolution reaction (HER). The negative charge transport through electrons is compensated by charge transport through ions in the cell. The production of H₂ from organic matter in an MEC is not a spontaneous process, but requires a voltage input that is delivered by the power supply. According the Nernst equation, 0.14 V would be required to produce H₂ from acetate under standard biological conditions (298 K, P = 1 bar, pH 7). In practice, 0.4-1.0 V is applied to produce H₂ at a measurable rate [1].

To decrease the energy input (kWh m⁻³ H₂), and increase the H₂ production rate (i.e. m³ H₂ m⁻³ MEC d⁻¹) of an MEC, a catalyst is used at the cathode [1]. The catalyst decreases the HER activation overpotential, i.e. the activation energy for the charge transfer reaction at the cathode surface [2]. The first MECs used a cathode with Pt catalyst. However, the high costs of Pt have stimulated the search for alternative catalysts, such as non-noble transition metals.

Previous studies showed that cathodes based on non-noble metal catalysts such as Fe [3-4] and Ni [4-8], could be employed in MECs. For example, a continuous flow membrane-less MEC with Ni based gas diffusion cathode produced 4 m³ H₂ m⁻³ MEC day⁻¹ [7]. Furthermore, cathodes based on alloys of these metals could be employed in MECs. Although theoretically not well understood [9-11], metal alloys effectively decrease the HER activation overpotential. For MECs, Ni alloys and tungsten carbide (WC) were applied as HER catalyst [7,12-15]. For alkaline water electrolyzers, various other alloys were applied as HER catalyst [16-18]. The performance of these alloys in MECs however, is not necessarily the same as in water electrolyzers, because MECs and water electrolyzers operate under different conditions [11]. To choose the right alloy as HER catalysts for an

MEC, a comparison of various alloys under typical MEC cathode conditions (e.g. pH) is thus relevant.

MEC cathode pH depends on MEC design. In literature, two types of MEC design can be distinguished: MECs without a membrane, and MECs with a membrane that separates the cell in an anode and a cathode chamber [1]. In MECs without a membrane, HER catalysts typically work around neutral pH (i.e. wastewater pH) [19]. Around neutral pH, there is a low concentration of H^+ and OH^- and therefore, the HER is easily transport limited, which results in a considerable concentration overpotential. Buffers can overcome this transport limitation, but this strongly depends on pH, buffer pK_a and concentration, current density, and hydrodynamic conditions [20]. In MECs with a membrane, the transport of cations other than protons through the membrane causes an increased catholyte pH [21-22], and thus HER catalysts typically work at mild alkaline pH ($pH > 12$). At alkaline pH, the HER is not mass transport limited, and thus no buffer is required [20], but the MEC suffers from voltage losses that arise from the pH gradient between anode and cathode [21-22].

In this study, we extended the investigated range of alloys with nickel-iron-molybdenum (NiFeMo) and cobalt molybdenum (CoMo) alloys as possible HER catalysts in an MEC. These alloys are known to have a high catalytic activity under strong alkaline conditions in water electrolyzers [16-17], but a high catalytic activity around neutral and mild alkaline pH as encountered in MECs has yet to be proven. Therefore, the catalytic activity of these alloys was compared in a 0.1 M phosphate buffered electrolyte of pH 6. The pH of this electrolyte differs most from a strongly alkaline electrolyte, while the high buffer concentration improves mass transport. After characterization of conditions and catalytic activity, a catalyst was selected and further characterized in an MEC.

6.2 Materials and Methods

6.2.1 Cathode preparation

Each cathode was prepared by electrodeposition of metals from an aqueous deposition

6. Metal alloys as HER catalysts in MEC

bath on a new Cu sheet substrate. The use of Cu sheet instead of Ni foam [8] as substrate, enabled us to study the effect of the deposited metal (alloy) on overpotential without the contribution of a large specific surface area. Furthermore, Cu has a high overpotential for the HER compared to Ni, which will make it easier to distinguish the contribution of the deposited metal (alloy) to the HER overpotential.

Before electrodeposition, the Cu substrate was cleaned. For the cathode characterization experiments, a Cu piece (1.5 x 3.0 cm) was polished with abrasive paper and subsequently left overnight in 1 M HCl. For the MEC experiments, a Cu piece (10 x 10 cm) was polished with abrasive paper, subsequently immersed for 15 min in 1 M HCl, and finally immersed for 15 min in an ultrasonic bath. The deposition bath contained one or more metals (Table 1), 0.15 M $\text{Na}_3\text{C}_6\text{H}_5\text{O}_7$ (trisodium citrate) and 0.5 M NaHCO_3 . The pH was adjusted with 1 M HCl or 1 M NaOH.

Table 1 Metal composition and pH of electrodeposition bath, current density (j), deposition time, and potential (vs NHE) of the working electrode at the start (E_0) and at the end (E_{end}) of electrodeposition.

Bath	NiCl_2 (M)	CoCl_2 (M)	FeCl_3 (M)	Na_2MoO_4 (M)	pH (-)	j (A m^{-2})	Time (h)	E_0 (V)	E_{end} (V)
Ni_{100}	0.250				10.5	50	3	-1.08	-1.05
$\text{Ni}_{85}\text{Mo}_{15}$	0.213			0.038	10.5	100	6	-1.09	-0.95
$\text{Ni}_{64}\text{Fe}_{18}\text{Mo}_{18}$	0.160		0.045	0.045	10.5	200	6	-1.23	-1.14
$\text{Ni}_{76}\text{Fe}_{16}\text{Mo}_8$	0.190		0.040	0.020	10.5	200	6	-1.40	-1.19
$\text{Co}_{75}\text{Mo}_{25}^{\text{a}}$		0.188		0.063	6.6	100	3	-1.51	-1.13

^a This deposition bath of $\text{Co}_{75}\text{Mo}_{25}$ contained 0.5 M $\text{Na}_3\text{C}_6\text{H}_5\text{O}_7$ (trisodium citrate), and did not contain NaHCO_3 . The pH was adjusted to pH 6.6 [23].

The Cu substrate was connected as the working electrode to a potentiostat/galvanostat (Autolab PGSTAT100, Metrohm Autolab B.V., Utrecht, The Netherlands). An Ir/Ta electrode (80%/20%, Magneto Special Anodes BV, Schiedam, The Netherlands) was used as the counter electrode. The metals were deposited in galvanostatic mode (i.e. at constant current, Table 1) [23]. The potential during electrodeposition was measured (Table 1).

6.2.2 Cathode characterization

Each prepared cathode was characterized in an electrochemical cell. The electrochemical cell contained a sample holder, which exposed 0.8 cm^2 of the cathode to the electrolyte. The cathode was connected as working electrode, and a Pt plate (2 cm^2) was connected as counter electrode of a potentiostat/galvanostat (μ Autolab III, Metrohm Autolab B.V., Utrecht, The Netherlands). A 3 M KCl Ag/AgCl electrode (+0.210 V vs NHE) was connected as reference electrode. The electrolyte contained 0.50 M Na_2SO_4 solution and 0.10 M NaH_2PO_4 , and was adjusted to pH 6.0 with NaOH. The temperature of the electrolyte was controlled at 25 °C. To maintain a constant H_2 pressure, and to minimize O_2 production at the Pt counter electrode, H_2 was continuously flushed through the electrolyte ($p_{\text{H}_2} = 1 \text{ bar}$). The electrolyte was continuously mixed with a magnetic stirrer. The HER potential was obtained in a series of measurements at constant current densities of respectively 75, 50, 25, 10, 5, 2.5, 1, 0.1, and 0.01 A m^{-2} . The HER potential was measured each 10 s, for 50 min at 75 A m^{-2} , and for 25 min at all other current densities. This sequence was performed 5 times for each cathode to check if measurements were reproducible. For each current density the results of the last 100 s of the 5th sequence were averaged and used for further analysis. The cathode overpotential was calculated as described previously [8].

The elemental composition of the cathodes was measured with a scanning electron microscope (SEM) equipped with an energy dispersive X-ray spectroscope (EDX, Noran system six model 300, Thermo Fisher Scientific, Waltham, USA). The acceleration voltage was 15 kV.

The specific surface area of the cathodes was determined for a spot size of $5 \times 5 \text{ }\mu\text{m}$ with an atomic force microscope (AFM, Nanoscope IIIa, Bruker AXS, Santa Barbara, CA, USA) in contact mode.

6.2.3 Cathode application in an MEC

The MEC and its setup were the same as used in a previous study [8], except for the

6. Metal alloys as HER catalysts in MEC

membrane and cathode. The membrane was a heterogeneous anion exchange membrane from Ralex (HMA-PES, Mega A.S., Stráž pod Ralskem, Czech). The cathode was prepared according to 2.1 from the best alloy. The anode and cathode chamber were operated as described previously [8]. The anolyte contained (in demineralized water): 2.72 g/L $\text{NaCH}_3\text{COO}\cdot 3\text{H}_2\text{O}$, 0.68 g/L KH_2PO_4 , 0.87 g/L K_2HPO_4 , 0.74 g/L KCl, 0.58 g/L NaCl, 0.28 g/L NH_4Cl , 0.1 g/L $\text{CaCl}_2\cdot 2\text{H}_2\text{O}$, 0.01 g/L $\text{MgSO}_4\cdot 7\text{H}_2\text{O}$ and 0.1 mL/L of a trace element mixture [24]. The catholyte consisted of 0.1 M KCl. The temperature of the MEC was controlled at 30 ± 1 °C.

To allow a fast startup of the MEC, a cathode of sintered Ti (10 x 10 x 0.2 cm) with 5 g m^{-2} projected area Pt coating was used (Magneto Special Anodes BV). This cathode has a low HER overpotential and therefore, bioanode development is not limited by poor cathode performance. The MEC anode was inoculated with 10 mL effluent of a previously operated MEC [8], and initially operated at an applied cell voltage of 0.5 V. The voltage was increased in steps of 0.1 V each time the current had stabilized, till maximally 1.0 V. Subsequently, the sintered Ti-Pt cathode was replaced by a freshly prepared, alloy coated cathode. This procedure was performed twice (run 1 and run 2), each time with a new graphite felt anode, and newly prepared alloy cathode.

For both runs, a polarization curve of the alloy coated cathode was constructed by measuring current, cathode potential and cathode pH at applied cell voltages of 1.0, 0.9, 0.8, 0.7, 0.6 and 0.5 V. Each cell voltage was applied for 1 hour. Measurements were recorded each 5 min, and the last 5 recorded measurements were averaged. For run 1, also anode potential and anode pH were measured. Equilibrium voltage, anode and cathode (over)potential, membrane plus ionic voltage loss, and their contributions to the overall electricity input were calculated as described previously [8]. For calculation of the equilibrium anode potential, the bicarbonate and acetate concentrations must be known. Their concentrations were not measured during polarization however. Nevertheless, within their applied concentration range, they only have a small effect on the equilibrium anode potential. Therefore, influent values were assumed for calculation of the equilibrium potential.

6.3 Results and Discussion

6.3.1 HER near neutral pH is largely mass transport controlled

The catalytic activity of Pt, Cu and each electroplated cathode was characterized through measurements of the cathode overpotential (η) at various current densities (j) (Figure 1 A and B).

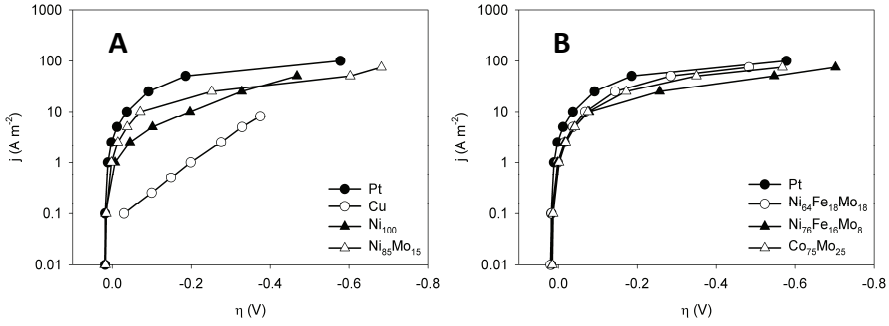


Figure 1 A and B Performance of various catalysts in 0.1 M NaH₂PO₄ + 0.5 M Na₂SO₄ at pH 6.0 and 25 °C.

If transport is not limiting, $\log(j)$ linearly increases with increasing η for $|\eta| > RT/\alpha F$, with R the universal gas constant (8.314 J mol⁻¹ K⁻¹), T the absolute temperature (298 K), α the transfer coefficient (-), and F the Faraday constant (96485 C mol⁻¹). Pure Cu follows this so-called Tafel behavior. However, Pt and the electroplated cathodes did not show a linear increase of $\log(j)$ with increasing η , but $\log(j)$ leveled off with increasing η (Figure 1 A and B). Limited transport of H⁺ towards the surface (or OH⁻ away from the surface) results in a H⁺ concentration that is lower at the surface than in the bulk [20,25]. The shape of the η - j curve can then be interpreted with a concentration corrected Tafel relation [2]:

$$j = j_0 \left(\frac{H_{surface}^+}{H_{bulk}^+} \right) e^{\frac{-\alpha \eta F}{RT}} \quad (1)$$

6. Metal alloys as HER catalysts in MEC

with j_0 the exchange current density ($A\ m^{-2}$), which is a measure for the electrode kinetics [26], $H^+_{surface}$ the proton concentration at the surface (unknown) and H^+_{bulk} the proton concentration in the bulk (10^{-6} M). The equilibrium potential and thus η is calculated using the bulk pH value, and thus η includes activation and concentration overpotential. It can be assumed that H_2 diffusion is not limiting the current density [27].

The current density must equal the charge transport to the cathode surface. A high concentration of background electrolyte (0.5 M Na_2SO_4) was used and therefore, transport due to migration was neglected. The diffusion layer thickness was constant through controlled convection with a magnetic stirrer. The species considered in diffusive transport are buffer species, protons and hydroxide. At bulk pH 6, the dominant buffer species are $H_2PO_4^-$ and HPO_4^{2-} and therefore, the transport flux ($mol\ m^{-2}\ s^{-1}$) of other phosphate buffer species and protons could be neglected [20]. The current density must thus equal the transport flux of three species:

$$j = F \left(-J_{OH^-} - J_{H_2PO_4^{2-}} - 2J_{HPO_4^{2-}} \right) \quad (2)$$

Assuming that the total buffer concentration C_T equals $[H_2PO_4^-] + [HPO_4^{2-}]$, and that the diffusion coefficients of $H_2PO_4^-$ and HPO_4^{2-} are equal, the flux of HPO_4^{2-} is opposite to the flux of $H_2PO_4^-$. The transport equation can then be written as:

$$j = F \left[\frac{D_{OH^-}}{\delta} \left(\frac{K_w}{H^+_{surface}} - \frac{K_w}{H^+_{bulk}} \right) + \frac{D_A}{\delta} C_T \left(\frac{H^+_{bulk}}{H^+_{bulk} + K_{a2}} - \frac{H^+_{surface}}{H^+_{surface} + K_{a2}} \right) \right] \quad (3)$$

with D_{OH^-} the diffusion coefficient of hydroxide ($5.3 \cdot 10^{-9}\ m^2\ s^{-1}$ at 298 K [28]) and D_A the diffusion coefficient of buffer (average value for $H_2PO_4^-$ and HPO_4^{2-} , which is $1.3 \cdot 10^{-9}\ m^2\ s^{-1}$ at 298 K [28]), K_w the water dissociation constant ($10^{-14}\ M^2$), K_{a2} the acid dissociation

constant of H_2PO_4^- ($K_{a2}=10^{-6.4}$ M, predicted with OLI StreamAnalyzer 2.0, OLI Systems, Morris Plains, NJ, USA), and δ the diffusion layer thickness. Under conditions of controlled convection, it can be safely assumed that the diffusion layer thickness was about 90 μm [2].

Equations 1 and 3 were combined and solved using MathCad (vs 14, PTC, Needham, USA) to yield an expression of η as function of j (Appendix – Chapter 6). This expression allows to study the effect of the variables α and j_0 (i.e. catalytic activity) on the shape of η - j curves for the HER in a near neutral pH electrolyte. Figure 2 shows how materials with high and low catalytic activities can lead to different shapes of the η - j curves.

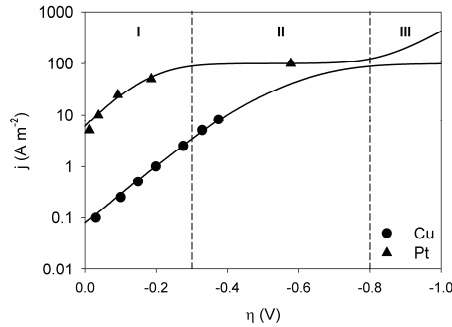


Figure 2 Current density (j) as function of measured overpotential (η) for Cu and Pt (symbols). A transport corrected Tafel relation (lines) was fitted (fitting parameter: α) through the data by minimizing the sum of squared differences between this relation and experimental data. Therefore, the required values of j_0 for Pt and Cu were estimated using the linear approximation at low overpotential (section 6.3.2 and Table 2). Minimization was done with the quasi-Newton method in MathCad. For Cu the fit yielded $\alpha=0.33$, for Pt $\alpha=0.51$.

For the η - j curve of a material with high catalytic activity for the HER, such as Pt, 3 limiting regions can be identified (Figure 2). In region I ($\eta = 0$ to -0.3 V), $\log(j)$ increases non-linearly with η . This region is characterized by a transition from activation control to mass transport control of the HER. In region II ($\eta = -0.3$ to -0.8 V), $\log(j)$ hardly increases with η , because the HER is mainly mass transport controlled. The large increase in overpotential in this region is caused by a large increase in pH at the cathode surface that is required for

6. Metal alloys as HER catalysts in MEC

the OH^- flux [20,25]. In region III, (η more negative than -0.8 V), $\log(j)$ increases linearly with η . In this region, the reaction is activation controlled, because the OH^- flux is not limiting.

For the η - j curve of a material with low catalytic activity and thus high activation overpotential for the HER, such as Cu, the transition from activation to mass transport control extents over a large η range (regions I and II in Figure 2). In region III, the HER on Cu is mainly mass transport controlled, and at more negative values of η , the HER would be again activation controlled (outside the range of Figure 2).

This analysis demonstrates that even in presence of 0.100 M phosphate buffer, the HER suffers from mass transport limitation at current densities above 25 A m^{-2} in a near neutral pH electrolyte. Also in a previous study (Figure 1 in [13]), the effect of transport on the HER current density was slightly visible at 25 A m^{-2} . This implies that an MEC operating at neutral cathode pH requires a high concentration of buffer to decrease the cathode overpotential at 25 A m^{-2} and higher. The HER does not suffer from mass transport limitation at alkaline conditions as follows from the combined expression (Appendix – Chapter 6). The HER at the alkaline conditions encountered in an MEC with membrane will be further investigated in section 6.3.4.

6.3.2 Alloys have high exchange current densities for HER near neutral pH

Materials with high catalytic activity are characterized by a high value for the exchange current density (j_0). To estimate j_0 at pH 6 at the cathode surface, the HER should not be mass transport controlled, which is however the case at high overpotentials (Figure 2). Therefore, j_0 was estimated at overpotentials at which only activation controls the reaction, using the linear approximation that is valid at $|\eta| < RT/\alpha F$ [26,29]:

$$j = j_0 \frac{RT}{F} \eta \quad (4)$$

Table 2 lists the values of j_0 that were determined from the data of Figure 1A and B. The

value of j_0 of the commercial Pt sheet is comparable to values obtained in previous studies under acidic and alkaline conditions [29-30]. The j_0 values for electroplated Ni, and NiMo and CoMo alloys are higher, whereas j_0 values for NiFeMo alloys are lower than previously reported j_0 values of these catalysts [16-17,31-32]. The difference between measured and literature values are likely caused by differences in pH (pH 6 vs pH < 0 or pH > 14), electrolyte conditions (presence of buffer) and cathode composition (e.g. metal substrate, alloy composition). As was also pointed out by Petrii and Tsirlina [11], variation in measurement conditions largely influences electrocatalytic data. Thus, the estimated values of j_0 (Table 2) cannot be universally applied, but can be used to compare activities of different metal alloys under equal conditions.

All studied alloys have a higher value for j_0 than Ni in 100 mM phosphate buffer of pH 6. The high catalytic activity of Ni₈₅Mo₁₅ alloy was also observed by Hu et al., who measured in a 100 mM phosphate buffer of pH 7 [12-13]. To our knowledge, NiFeMo and CoMo alloys have only been investigated as HER catalyst at alkaline pH [16-17], and not around neutral pH. These measurements confirm that also around neutral pH, alloys demonstrate enhanced HER catalysis compared to the pure metals.

Table 2 Exchange current densities of the studied cathodes; uncorrected (j_0) and corrected for specific surface area (corrected j_0). Values were calculated from the slope of the linear relation that was fitted through the origin and data points with $\eta < 0.04$ V. The correlation coefficient r^2 was > 0.9 for all cathodes, except Pt ($r^2=0.8$) and Ni ($r^2=0.7$). The formula of the electrodeposited cathodes is the deposition bath composition.

<i>Cathode</i>	<i>j_0 (A m⁻²)</i>	<i>corrected j_0 (A m⁻²)</i>
Pt	7.3	7.3
Cu ^a	0.08	-
Ni ₁₀₀	1.5	1.3
Ni ₈₅ Mo ₁₅	3.5	3.2
Ni ₆₄ Fe ₁₈ Mo ₁₈	3.6	2.6
Ni ₇₆ Fe ₁₆ Mo ₈	3.3	2.4
Co ₇₅ Mo ₂₅	3.1	2.8

^aThe surface area of Cu was not measured.

6.3.3 Composition and specific surface area confirm enhanced HER catalysis by alloys

After electrochemical characterization, the elemental composition of each cathode was

6. Metal alloys as HER catalysts in MEC

determined with EDX (Appendix – Chapter 6). Next to the deposited metals, carbon and oxygen were measured for the cathodes.

Carbon was only measured for cathodes that had been stored in acetone, and therefore, likely originated from impurities present in the acetone. The compositions as measured by EDX were thus corrected by excluding carbon (Table 3).

Oxygen was measured for all cathodes, and can be mainly attributed to formation of a surface metal oxide film (passivation) during exposure of the cathodes to ambient air. The passivation layer is removed when the cathodes are connected cathodically [33]. However, Mo can retain an oxide film which is not cathodically reduced [13,34], and this permanent oxide film cannot be distinguished from the passivation layer with EDX. Compositions excluding oxygen were also calculated (Table 3).

The compositions of the deposited alloys do not correspond to the concentration ratios of the metal ions in the baths. This was expected because under conditions of the deposition bath, standard electrode potentials and thus overpotentials decrease in the order $\text{Ni}^{2+}/\text{Ni} \approx \text{Co}^{2+}/\text{Co} > \text{Fe}^{2+}/\text{Fe} > \text{MoO}_4^{2-}/\text{Mo}$ [35]. A higher overpotential would result in a higher deposition rate. However, this does not explain the relatively high Mo content in the alloys. Zech et al. [36] demonstrated that codeposition of iron group metals enhances the deposition rate of the metals with a lower standard electrode potential, whereas it slows down the deposition rate of metals with a higher standard electrode potential. Enhanced Mo deposition, which was also noted in other studies [13,23,37], would explain the high Mo content in the alloys.

The specific surface area, as determined with AFM, was highest for the NiFeMo alloys. The exchange current densities were corrected for specific surface area (Table 2). The values of the exchange current densities after correction confirm that improved HER catalysis is obtained through a synergistic catalytic effect of the alloy, and not only through an increase in specific surface area [16]. $\text{Ni}_{85}\text{Mo}_{15}$ had the highest exchange current density after correction.

Table 3 Approximate elemental composition (determined with EDX), and specific surface area (determined with AFM) of cathodes prepared with electrodeposition. The numbers in parentheses indicate the composition excluding oxygen.

Bath composition	Deposit composition					Specific surface area (m ² /m ²)
	Ni (%)	Co (%)	Fe (%)	Mo (%)	O (%)	
Pt						1.0
Ni ₁₀₀	94 (100)				6 (0)	1.2
Ni ₈₅ Mo ₁₅	40 (66)			21 (34)	39 (0)	1.1
Ni ₆₄ Fe ₁₈ Mo ₁₈	39 (48)		22 (26)	20 (25)	19 (0)	1.4
Ni ₇₆ Fe ₁₆ Mo ₈	36 (51)		17 (24)	18 (25)	29 (0)	1.4
Co ₇₅ Mo ₂₅		47 (67)		23 (33)	30 (0)	1.1

6.3.4 High H₂ production rate for MEC with CoMo coated Cu-sheet cathode and membrane

An MEC with 100 cm² CoMo coated Cu cathode was operated twice. CoMo alloy was chosen, because it had not been studied in an MEC before, and was expected to be more stable than NiMo alloy [16] and NiFeMo under alkaline conditions [18]. The MEC with membrane was operated without pH control of anode and cathode, and therefore the cathode pH was above 12. Although this leads to losses caused by a membrane pH gradient, mass transport limitation of the HER is minimized (section 3.1), no buffer is required, and H₂ consumption through methanogenesis is avoided.

The performance of the CoMo coated cathode in the MEC was reproducible (Figure 3). A Tafel relation was fitted through data of both runs. From the fit a value of 2.8 A m⁻² for j_0 was obtained. The specific surface area as determined with AFM was 1.0 m² m⁻². Taking into account the specific surface area, the value of j_0 is consistent with the value at pH 6 that was estimated with the linear approximation in the characterization experiments (Table 2). For the fitted Tafel relation the slope⁻¹ = 0.11 V (α = 0.55), which is consistent with slope⁻¹ = 0.116 V (α =0.5) for CoMo alloy under alkaline conditions that can be found in literature [16]. The average composition of the 2 tested CoMo coated cathodes was 44 % Co, 27 % Mo, and 26 % O, which is comparable to the composition measured for the CoMo alloy of the characterization experiment.

6. Metal alloys as HER catalysts in MEC

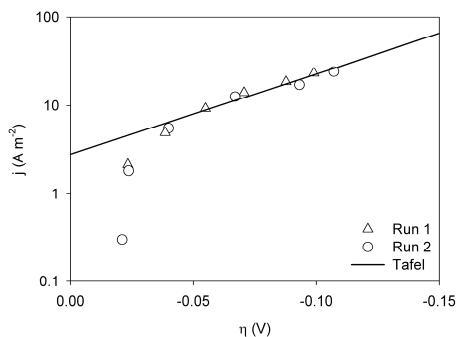


Figure 3 Polarization of the CoMo coated Cu cathode (duplicate runs) in an MEC with membrane and without pH control of the cathode (cathode pH >12). Linear regression ($r^2=0.95$) for data with η more negative than -0.04 yielded a Tafel relation with $j_0=2.8 \text{ A m}^{-2}$ and $\text{slope}^{-1} = 0.11 \text{ V}$ ($\alpha=0.55$).

The MEC with low surface area, CoMo coated cathode produced H_2 at comparable rates (cathodic H_2 recovery always above 90%) and energy inputs (Figure 4) as a similar MEC with a high surface area, Ni foam cathode studied previously [8]. The voltage input for the cathode was decreased because of enhanced HER catalysis by the CoMo coated cathode (23 A m^{-2} at $\eta = -0.1 \text{ V}$) as compared to the Ni foam cathode (5 A m^{-2} at $\eta = -0.1 \text{ V}$). The voltage input for the membrane however, was increased compared to the previous study [8], because of the high resistance of the heterogeneous Ralex membrane compared to the homogeneous Neosepta membrane [38] used previously [8].

The costs of the catalyst will depend on the mode of application (e.g. electrodeposition from a solution, or as a powder with a binder [5]), and the loading (g/m^2). Nevertheless, the costs for $\text{Co}_{75}\text{Mo}_{25}$ alloy are estimated at 1 euro/g (based on prices of Alfa Aesar and Sigma-Aldrich), whereas for Pt at 45 euro/g (based on prices of Johnson Matthey). Thus, although CoMo has a 2 to 3 times lower catalytic activity than Pt (Table 2), it is 40 times cheaper than Pt.

The results show that a CoMo coated cathode can be successfully applied in an MEC with membrane. Experiments are required to further improve HER catalysis, for example through the use of high surface area cathodes [3,8], and to test the stability of the CoMo cathode. The long-term stability of CoMo cathodes has already been

demonstrated under strong alkaline conditions [16]. The stability in MECs, fed with different types of wastewaters, remains to be proven.

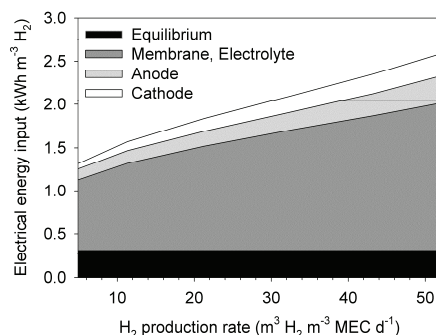


Figure 4 Overall performance of the MEC with a CoMo coated Cu cathode. The contributions to the electrical energy input of the equilibrium voltage, membrane (i.e. pH gradient plus transport losses [22]) and electrolyte voltage losses, anode overpotential and cathode overpotential are specified [8]. The H₂ production rate is based on measured current densities, and an assumed cathodic H₂ recovery of 90%.

6.4 Conclusions

This study demonstrates that near neutral pH, Cu sheet cathodes coated with NiMo, NiFeMo or CoMo alloy have a high catalytic activity for the HER compared to cathodes that consist of only Ni. However, the catalytic activity of these alloys cannot be fully exploited near neutral pH because of mass transport limitation. Their catalytic activity is best exploited at alkaline pH where mass transport is not limiting. This was demonstrated in an MEC with CoMo coated Cu cathode and anion exchange membrane, which reached a production rate of 50 m³ H₂ m⁻³ MEC d⁻¹ (at STP) at an electricity input of 2.5 kWh m⁻³ H₂.

6.5 Acknowledgements

This work was performed in the TTIW-cooperation framework of Wetsus, centre of excellence for sustainable water technology (www.wetsus.nl). Wetsus is funded by the Dutch Ministry of Economic Affairs, the European Union Regional Development Fund, the Province of Fryslân, the City of Leeuwarden and the EZ/Kompas program of the

“Samenwerkingsverband Noord-Nederland”. The authors like to thank Jerome Saas and Suman Bajracharya for performing part of the experiments, and the participants of the Wetsus research theme “Bio-energy” for fruitful discussions and financial support.

6.6 References

- [1] Logan B E, Call D, Cheng S, Hamelers H V M, Sleutels T H J A, Jeremiasse A W, et al. Microbial electrolysis cells for high yield hydrogen gas production from organic matter. *Environ Sci Technol* 2008; 42: 8630-40
- [2] Bockris J O M, Reddy A K N, Gamboa-Aldeco M. *Modern Electrochemistry 2A: Fundamentals of Electrodics*. ed. New York: Kluwer Academic; 2000.
- [3] Call D F, Merrill M D, Logan B E. High Surface Area Stainless Steel Brushes as Cathodes in Microbial Electrolysis Cells. *Environ Sci Technol* 2009; 43: 2179-83
- [4] Selembo P A, Merrill M D, Logan B E. The use of stainless steel and nickel alloys as low-cost cathodes in microbial electrolysis cells. *J Power Sources* 2009; 190: 271-8
- [5] Selembo P A, Merril M D, Logan B E. Hydrogen production with nickel powder cathode catalysts in microbial electrolysis cells. *Int J Hydrogen Energy* 2010; 35: 428-37
- [6] Hrapovic S, Manuel M F, Luong J H T, Guiot S R, Tartakovsky B. Electrodeposition of nickel particles on a gas diffusion cathode for hydrogen production in a microbial electrolysis cell. *Int J Hydrogen Energy* 35: 7313-20
- [7] Manuel M F, Neburchilov V, Wang H, Guiot S R, Tartakovsky B. Hydrogen production in a microbial electrolysis cell with nickel-based gas diffusion cathodes. *J Power Sources* 2010; 195: 5514-9
- [8] Jeremiasse A W, Hamelers H V M, Saakes M, Buisman C J N. Ni foam cathode enables high volumetric H₂ production in a microbial electrolysis cell. *Int J Hydrogen Energy* 2010; 35: 12716-23
- [9] Jaksic M M. Electrocatalysis of hydrogen evolution in the light of the brewer-engel theory for bonding in metals and intermetallic phases. *Electrochim Acta* 1984; 29: 1539-50
- [10] Ezaki H, Morinaga M, Watanabe S. Hydrogen overpotential for transition metals and alloys, and its interpretation using an electronic model. *Electrochim Acta* 1993; 38: 557-64
- [11] Petrii O A, Tsirlina G A. Electrocatalytic activity prediction for hydrogen electrode reaction: intuition, art, science. *Electrochim Acta* 1994; 39: 1739-47
- [12] Hu H, Fan Y, Liu H. Hydrogen production in single-chamber tubular microbial electrolysis cells using non-precious-metal catalysts. *Int J Hydrogen Energy* 2009; 34: 8535-42
- [13] Hu H, Fan Y, Liu H. Optimization of NiMo catalyst for hydrogen production in microbial electrolysis cells. *Int J Hydrogen Energy* 2010; 35: 3227-33
- [14] Wang L, Chen Y, Ye Y, Lu B, Zhu S, Shen S. Evaluation of low-cost cathode catalysts for high yield biohydrogen production in microbial electrolysis cell. *Water Sci Technol* 2011; 63: 440-8

- [15] Harnisch F, Sievers G, Schroder U. Tungsten carbide as electrocatalyst for the hydrogen evolution reaction in pH neutral electrolyte solutions. *Appl Catal B: Environ* 2009; 89: 455-8
- [16] Fan C, Piron D L, Sleb A, Paradis P. Study of Electrodeposited Nickel-Molybdenum, Nickel-Tungsten, Cobalt-Molybdenum, and Cobalt-Tungsten as Hydrogen Electrodes in Alkaline Water Electrolysis. *J Electrochem Soc* 1994; 141: 382-7
- [17] Arul Raj I. On the catalytic activity of Ni-Mo-Fe composite surface coatings for the hydrogen cathodes in the industrial electrochemical production of hydrogen. *Appl Surf Sci* 1992; 59: 245-52
- [18] Tilak B V, Ramamurthy A C, Conway B E. High performance electrode materials for the hydrogen evolution reaction from alkaline media. *Proc Indian Acad Sci (Chem Sci)* 1986; 97: 359-93
- [19] Call D, Logan B E. Hydrogen production in a single chamber microbial electrolysis cell lacking a membrane. *Environ Sci Technol* 2008; 42: 3401-6
- [20] Jeremiasse A W, Hamelers H V M, Kleijn J M, Buisman C J N. Use of biocompatible buffers to reduce the concentration overpotential for hydrogen evolution. *Environ Sci Technol* 2009; 43: 6882-7
- [21] Rozendal R A, Hamelers H V M, Buisman C J N. Effects of membrane cation transport on pH and microbial fuel cell performance. *Environ Sci and Technol* 2006; 40: 5206-11
- [22] Sleutels T H J A, Hamelers H V M, Rozendal R A, Buisman C J N. Ion transport resistance in microbial electrolysis cells with anion and cation exchange membranes *Int J Hydrogen Energy* 2009; 34: 3612-20
- [23] Gómez E, Pellicer E, Vallés E. Influence of the bath composition and the pH on the induced cobalt-molybdenum electrodeposition. *J Electroanal Chem* 2003; 556: 137-45
- [24] Zehnder A J B, Huser B A, Brock T D, Wuhrmann K. Characterization of an acetate-decarboxylating, non-hydrogen-oxidizing methane bacterium. *Arch Microbiol* 1980; 124: 1-11
- [25] Harris L B. Change in pH near the cathode during the electrodeposition of a bivalent metal. *Analysis. J Electrochem Soc* 1973; 120: 1034-40
- [26] Bard A J, Faulkner L R. *Electrochemical methods: fundamentals and applications*. 2nd ed. New York: John Wiley & Sons; 2001.
- [27] Conway B E, Tilak B V. Interfacial processes involving electrocatalytic evolution and oxidation of H₂, and the role of chemisorbed H. *Electrochim Acta* 2002; 47: 3571-94
- [28] Lide R L. *CRC Handbook of Chemistry and Physics*. 85th ed. Boca Raton: CRC Press; 2005.
- [29] Markovic N M, Grgur B N, Ross P N. Temperature-Dependent Hydrogen Electrochemistry on Platinum Low-Index Single-Crystal Surfaces in Acid Solutions. *J Phys Chem B* 1997; 101: 5405-13
- [30] Schmidt T J, Ross P N, Markovic N M. Temperature dependent surface electrochemistry on Pt single crystals in alkaline electrolytes Part 2. The hydrogen evolution/oxidation reaction. *J Electroanal Chem* 2002; 524: 252-60
- [31] Highfield J G, Claude E, Oguro K. Electrocatalytic synergism in Ni/Mo cathodes for hydrogen evolution in acid medium: a new model. *Electrochim Acta* 1999; 44: 2805-14

6. Metal alloys as HER catalysts in MEC

- [32] Couper A M, Pletcher D, Walsh F C. Electrode materials for electrosynthesis. *Chem Rev* 1990; 90: 837-65
- [33] Huot J-Y, Trudeau M, Brossard L, Schulz R. Electrochemical and Electrocatalytic Behavior of an Iron-Base Amorphous Alloy in Alkaline Solutions at 70[degree]C. *J Electrochem Soc* 1989; 136: 2224-30
- [34] Eley D D, Pines H, Weisz P B. *Advances in catalysis*. ed. Academic Press; 1992.
- [35] Bratsch S G. Standard Electrode Potentials and Temperature Coefficients in Water at 298.15 K. *J Phys Chem Ref Data* 1989; 18: 1-21
- [36] Zech N, Podlaha E J, Landolt D. Anomalous Codeposition of Iron Group Metals: I. Experimental Results. *J Electrochem Soc* 1999; 146: 2886-91
- [37] Gómez E, Pellicer E, Vallés E. Detection and characterization of molybdenum oxides formed during the initial stages of cobalt–molybdenum electrodeposition. *J Appl Electrochem* 2003; 33: 245-52
- [38] Dlugolecki P, Nymeijer K, Metz S, Wessling M. Current status of ion exchange membranes for power generation from salinity gradients. *J Membr Sci* 2008; 319: 214-22

7. General discussion and outlook

This chapter presents an overview of the most important results of this thesis, as well as the perspectives of this relatively new technology for the production of H_2 . We discuss upscaling of the MEC, the expected energy input that is needed, and costs for H_2 production on a larger scale to evaluate the economic viability. This is illustrated by a case study on the possible production of H_2 from wastewater of a vegetable oil refinery with an MEC.

7.1 MEC cathode

The first lab MECs made use of Pt-based cathodes for the HER in an MEC. Pt-based cathodes have low overpotentials at high current densities for the hydrogen evolution reaction (HER) (Table 1). However, their high costs have stimulated the search for an alternative cathode. In this thesis, two types of alternative cathodes have been described: 1) the microbial biocathode, and 2) non-noble metal cathodes. First, the performance and perspectives of both types of cathodes are discussed, and subsequently the feasibility of their application in an MEC is compared.

7.1.1 Microbial biocathode

The maximum current density that has been measured for the microbial biocathode was 3.3 A m^{-2} at an overpotential of -0.28 V (columns 3 & 4 Table 1). The maximum cathodic recovery of H_2 on electrons was 50 %. Various factors influence the current density and cathodic H_2 recovery of the microbial biocathode:

First, the number of microorganisms that have colonized the cathode material (e.g. graphite felt), and the rate at which these microorganisms accept electrons influence the current density. Furthermore, the presence of microorganisms that accept electrons for other processes than H_2 production, such as acetogenesis, [1] or that use H_2 for methanogenesis [2], decrease the cathodic H_2 recovery. To increase the current density and cathodic H_2 recovery, colonization and selection (i.e. enrichment) of microbial species that produce H_2 must be enhanced. Similar to what has been demonstrated for bioanodes [3], this may be achieved through optimization of operational conditions such as pH, cathode potential and medium composition. A first attempt was made in Chapter 4, which investigated the effect of cathode potential and carbon source (acetate versus bicarbonate) on microbial biocathode development and performance. Identification of microorganisms on the biocathode and their mode of H_2 production will help to improve the enrichment process. For example, if these microorganisms employ hydrogenases for hydrogen production, the type of hydrogenases ([NiFe] or [FeFe]; Chapter 1) likely influences the current density.

Second, mass transport of protons will eventually limit the current density of the biocathode, because the microbial biocathode operates at neutral pH. Chapter 2 demonstrated that around neutral pH, the selection of a buffer (i.e. pK_a), buffer concentration, and recirculation speed largely influence the cathode overpotential (or current density at a given overpotential). To improve mass transport, a high concentration of the right buffer could be used. However, such conditions may be challenging for practical application due to the associated chemical consumption. Chapter 4 demonstrated the use of a flow through microbial biocathode which also partly improves mass transport. Alternatively, a biocathode that operates at pH 12, which would not suffer from mass transport limitation by protons, could be envisioned. However, the proof-of-principle of such a biocathode has not been described so far.

Third, H_2 is lost via diffusion through membrane and tubing, which decreases the cathodic H_2 recovery. The amount of these losses however, will become relatively less if the H_2 production rate of the microbial biocathode is increased [4], which consequently results in an increased cathodic H_2 recovery.

Finally, scaling may form on the microbial biocathode, which shields the biocathode and thus influences its current density. This may occur particularly for MECs with a cation exchange membrane and phosphate or carbonate buffer in the catholyte. Transport of multivalent cations such as Ca^{2+} and Mg^{2+} through the cation exchange membrane increases their concentration in the catholyte. An increased concentration of multivalent cations together with phosphate species and a locally high pH increase the scaling tendency on the biocathode (Chapter 3). Use of an anion exchange membrane or a buffer that has low tendency to scale (Chapter 2) would prevent scaling on the biocathode.

7.1.2 Metal cathodes

Non-noble metal cathodes have high overpotentials compared to Pt, even at the low current densities encountered in MECs. To decrease the overpotential of cathodes based on non-noble metals, two strategies were investigated: 1) an increase in specific surface area of the non-noble metal, e.g. the Ni foam cathode of Chapter 5, and 2) the use of a

7. General discussion and outlook

non-noble metal alloy, e.g. the CoMo coated Cu cathode of Chapter 6.

Both strategies have been extensively studied for the HER under strong alkaline conditions (e.g. [5-6]). However, they have been limited studied for the HER under the neutral and mild alkaline conditions encountered in MECs. In this thesis, both strategies were applied to decrease the overpotential of a non-noble metal cathode in an MEC. The lowest overpotential was obtained with the CoMo coated Cu cathode, which was -0.1 V at 23 A m^{-2} (Table 1). The cathodic H_2 recovery was above 90 %.

Given the high current densities (36 A m^{-2} at an overpotential of -0.04 V; Table 1) obtained with a Pt coated sintered Ti cathode relative to a Pt coated Ti sheet cathode, current densities and thus H_2 production rates could be further increased through increasing the surface area of the metal alloy catalyst. Furthermore, long-term MEC experiments are required to test the stability of non-noble metal cathodes in an MEC.

7.1.3 Cathode comparison

Table 1 compares cathodes, described in this thesis and elsewhere, in terms of current density and cathode overpotential for the HER in an MEC, or under MEC conditions. Furthermore, it compares the specific surface area and catholyte conditions of the various cathodes.

The microbial biocathodes demonstrated high overpotentials and low current densities compared to metal cathodes that were tested around neutral pH. Thus, to make the microbial biocathode a viable alternative for metal cathodes around neutral pH, its current density needs to be increased, while its overpotential must be decreased. Furthermore, the cathodic H_2 recovery of the microbial biocathode needs to be increased. The low costs, regenerative character, and stability against corrosion compared to non-noble metal cathodes however, stimulate further research and development of the microbial biocathode.

So far, non-noble metal cathodes have been mainly studied in buffered catholyte of (near) neutral pH (Table 1). Chapters 2 and 6 however, demonstrated a large effect of mass transport on cathode overpotential near neutral pH. This effect was negligible at

pH > 12, which is a typical catholyte pH for an MEC with membrane. At such a pH, buffer can thus be excluded, and the catholyte could contain only a salt to decrease the internal resistance. Therefore, the metal cathodes in this thesis (chapter 5 and 6) were applied in unbuffered catholyte of an MEC with membrane (catholyte pH >12; Table 1). The catholyte consisted of 0.1 M KCl.

The effect of catholyte composition on the activation overpotential of the HER was not investigated in this thesis. However, based on previous studies, it is expected that K^+ and Cl^- ions do not increase the activation overpotential (“poisoning”) of non-noble metal cathodes [7]. Impurities such as H_2S however, can poison the non-noble metal cathode [7]. H_2S formation due to biological sulfate reduction in the anode chamber and its subsequent transfer to the cathode must thus be prevented.

The cathodes based on NiMo and CoMo alloys are among the non-noble metal cathodes with the highest intrinsic performance (i.e. high current density at low overpotential and low specific surface area; Table 1). These cathodes thus seem very suitable for application in an MEC.

Table 1 Performance of cathodes with respect to the HER in an MEC, or under MEC conditions (A_{sp} = specific surface area, η = overpotential, j = current density, ND = no data, SS = stainless steel, PBS = phosphate buffer solution, CBS = carbonate buffer solution, GDC = gas diffusion cathode, MEA = membrane electrode assembly).

Cathode	A_{sp} ($m^2 m^{-2}$)	η (V)	j ($A m^{-2}$)	pH	Catholyte	Reference	Comment
<i>Noble metal or metal alloys</i>							
GDC of carbon paper + PdPt alloy	ND	ND	ND	ND	GDC	[8]	MEA
Commercial GDC + Pt	ND	ND	ND	ND	GDC	[9]	
Ti mesh + Pt	1.7	-0.15	5.3	12	0.01 M PBS	[10]	
Carbon paper + Pd nanoparticles	ND	-0.13	>10	7	0.05 M PBS	[11]	Performance in linear sweep voltammetry (2 mV/s).
Ti sheet + Pt/Ir	1	-0.05	15	6.4	0.05 M PBS + 1 M KCl	Chpt. 2 [12]	Not studied in MEC
Sintered Ti + Pt	ND	-0.04	36	>12	0.1 M KCl	Unpublished data	High surface area cathode
<i>Nickel</i>							
Carbon cloth + Ni	ND	-0.08	6.3	7	0.002 M PBS	[13]	Performance in linear sweep voltammetry (2 mV/s).
Carbon cloth + NiOx	ND	-0.38	6.3	7	0.002 M PBS	[13]	Performance in linear sweep voltammetry (2 mV/s).
GDC of carbon paper + Ni	ND	ND	ND	ND	GDC	[14]	Cathode potential: -1.08 V vs NHE at 6 $A m^{-2}$.
GDC of carbon paper + Ni	ND	ND	ND	ND	GDC	[15]	
Ni foam	128	-0.23	22.8	>12	0.1 M KCl	Chpt. 5 [16]	
GDC of Ni foam	4.4	ND	15	ND	GDC	Unpublished data	MEA. Membrane + cathode potential losses = 0.78 V.
Cu-Ni	1.2	-0.33	25	6	0.5 M Na ₂ SO ₄ + 0.1 M NaH ₂ PO ₄	Chpt. 6	Characterized with Tafel parameters. Not in MEC.
<i>Alloys</i>							
Carbon cloth + FeCoTMPP	ND	ND	ND	7	0.05 M PBS + salts	[17]	
Carbon cloth + CoTMPP	ND	ND	ND	7	0.05 M PBS + salts	[18]	
304 SS brush	37	-0.29	9	7	0.05 M PBS + medium	[19]	For half SS brush.
Sheets of Ni alloys (+ NiOx)	ND	ND	ND	7	0.05 M PBS + medium	[20]	Catalytic activity characterized with Tafel parameters.
Sheets of SS alloys (+ NiOx)	ND	ND	ND	7	0.05 M PBS + medium	[20]	Catalytic activity characterized with Tafel parameters.

Cathode	A_p (m ² m ⁻²)	η (V)	j (A m ⁻²)	pH	Catholyte	Reference	Comment
Graphite + W ₂ C	ND	-0.3	88	7	0.1 M PBS	[21]	Not studied in MEC
Carbon cloth + NiMo	ND	-0.08	8	7	0.32 M PBS	[22]	Performance in chronopotentiometry.
Carbon cloth + NiW	ND	-0.08	8	7	0.32 M PBS	[22]	Performance in chronopotentiometry.
Carbon cloth + NiMo	ND	-0.1	25	7	0.32 M PBS	[23]	Performance in chronopotentiometry.
SS 316L sheet	1	-0.3	11.2	8	0.5 M PBS	[24]	
SS 316L sheet	ND	-0.34	13.5	4-5	1 M PBS	[25]	Not studied in MEC, but in water electrolyzer.
GDC of carbon paper + NiMoCrFe	ND	ND	ND	ND	GDE	[15]	
GDC of carbon paper + NiCrFe	ND	ND	ND	ND	GDE	[15]	
GDC of carbon paper + NiCrMn	ND	ND	ND	ND	GDE	[15]	
Commercial SS 304 mesh	~3	-0.8	12	7	0.05 M PBS + medium	[26]	
Commercial SS 304 sheet	ND	ND	ND	7.1	0.05 M PBS + medium	[27]	
Commercial SS 304 sheet	ND	ND	ND	8.9	0.08 M CBS + medium	[27]	
Commercial SS 304 mesh	ND	ND	ND	7.1	0.05 M PBS + medium	[27]	
Commercial SS 304 mesh	ND	ND	ND	8.9	0.08 M CBS + medium	[27]	
Cu + NiWP	ND	-0.27	7	7	0.05 M PBS + medium	[28]	
Cu + NiCeP	ND	ND	ND	7	0.05 M PBS + medium	[28]	
Cu-NiMo	1.1	-0.25	25	6	0.5 M Na ₂ SO ₄ + 0.1 M NaH ₂ PO ₄	Chpt. 6	Characterized with Tafel parameters. Not in MEC.
Cu-NiFeMo	1.4	-0.26	25	6	0.5 M Na ₂ SO ₄ + 0.1 M NaH ₂ PO ₄	Chpt. 6	Characterized with Tafel parameters. Not in MEC.
Cu-CoMo	1.1	-0.17	25	6	0.5 M Na ₂ SO ₄ + 0.1 M NaH ₂ PO ₄	Chpt. 6	Characterized with Tafel parameters. Not in MEC.
Cu-CoMo	1	-0.1	23	>12	0.1 M KCl	Chpt. 6	Characterized with Tafel parameters.
<i>Microbial biocathodes</i>							
Graphite felt + microbial culture	ND	-0.28	1.9-3.3	7	0.01 M PBS + medium with CBS	Chpt. 3 [29]	
Graphite felt + microbial culture	ND	-0.28	2.7	7	0.01 M PBS + medium with acetate	Chpt. 4	Not studied in MEC

7.2 MEC design

7.2.1 Application of an ion exchange membrane

In literature, two MEC designs have been described: with an ion exchange membrane that separates the anode and cathode chamber, and without a membrane. MECs with a membrane have several advantages over without a membrane, such as negligible concentration overpotential at the cathode, and no need for buffering and recirculation of the catholyte. Furthermore, pure H_2 can be produced because methanogenesis at the cathode is avoided, and H_2 is not mixed with CO_2 from the anode. Part of the total voltage input of an MEC with membrane however, is lost due to a membrane pH gradient and membrane resistance (Chapters 5 and 6). To increase the H_2 production rate of an MEC (or decrease the voltage input), further research should thus focus on decreasing this membrane associated voltage loss. Furthermore, the long term stability of membranes in an MEC has still to be proven. Nevertheless, the advantages of an MEC with membrane favor its application for high rate production of pure H_2 .

7.2.2 Scaling up microbial electrolysis: stack design

The laboratory MEC, studied in chapters 5 and 6 had a MEC liquid volume of 0.04 L and produced $2 \text{ L } H_2 \text{ day}^{-1}$, i.e. $50 \text{ L } H_2 \text{ L}^{-1} \text{ MEC day}^{-1}$. To reach a comparable H_2 production rate on a cubic meter scale, a large electrode area must be fitted in 1 m^3 of MEC. This may be achieved with a stack design [30] with flow-through anode [31] and membranes.

There are two ways of stacking: monopolar and bipolar (Figure 1) [32]. In a monopolar stack, electrode pairs (anode and cathode) are connected in parallel, whereas in a bipolar stack, electrode pairs are connected in series to the power supply. The bipolar stack does not require a current collector for each pair of electrodes, but only for the two end electrodes (Figure 1). This decreases ohmic losses. An advantage of the monopolar stack compared to the bipolar stack is that both sides of the cathode can be used. The principle of a monopolar or bipolar MEC stack has not been proven yet, but it has been shown already that a bipolar microbial fuel cell (MFC) stack is feasible ([33-34]).

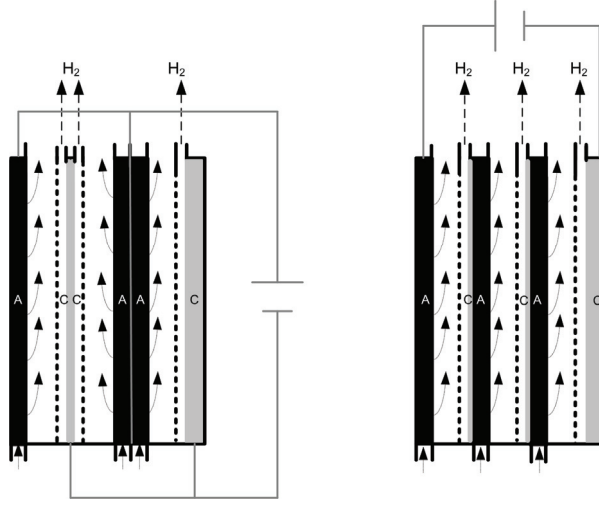


Figure 1 Left: lay-out of a monopolar MEC stack with 3 electrode pairs (anode and cathode). Right: lay-out of a bipolar stack with 3 electrode pairs. The number of depicted monopolar plates (2) or bipolar plates (2) is arbitrary. A = anode, C = cathode, dotted lines are membranes. Flow-through anodes are depicted.

The volumetric H_2 production rate of a monopolar or bipolar stack can be calculated with:

$$r = j \cdot A \cdot \left(\frac{1}{F} \right) \cdot \left(\frac{1}{n} \right) \cdot V_m \cdot N \cdot r_{cat} \quad (1)$$

with r the H_2 production rate ($m^3 H_2 m^{-3} MEC s^{-1}$), j the current density of the stack ($A m^{-2}$), A the surface area of the electrodes ($1 m^2$), F the Faraday constant ($96485 C mol^{-1}$), n the number of electrons per H_2 ($n=2$), V_m the molar volume at standard temperature and pressure (STP, 273.15 K, $10^5 Pa$, $V_m = 0.023 m^3/mol$), N the amount of electrode pairs per $m^3 MEC$, and r_{cat} the cathodic H_2 recovery (a value of 0.9 is assumed).

According to equation 1, the more electrode pairs are fitted in $1 m^3$ at a certain current density, the higher the volumetric H_2 production rate that can be achieved with an MEC stack (Figure 2). More electrode pairs per $1 m^3$ implies less spacing between electrodes, and thus also a lower internal resistance. However, less spacing between electrodes increases the chance of clogging if the MEC is fed with wastewater. If 100

7. General discussion and outlook

electrode pairs are to be fitted in 1 m^3 , the width available per electrode pair is 1.0 cm. Each anode could for example consist of 2.5 mm graphite felt, and each cathode of 0.5 mm CoMo-coated Cu sheet. Each pair of electrodes is separated by an anion exchange membrane (thickness $< 0.1 \text{ cm}$). This means that about 0.6 cm remains through which electrolytes can be pumped. The MEC could operate without catholyte recycle, or without catholyte at all. Experiments in our lab with a membrane electrode assembly (MEA) composed of an anion exchange membrane and a Ni foam cathode showed similar performance for the cathode operated with catholyte, and the cathode operated as a gas diffusion cathode. The largest part of this 0.6 cm can thus be used for the anolyte. The anolyte can be pumped through a serpentine flow channel to make optimal use of the graphite felt [31].

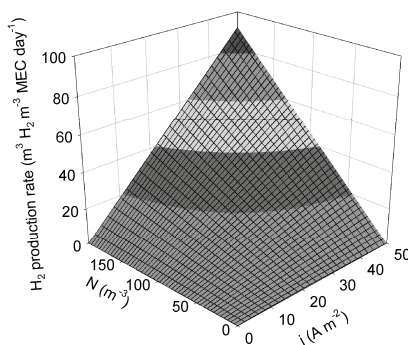


Figure 2 H_2 production rate (at standard T and p) as function of the amount of electrode pairs per m^{-3} (N) and current density (j). A cathodic H_2 recovery of 0.9 was assumed.

7.3 Electrical energy input

The electrical energy input of a continuously fed MEC mainly consists of the electrical energy input of the MEC, and of pumps that recycle electrolytes. These electrical energy requirements depend on the MEC design. Here we only consider the stack design (7.3.2).

7.3.1 Electrical energy input of the MEC

The current densities measured at different electrical energy inputs for the MEC with a CoMo-coated Cu cathode (chapter 6) were extrapolated to H_2 production rates for an MEC

stack with 100 electrode pairs per m^3 (Figure 3).

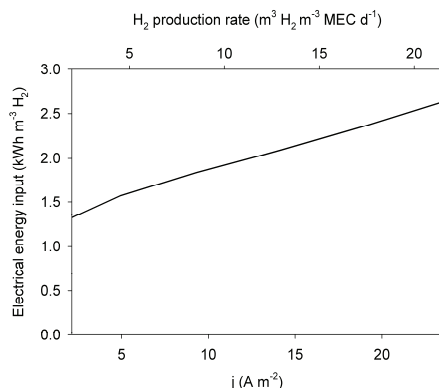


Figure 3 Electrical energy input at measured current densities (j) for the MEC described in chapter 6 (excluding electrical energy of pumps). The current densities (primary x-axis) were converted to H_2 production rates (secondary x-axis) for an MEC stack with 100 electrode pairs per m^3 . A cathodic H_2 recovery of 0.9 was assumed.

The individual cell thickness in the MEC stack is larger (1.0 cm) than that of the single MEC (0.4 cm) of Chapter 5 and 6, which results in a lower H_2 production rate per m^3 MEC. An individual cell thickness of 1.0 instead of 0.4 cm however, seems more reasonable for practical application. A state-of-the-art laboratory MEC produces 22 A m^{-2} at 1.0 V. If this is extrapolated to an MEC stack with 100 cells, this MEC stack could produce $20 \text{ m}^3 \text{H}_2 \text{m}^{-3} \text{MEC day}^{-1}$, at an electrical energy input of $2.6 \text{ kWh m}^{-3} \text{H}_2$.

7.3.2 Electrical energy input for pumping electrolytes

So far, the input of electrical energy for pumping the electrolytes through anode and cathode chamber of an MEC has not been considered. For continuously fed MECs however, pumping contributes to the total energy consumption and thus must be taken into account. We here only elaborate on the energy requirement for pumping anolyte, because an MEC could operate without catholyte recycle or without catholyte at all (7.3.2).

Sleutels et al. [35] demonstrated current densities of more than 20 A m^{-2} at a linear flow speed of 1.4 cm min^{-1} perpendicular to the graphite felt anode, and an applied

7. General discussion and outlook

voltage of 1.0 V. They also showed that an increase in linear flow speed from 1.4 to 2.7 cm min⁻¹ increased the current density from 3.8 to 5 A m⁻² with the same MEC but at an applied cell voltage of 0.8 V. A further increase to 5.4 cm min⁻¹ however, did not lead to a considerable increase of current density for a 3 mm graphite felt bioanode [36]. Thus, given these experimental findings, it should be possible to achieve current densities of 22 A m⁻² below linear flow speeds of 2 cm min⁻¹.

The power requirement for pumping, P_{pump} (W m⁻³ MEC stack), can be calculated with:

$$P_{pump} = Q \cdot \Delta P \cdot N \cdot \frac{1}{\eta_{pump}} \quad (2)$$

with Q the volumetric recycle rate (m³ s⁻¹), ΔP the pressure drop over the anode chamber (Pa = N m⁻²), and η_{pump} the pump efficiency ($\eta = 0.7$, based on [37]). The volumetric recycle rate Q equals the product of anode surface area ($A = 1$ m²) and the linear flow speed perpendicular to this surface area.

The ΔP over the anode chamber, measured for a lab MEC with flow-through anode, was 2·10⁴ Pa at a linear flow speed of 12 cm min⁻¹ perpendicular to the graphite felt anode. The ΔP is mainly caused by the resistance of the 2.5 mm graphite felt. Assuming that ΔP is proportional to Q , ΔP would be 3.3 · 10³ Pa at a linear flow speed of 2 cm min⁻¹.

The energy requirement for pumping in kWh m⁻³ H₂ can then be estimated through dividing the power requirement for pumping by the volumetric H₂ production rate. At a linear flow speed of 2 cm min⁻¹, and 20 m³ H₂ m⁻³ MEC day⁻¹, the electrical energy input for pumping would be below 0.2 kWh m⁻³ H₂ (at STP).

7.3.3 Other inputs

The total electrical energy input would thus be 2.8 kWh m⁻³ H₂ to produce 20 m³ H₂ m⁻³ MEC day⁻¹. However, energy required for processes such as pre-treatment of the waste

stream, H_2 purification and compression, and heating of the MEC have not been taken into account. These processes however, are application dependent and must thus be evaluated for each business case. For comparison, the electrical energy requirement for commercial water electrolyzers is 5 - 7 kWh $m^{-3} H_2$ [38] (Table 2). This energy requirement includes compression to 10-30 bars (H_2 purity >99.9 %). If H_2 compression would take place in the cathode chamber of the MEC, an extra electrical energy input of 0.06 kWh $m^{-3} H_2$ (0.03 V; at 298 K) per tenfold increase in pressure is theoretically required [39].

Table 2 H_2 production rate, electrical energy input and delivered pressure of a MEC stack (theoretical estimations) and some commercial water electrolyzers (data retrieved from www.protonenergy.com, www.linde-gas.com and from personal communication with Fred Hage from Linde).

Production line	H_2 production rate ($m^3 H_2 m^{-3} MEC day^{-1}$)	Electrical energy input (kWh $m^{-3} H_2$)	Delivery Pressure (bars)
MEC	20	2.8	1
Hogen® S series	8-31.5	6.7	13.8
Hogen® H series	17-51	6.8-7.3	15
Hogen® C series	60-180	5.8-6.0	30
Linde Hydross	36	~5	25

7.4 Monetary evaluation

MEC costs consist of capital costs and operational costs. The capital costs are the costs of the MEC system (e.g. MEC, peripherals). The operational costs consist of maintenance, electricity and substrate costs. However, waste streams usually have no or even negative monetary value and therefore, substrate costs are neglected. We thus only consider the capital, maintenance and electricity costs.

To calculate the MEC capital costs (Capex in Table 3), we need to know the costs and lifetimes of parts that are used in an MEC. The costs of the parts in Table 3 are based on up-to-date prices of parts used in the lab MEC of Chapter 5. Only the heterogeneous anion exchange membrane from Ralex is replaced by the cheaper, but equally performing Qianqiu membrane [40-41], and the housing is based on HDPE. The actual costs of current collectors and electrodes will vary with the type of MEC stack (monopolar or bipolar). It is

7. General discussion and outlook

difficult to estimate the lifetime of MEC components without durability tests. Nevertheless, the predicted lifetimes of MEC parts presented in Table 3 seem reasonable, considering that anodes and cathodes last 8-15 years in chlor-alkali electrolysis [32], and considering the mild conditions of MECs compared to chlor-alkali electrolyzers.

The maintenance costs in Table 3 are estimated at 3 % of the costs of the parts [42]. The H_2 costs excl. the costs for electrical energy input are $\text{€ } 0.22 \text{ m}^{-3} H_2$.

Table 3 Overview of capital and maintenance costs of a 1 m^3 MEC stack producing $20 \text{ m}^3 H_2 \text{ day}^{-1}$.

Part	Costs (€)	Predicted lifetime (y)	Annual Costs (€ y^{-1})			Costs H_2 ($\text{€ m}^{-3} H_2$) ^j
			Capex ^h	Main. ⁱ	Total	
Anode current collector	500 ^a	10 ^f	70	10	80	0.01
Anode	4000 ^b	10 ^f	540	120	660	0.10
Cathode	1500 ^c	10 ^f	200	50	250	0.04
AEM	1000 ^d	10 ^g	140	30	170	0.02
Housing (e.g. HDPE)	2500 ^e	20	220	80	300	0.05
Other (e.g. circuit)	100	20	10	0	10	0.00
Total	9600	-	1180	290	1470	0.22

a: Estimation based on price Pt/Ir: 80/20 wire, Advent Research Materials, Oxford, UK, b: 100 m^2 of graphite felt, Fiber Materials Inc, Biddeford, USA, c: 100 m^2 of Ni foam, Heze Jiaotong Group Corporation, d: 100 m^2 of Qianqiu heterogeneous anion exchange membranes (AEM), Hangzhou QianQiu Industry Co, China, e: Based on price of polypropylene, f: Based on lifetime in Chlor alkali industry [32], g: Based on expected lifetime of comparable Ralex heterogeneous membranes (www.mega.cz), h: Annuity depreciation: discount rate 6 % [42], i: Maintenance and operation: 3 % of construction costs [42], j: Assuming 8,000 hours of operation per year [42], excluding costs of electrical energy input, at standard temperature and pressure.

In 7.4 the electrical energy input was calculated at $2.8 \text{ kWh m}^{-3} H_2$. The costs for electrical energy depend from the energy source. For nuclear power, which is produced for about 0.04 € kWh^{-1} (www.ecn.nl, visited 24-05-2011, [43]), the electricity costs would be $0.11 \text{ € m}^{-3} H_2$. For wind power, which is produced for about 0.06 € kWh^{-1} , the electricity costs would be $0.17 \text{ € m}^{-3} H_2$ (www.ecn.nl, [43]). The total H_2 costs (Table 4) for an upscaled MEC would be comparable to the costs for water electrolyzers and distributed biomass gasification plants. The H_2 costs for steam methane reforming however, are still much lower.

The price of distributed H_2 is about $\text{€ } 0.35 \text{ m}^{-3} H_2$ (at STP) [44]. To produce H_2 below this price, the costs need to be decreased. This can be achieved through a decrease

in electricity costs, and/or capital and maintenance costs per $\text{m}^3 \text{H}_2$. The costs of parts and the H_2 production rate determine the capital and maintenance costs per $\text{m}^3 \text{H}_2$. Although the costs of parts may be decreased, most can be gained from an increase in H_2 production rate. Figure 4 shows the effect of H_2 production rate and electrical energy input on the total costs per $\text{m}^3 \text{H}_2$.

Table 4 Total H_2 costs (capital, maintenance, operation and electricity costs) at present for various H_2 production methods, and expected total H_2 costs for an MEC based on currently used materials and achieved current densities.

<i>Production method</i>	<i>Costs ($\text{€ m}^{-3} \text{H}_2$)^a</i>	<i>References</i>
Steam methane reforming	0.10 ^b -0.23 ^c	[45]
Biomass gasification	0.33 ^c -0.62 ^b	[43,45]
Water electrolysis, nuclear electricity ^d	0.25-0.35	[43,45]
Water electrolysis, green electricity ^e	0.40-0.46	[43,45]
MEC, nuclear electricity ^d	0.33 ^d	
MEC, green electricity ^e	0.39 ^e	

a: without liquefaction, and without carbon capture and storage, at standard temperature and pressure, b: centralized H_2 production, c: distributed H_2 production, d: based on an electricity price for nuclear power of 0.04 € kWh^{-1} (www.ecn.nl) [43], e: based on an electricity price for wind power of 0.06 € kWh^{-1} (www.ecn.nl) [43].

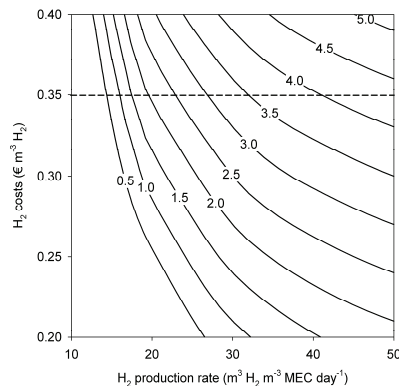


Figure 4 The total costs of H_2 as function of H_2 production rate and for different electrical energy inputs in $\text{kWh m}^{-3} \text{H}_2$. For capex, maintenance and operation, costs of 1500 € y^{-1} were assumed (Table 3), and for green electricity of 0.06 € kWh^{-1} . The distributed H_2 price of $0.35 \text{ € m}^{-3} \text{H}_2$ is indicated with the dashed line.

7. General discussion and outlook

This monetary evaluation thus demonstrates that it seems possible to design an MEC that can be cost-effective, especially if a waste stream is used that otherwise would be treated without energy or product recovery.

7.5 Possible MEC applications

7.5.1 Waste streams

So far, only the H_2 production aspect of an MEC has been considered, assuming that the substrate supply for the bioanode is not a limiting factor. However, to reach a current density of 22 A m^{-2} , $16\text{ kg chemical oxygen demand (COD) m}^{-3}\text{ MEC day}^{-1}$ must be converted into electrons in the MEC stack. If, based on results of Sleutels et al [35], an anodic coulombic efficiency of 50 % is assumed, a conversion rate of $32\text{ kg COD m}^{-3}\text{ MEC day}^{-1}$ would be required. An MEC would thus be especially attractive for treatment of concentrated and high temperature waste streams from industries that use H_2 in their process scheme, or that can sell the H_2 to a local user. Waste streams that qualify for this originate for example from food (e.g. vegetable oil and fats industry), pharmaceutical and chemical industry [46-49].

7.5.2 Example of a business case: vegetable oil industry

Hydrogen is used in the vegetable food industry to hydrogenate vegetable oils. Hydrogenation increases the content of saturated fatty acids and consequently, turns oils into fats that are less susceptible to oxidation. Although there is a trend to decrease the use of saturated fatty acids in food products due to their health risks, hydrogenated vegetable oils are still being used, for example, in the production of hardened fats for cookies [50] (www.mvo.nl, visited 15-04-2011).

The amount of unsaturated fatty acid bonds in an oil is expressed with the iodine value (IV). About 0.4 m^3 of H_2 (at STP) is required to decrease the IV of 450 kg of oil with 1 IV [51]. For example, if 1 ton of soybean oil with a typical IV value of 130 [52] must be decreased to an IV of 70 [50], $50\text{-}60\text{ m}^3 H_2$ would be required.

The vegetable oil refineries in India described by Pandey et al. [53] and Rajkumar et al. [54] use 50-60 tonnes of soybean oil per day. Assuming that all soybean oil is hydrogenated from an IV of 130 to 70, maximally 3600 m³ H₂ would be daily required.

The refinery described by Pandey et al. produced 65 m³ wastewater day⁻¹ with about 29 kg COD m⁻³ wastewater. The volume of the MEC that is required can be calculated with a mass balance equation:

$$\frac{dCOD}{dt} \cdot V = Q \cdot COD_{in} - Q \cdot COD_{out} + r_{COD} \cdot V \quad (3)$$

with COD the COD concentration in the MEC (kg COD m⁻³ MEC), V the total volume of the MEC (m³), Q the wastewater flow rate (65 m³ day⁻¹), COD_{in} the influent COD concentration (29 kg COD m⁻³ wastewater), COD_{out} the effluent COD concentration (kg COD m⁻³), and r_{COD} the COD conversion rate (-32 kg COD m⁻³ MEC day⁻¹). At steady state ($dCOD/dt = 0$) and a COD conversion of 90 % ($COD_{out} = 2.9$ kg COD m⁻³ wastewater), an MEC of 53 m³ would be required. The hydraulic retention time (HRT), defined as the volume of the MEC divided by the wastewater flow rate, is 19.6 hours. The organic loading rate (OLR), which is defined as:

$$OLR = \frac{Q \cdot COD_{in}}{V} \quad (4)$$

is about 36 kg COD m⁻³ MEC day⁻¹, which is similar to a highly loaded anaerobic reactor [46]. This MEC could produce 1060 m³ H₂ day⁻¹ from its wastewater, which comprises at least 30 % of the total H₂ requirement of the described vegetable oil refinery.

7.6 Conclusions

The microbial biocathode demonstrated high overpotentials and low current densities compared to metal cathodes. Non-noble metal cathodes that have a high surface area or that consist of metal alloys have been successfully applied in MECs. The metal cathodes based on NiMo or CoMo alloy are among the non-noble metal cathodes with the highest

7. General discussion and outlook

performance. These cathodes thus seem very suitable for application in an MEC. To produce H_2 at high rate and with high purity, MECs with an ion exchange membrane are preferred over MECs without a membrane. The use of a membrane however, leads to a substantial voltage loss. Future studies should thus focus on decreasing this voltage loss. The monopolar or bipolar MEC stack, in which flow-through anodes are stacked with cathodes, seems an effective design to produce green H_2 that can be cost competitive with H_2 from distributed biomass gasification and water electrolysis.

7.7 Acknowledgements

The help of David Vermaas and Jan Post with pressure drop measurements and calculations, and the contributions of Henk Dijkman and Oane Galama to the cost calculations are kindly acknowledged.

7.8 References

- [1] Nevin K P, Woodard T L, Franks A E, Summers Z M, Lovley D R. Microbial Electrosynthesis: Feeding Microbes Electricity To Convert Carbon Dioxide and Water to Multicarbon Extracellular Organic Compounds. *mBio* 2010; 1:
- [2] Lee H-S, Torres C s I, Parameswaran P, Rittmann B E. Fate of H₂ in an Upflow Single-Chamber Microbial Electrolysis Cell Using a Metal-Catalyst-Free Cathode. *Environ Sci Technol* 2009; 43: 7971-6
- [3] Pham T H, Aelterman P, Verstraete W. Bioanode performance in bioelectrochemical systems: recent improvements and prospects. *Trends Biotechnol* 2009; 27: 168-78
- [4] Rozendal R A, Hamelers H V M, Euverink G J W, Metz S J, Buisman C J N. Principle and perspectives of hydrogen production through biocatalyzed electrolysis. *Int J Hydrogen Energy* 2006; 31: 1632-40
- [5] Rausch S, Wendt H. Morphology and utilization of smooth hydrogen-evolving raney nickel cathode coatings and porous sintered-nickel cathodes. *J Electrochem Soc* 1996; 143: 2852-62
- [6] Fan C, Piron D L, Sleb A, Paradis P. Study of Electrodeposited Nickel-Molybdenum, Nickel-Tungsten, Cobalt-Molybdenum, and Cobalt-Tungsten as Hydrogen Electrodes in Alkaline Water Electrolysis. *J Electrochem Soc* 1994; 141: 382-7
- [7] Vetter K J. *Electrochemical kinetics: theoretical and experimental aspects*. ed. New York: Academic press; 1967.
- [8] Tartakovsky B, Manuel M-F, Neburchilov V, Wang H, Guiot S R. Biocatalyzed hydrogen production in a continuous flow microbial fuel cell with a gas phase cathode. *J Power Sources* 2008; 182: 291-7
- [9] Tartakovsky B, Manuel M-F, Wang H, Guiot S R. High rate membrane-less microbial electrolysis cell for continuous hydrogen production. *Int J Hydrogen Energy* 2009; 34: 672-7
- [10] Sleutels T H J A, Hamelers H V M, Rozendal R A, Buisman C J N. Ion transport resistance in microbial electrolysis cells with anion and cation exchange membranes *Int J Hydrogen Energy* 2009; 34: 3612-20
- [11] Huang Y-X, Liu X-W, Sun X-F, Sheng G-P, Zhang Y-Y, Yan G-M, et al. A new cathodic electrode deposit with palladium nanoparticles for cost-effective hydrogen production in a microbial electrolysis cell. *Int J Hydrogen Energy* 2011; 36: 2773-6
- [12] Jeremiasse A W, Hamelers H V M, Kleijn J M, Buisman C J N. Use of biocompatible buffers to reduce the concentration overpotential for hydrogen evolution. *Environ Sci Technol* 2009; 43: 6882-7
- [13] Selembo P A, Merrill M D, Logan B E. Hydrogen production with nickel powder cathode catalysts in microbial electrolysis cells. *Int J Hydrogen Energy* 2010; 35: 428-37
- [14] Hrapovic S, Manuel M F, Luong J H T, Guiot S R, Tartakovsky B. Electrodeposition of nickel particles on a gas diffusion cathode for hydrogen production in a microbial electrolysis cell. *Int J Hydrogen Energy* 35: 7313-20
- [15] Manuel M F, Neburchilov V, Wang H, Guiot S R, Tartakovsky B. Hydrogen production in a microbial electrolysis cell with nickel-based gas diffusion cathodes. *J Power Sources* 2010; 195: 5514-9

7. General discussion and outlook

- [16] Jeremiasse A W, Hamelers H V M, Saakes M, Buisman C J N. Ni foam cathode enables high volumetric H₂ production in a microbial electrolysis cell. *Int J Hydrogen Energy* 2010; 35: 12716-23
- [17] Cheng S, Logan B E. Evaluation of catalysts and membranes for high yield biohydrogen production via electrohydrogenesis in microbial electrolysis cells (MECs). *Water Sci Technol* 2008; 58: 853-7
- [18] Cheng K Y, Ho G, Cord-Ruwisch R. Affinity of microbial fuel cell biofilm for the anodic potential *Environ Sci and Technol*
- [19] Call D F, Merrill M D, Logan B E. High Surface Area Stainless Steel Brushes as Cathodes in Microbial Electrolysis Cells. *Environ Sci Technol* 2009; 43: 2179-83
- [20] Selembo P A, Merrill M D, Logan B E. The use of stainless steel and nickel alloys as low-cost cathodes in microbial electrolysis cells. *J Power Sources* 2009; 190: 271-8
- [21] Harnisch F, Sievers G, Schroder U. Tungsten carbide as electrocatalyst for the hydrogen evolution reaction in pH neutral electrolyte solutions. *Appl Catal B: Environ* 2009; 89: 455-8
- [22] Hu H, Fan Y, Liu H. Hydrogen production in single-chamber tubular microbial electrolysis cells using non-precious-metal catalysts. *Int J Hydrogen Energy* 2009; 34: 8535-42
- [23] Hu H, Fan Y, Liu H. Optimization of NiMo catalyst for hydrogen production in microbial electrolysis cells. *Int J Hydrogen Energy* 2010; 35: 3227-33
- [24] DeSilva Munoz L, Erable B, Etcheverry L, Riess J, Basseguy R, Bergel A. Combining phosphate species and stainless steel cathode to enhance hydrogen evolution in microbial electrolysis cell (MEC). *Electrochem Commun* 2010; 12: 183-6
- [25] De Silva Muñoz L, Bergel A, Féron D, Basséguy R. Hydrogen production by electrolysis of a phosphate solution on a stainless steel cathode. *Int J Hydrogen Energy* 2010; 35: 8561-8
- [26] Zhang Y, Merrill M D, Logan B E. The use and optimization of stainless steel mesh cathodes in microbial electrolysis cells. *Int J Hydrogen Energy* 2010; 35: 12020-8
- [27] Ambler J R, Logan B E. Evaluation of stainless steel cathodes and a bicarbonate buffer for hydrogen production in microbial electrolysis cells using a new method for measuring gas production. *Int J Hydrogen Energy* 2011; 36: 160-6
- [28] Wang L, Chen Y, Ye Y, Lu B, Zhu S, Shen S. Evaluation of low-cost cathode catalysts for high yield biohydrogen production in microbial electrolysis cell. *Water Sci Technol* 2011; 63: 440-8
- [29] Jeremiasse A W, Hamelers H V M, Buisman C J N. Microbial electrolysis cell with a microbial biocathode. *Bioelectrochemistry* 2010; 78: 39-43
- [30] Rozendal R A, 2007. Hydrogen Production through Biocatalyzed Electrolysis, Department of Environmental Technology. Wageningen University, Wageningen.
- [31] Sleutels T H J A, Lodder R, Hamelers H V M, Buisman C J N. Improved performance of porous bio-anodes in microbial electrolysis cells by enhancing mass and charge transport. *Int J Hydrogen Energy* 2009; 34: 9655-61
- [32] Stegen, 2000. The state of the art of modern chlor alkali electrolysis with membrane cells. University of Twente, Enschede.

- [33] Shin S H, Choi Y J, Na S H, Jung S H, Kim S. Development of bipolar plate stack type microbial fuel cells. *Bull Korean Chem Soc* 2006; 27: 281-5
- [34] Dekker A, Heijne A T, Saakes M, Hamelers H V M, Buisman C J N. Analysis and Improvement of a Scaled-Up and Stacked Microbial Fuel Cell. *Environ Sci Technol* 2009; 43: 9038-42
- [35] Sleutels T, 2010. Microbial electrolysis: Kinetics and cell design, Environmental Technology. Wageningen University, Wageningen.
- [36] Sleutels T H J A, Hamelers H V M, Buisman C J N. Effect of mass and charge transport speed and direction in porous anodes on microbial electrolysis cell performance. *Bioresour Technol* 2011; 102: 399-403
- [37] Kaya D, Yagmur E A, Yigit K S, Kilic F C, Eren A S, Celik C. Energy efficiency in pumps. *Energy Convers Manage* 2008; 49: 1662-73
- [38] Kinoshita K. Electrochemical oxygen technology. ed. New York: John Wiley & Sons, Inc.; 1992.
- [39] Logan B E, Call D, Cheng S, Hamelers H V M, Sleutels T H J A, Jeremiasse A W, et al. Microbial electrolysis cells for high yield hydrogen gas production from organic matter. *Environ Sci Technol* 2008; 42: 8630-40
- [40] Dlugolecki P, Nymeijer K, Metz S, Wessling M. Current status of ion exchange membranes for power generation from salinity gradients. *J Membr Sci* 2008; 319: 214-22
- [41] Veerman J, de Jong R M, Saakes M, Metz S J, Harmsen G J. Reverse electrodialysis: Comparison of six commercial membrane pairs on the thermodynamic efficiency and power density. *J Membr Sci* 2009; 343: 7-15
- [42] Post J W, 2009. Blue Energy: electricity production from salinity gradients by reverse electrodialysis, Sub-department of Environmental Technology. Wageningen University, Wageningen.
- [43] Ewan B C R, Allen R W K. A figure of merit assessment of the routes to hydrogen. *Int J Hydrogen Energy* 2005; 30: 809-19
- [44] Agency I E, 2007. Hydrogen Production & Distribution, IEA Energy Technology Essentials. IEA.
- [45] Lemus R G, Martínez Duart J M. Updated hydrogen production costs and parities for conventional and renewable technologies. *Int J Hydrogen Energy* 2010; 35: 3929-36
- [46] Tchobanoglous G, Burton F L, Stensel H D. Wastewater engineering: treatment and reuse. 3rd ed. New York: Metcalf & Eddy, McGraw-Hill; 2003.
- [47] Pant D, Van Bogaert G, Diels L, Vanbroekhoven K. A review of the substrates used in microbial fuel cells (MFCs) for sustainable energy production. *Bioresour Technol* 2010; 101: 1533-43
- [48] Chelliapan S, Sallis P J. Application of anaerobic biotechnology for pharmaceutical wastewater treatment. *IIOAB J* 2011; 2: 13-21
- [49] Chen B, Dingerdissen U, Krauter J G E, Lansink Rotgerink H G J, Möbus K, Ostgard D J, et al. New developments in hydrogenation catalysis particularly in synthesis of fine and intermediate chemicals. *Appl Catal, A* 2005; 280: 17-46
- [50] Jang E S, Jung M Y, Min D B. Hydrogenation for Low Trans and High Conjugated Fatty Acids. *Compr Rev Food Sci F* 2005; 4: 22-30
- [51] Puri P. Hydrogenation of oils and fats. *J Am Oil Chem Soc* 1980; 57: A850-A4

7. General discussion and outlook

- [52] King J, Holliday R, List G, Snyder J. Hydrogenation of vegetable oils using mixtures of supercritical carbon dioxide and hydrogen. *J Am Oil Chem Soc* 2001; 78: 107-13
- [53] Pandey R A, Sanyal P B, Chattopadhyay N, Kaul S N. Treatment and reuse of wastes of a vegetable oil refinery. *Resour Conserv Recy* 2003; 37: 101-17
- [54] Rajkumar K, Muthukumar M, Sivakumar R. Novel approach for the treatment and recycle of wastewater from soya edible oil refinery industry--An economic perspective. *Resour Conserv Recy* 2010; 54: 752-8

Summary

Hydrogen gas, H_2 , is a valuable compound that is used on large scale as chemical and fuel for many applications. Most H_2 is produced through partial oxidation of fossil fuels. Fossil fuels however, are a finite resource and their combustion causes air pollution and CO_2 emission, which is believed to cause global warming. These issues raise the need for green H_2 without emissions. Thus, H_2 production technologies must be explored that do not require energy input from fossil fuels, but can use energy input from renewable sources. This thesis is about the production of H_2 from biomass through microbial electrolysis.

In a microbial electrolysis cell (MEC) electrochemically active microorganisms oxidize a substrate (e.g. acetate in a waste stream) into bicarbonate, protons and electrons, and transfer the electrons to the anode, the so-called bioanode. From the bioanode, the electrons travel through an electrical circuit with power supply, to the cathode. At the cathode, the electrons reduce protons or water to H_2 in the hydrogen evolution reaction (HER). The production of H_2 from organic matter in an MEC is not a spontaneous process, but requires a voltage input that is delivered by the power supply. To compensate for the negative electrical charge transport through the external circuit, ionic charge is transported between the electrodes inside the cell. To avoid H_2 losses through re-oxidation at the anode, and a decrease in H_2 purity through mixing with CO_2 , a membrane can be used to separate anode and cathode. Often, an anion or cation exchange membrane is used.

According to the Nernst equation, an applied voltage of 0.12 V would be required to produce H_2 from acetate under typical MEC conditions, while in practice, 0.4-1.0 V is applied. Part of this additional voltage is used as cathode overpotential to drive the HER at a certain rate. The cathode overpotential is the extra potential beyond the thermodynamic potential, and is expressed with a negative sign. The cathode overpotential represents an extra electrical energy input, and therefore it is relevant to decrease. This can be achieved with a catalyst, such as Pt. Previous MEC studies demonstrated overpotentials for Pt-based cathodes of a few hundred millivolts at H_2

Summary

production rates below $10 \text{ m}^3 \text{ H}_2 \text{ m}^{-3} \text{ MEC day}^{-1}$ (at standard temperature and pressure (STP)). The aim was to decrease this overpotential, while to increase the volumetric H_2 production rate of the MEC (i.e. $\text{m}^3 \text{ H}_2 \text{ m}^{-3} \text{ MEC day}^{-1}$). Furthermore, the cathode must be made of a low cost material, which decreases costs per $\text{m}^3 \text{ MEC}$, while an increased volumetric H_2 production rate decreases MEC size and thus total MEC costs. The objective of this PhD project therefore was: *To develop a low-cost cathode, capable of producing H_2 at high rate and low overpotential.*

First, the effect of mass transport on cathode overpotential at MEC relevant pH values is studied in **Chapter 2**. This chapter demonstrates that buffers decreased the overpotential of a Pt-based cathode. However, this effect was found to be strongly pH dependent. Furthermore, experimental data and a mass transport equation showed that by increasing the buffer concentration or linear flow speed (i.e. pump speed), or decreasing the current density (i) the overpotential decreases and (ii) the minimum overpotential is reached at a pH that approaches the buffer dissociation constant (pK_a). Thus, to decrease the cathode overpotential of an MEC, buffer (i.e. pK_a), buffer concentration, linear flow speed and current density must be well balanced with the desirable operational pH.

In **Chapter 3**, the H_2 producing microbial biocathode is studied as low-cost alternative for the Pt-based cathode. The proof-of-principle of such a biocathode was demonstrated previously. The microbial biocathode however, had not been applied in an MEC yet. This chapter demonstrates the application of the microbial biocathode in a continuous flow MEC. In this MEC, both anode and cathode reactions were thus catalyzed by microorganisms. Two of these MECs were simultaneously operated at an applied cell voltage of 0.5 V, and after a long development time produced $0.04 \text{ m}^3 \text{ H}_2 \text{ m}^{-3} \text{ MEC day}^{-1}$ (at STP; maximum current density: 1.4 A m^{-2}). After 1600 hours of operation, the current density of the MECs had decreased to 0.6 A m^{-2} , probably caused by precipitation of calcium phosphate on the biocathode.

The microbial biocathode is thus a candidate as low-cost substitute of the Pt-based cathode in MECs. However, the MEC with microbial biocathode showed a long

development time (i.e. slow startup), and low H_2 production rate. These limitations need to be resolved before the microbial biocathode can be a viable replacement of metal cathodes. In **Chapter 4** we hypothesized that the development time of the microbial biocathode could be decreased through applying a more negative cathode potential and/or feeding with an organic (acetate) instead of an autotrophic (bicarbonate) carbon source. Experiments showed however, that applying a more negative cathode potential did not decrease the development time of the microbial biocathode. Feeding with medium containing a low concentration of acetate (1 mM) instead of bicarbonate did decrease the development time with more than a factor 2. The enhanced development was likely caused by a higher biomass yield for acetate than for bicarbonate, which was supported by thermodynamic calculations. Furthermore, to increase the H_2 production rate, a flow through biocathode fed with acetate was investigated in this chapter. This biocathode produced $2.2 \text{ m}^3 \text{ H}_2 \text{ m}^{-3} \text{ reactor day}^{-1}$ (at STP; maximum current density: 2.7 A m^{-2}) at an overpotential of -0.28 V . The H_2 production rate of the microbial biocathode was 7 times higher than of a parallel flow biocathode used previously.

Next to the microbial biocathode, non-noble metal cathodes were studied as a substitute of the Pt-based cathode. Non-noble metals (e.g. Ni) have high HER overpotentials compared to Pt, even at the low current densities encountered in MECs. To decrease the overpotential of cathodes based on non-noble metals, two strategies were investigated: 1) an increase in specific surface area of the non-noble metal, and 2) the use of a non-noble metal alloy. Both strategies have been extensively studied for the HER under strong alkaline conditions. However, they have been limited studied for the HER under the neutral and mild alkaline conditions encountered in MECs.

In **Chapter 5**, the application of a Ni foam cathode with high specific surface area ($128 \text{ m}^2 \text{ m}^{-2}$ projected area) was studied in a continuous flow MEC with an anion exchange membrane and flow through bioanode. At an electrical energy input of $2.6 \text{ kWh m}^{-3} \text{ H}_2$ (applied cell voltage: 1.00 V), this MEC was able to produce over $50 \text{ m}^3 \text{ H}_2 \text{ m}^{-3} \text{ MEC d}^{-1}$ (at STP; $22.8 \pm 0.1 \text{ A m}^{-2}$). The high H_2 production rate was the result of a combination of MEC design, flow through bioanode, and Ni foam cathode. The Ni foam cathode had an

overpotential of -0.23 V at 22.8 A m^{-2} . The MEC performance however, decreased during 32 days of operation due to an increase in anode and cathode overpotentials. Scaling likely caused the increase in anode overpotential, but it remained unclear what caused the increase in cathode overpotential.

Chapter 6 demonstrates that a copper sheet coated with alloys of nickel-molybdenum, nickel-iron-molybdenum or cobalt-molybdenum alloy has a lower overpotential for the HER than a copper sheet coated with nickel, measured near neutral pH. However, the catalytic activity of these alloys cannot be fully exploited near neutral pH because of mass transport limitation. The catalytic activity is best exploited at alkaline pH where mass transport is not limiting. This was demonstrated with a similar MEC as in chapter 5, but with a cobalt-molybdenum coated cathode. This MEC produced $50 \text{ m}^3 \text{ H}_2 \text{ m}^{-3} \text{ MEC d}^{-1}$ (at STP) at an electricity input of $2.5 \text{ kWh m}^{-3} \text{ H}_2$. The overpotential of the cobalt molybdenum coated Cu cathode, was -0.1 V at 23 A m^{-2} .

Finally, **Chapter 7** compares the various studied cathodes. From this comparison follows that to make the microbial biocathode a viable alternative for metal cathodes around neutral pH, its H_2 production rate needs to be increased, while its overpotential must be decreased. Furthermore, the cathodic H_2 recovery of the microbial biocathode ($\leq 50 \%$) is much lower than that of metal cathodes ($> 90\%$), and thus needs to be increased. Cathodes based on nickel-molybdenum or cobalt-molybdenum alloy are among the best performing non-noble metal cathodes.

It seems that these cathodes can best be applied in an MEC with membrane, because an MEC with membrane has a high catholyte pH which results in a negligible concentration overpotential at the cathode. Furthermore, there is no need for buffering and recirculation of the catholyte, and pure H_2 can be produced because methanogenesis at the cathode is avoided and H_2 is not mixed with CO_2 from the anode. Chapters 5 and 6 demonstrated however, that the use of a membrane leads to a substantial voltage loss. Future studies should thus focus on decreasing this voltage loss.

Chapter 7 further shows that the MEC may be scaled up as a monopolar or bipolar stack design. Estimation of the capital and operational costs of such an MEC stack

demonstrates that it seems possible to design an MEC that can be cost competitive with H_2 from distributed biomass gasification and water electrolysis.

Samenvatting

Waterstofgas, H_2 , is een waardevolle stof die op grote schaal wordt gebruikt als chemisch product of brandstof voor vele toepassingen. De meeste waterstof wordt geproduceerd middels gedeeltelijke oxidatie van fossiele brandstoffen. Echter, fossiele brandstoffen raken uitgeput. Bovendien veroorzaakt verbranding van fossiele brandstoffen luchtvervuiling en emissie van CO_2 wat bij lijkt te dragen aan opwarming van de aarde. Dus, H_2 productietechnieken zijn nodig die geen fossiele energie gebruiken, maar hernieuwbare energie. Dit proefschrift beschrijft de productie van H_2 uit biomassa door middel van microbiële elektrolyse.

In een microbiële elektrolyse cel (MEC) zetten elektrochemisch actieve micro-organismen organische stof om in bicarbonaat, protonen en elektronen, en geven de elektronen vervolgens af aan de anode, de zogenaamde bioanode. De elektronen worden van de bioanode, via een elektrisch circuit met spanningsbron, getransporteerd naar de kathode. Aan de kathode reduceren de elektronen protonen of water tot H_2 . De productie van H_2 uit organisch materiaal in een MEC is geen spontaan proces, maar vereist een aangelegd voltage die wordt geleverd door de spanningsbron. Om te compenseren voor het negatieve ladingstransport door het elektrische circuit bewegen positief en negatief geladen ionen tussen de elektrodes in de cel. Ter voorkoming van H_2 verliezen door omzetting aan de anode en menging van het geproduceerde H_2 gas met CO_2 kan een membraan gebruikt worden die anode en kathode van elkaar scheidt. Vaak wordt dan een anion of kation uitwisselingsmembraan gebruikt.

Volgens de Nernst vergelijking is een aangelegd voltage van 0.12 V nodig om H_2 te produceren uit azijnzuur (acetaat) onder typische MEC condities. In de praktijk wordt een spanning van 0.4-1.0 V aangelegd. Een deel van deze extra spanning wordt gebruikt voor de kathode overpotentiaal om waterstof met een bepaalde snelheid te produceren. De kathode overpotentiaal is de extra potentiaal bovenop de thermodynamische potentiaal en is uitgedrukt met een negatief getal. De kathode potentiaal vertegenwoordigt een extra energieverbruik en daarom is het relevant deze te verlagen. Dit kan worden

bewerkstelligd door het toepassen van een katalysator, zoals platina (Pt). Voorgaande MEC studies demonstreerden overpotentialen voor Pt-gebaseerde kathoden van een aantal honderden millivolts bij productiesnelheden onder de $10 \text{ m}^3 \text{ H}_2 \text{ m}^{-3} \text{ MEC dag}^{-1}$ (bij standaard temperatuur en druk (STP)). Het is belangrijk om de kathode overpotentiaal te verlagen en tegelijkertijd de productiesnelheid ($\text{m.a.w. m}^3 \text{ H}_2 \text{ m}^{-3} \text{ MEC dag}^{-1}$) te verhogen van een MEC. Bovendien dient de kathode gemaakt te zijn van een goedkoop materiaal om daarmee de kosten per $\text{m}^3 \text{ MEC}$ te verlagen. Een hoge volumetrische waterstofproductie en lage kathode kosten verlagen de totale kosten van een MEC. Het doel van dit PhD project was daarom: Het ontwikkelen van een goedkope kathode met een hoge H_2 productiesnelheid bij lage overpotentiaal.

Eerst is het effect van massa transport op de kathode overpotentiaal bij MEC relevante pH waarden bestudeerd in **Hoofdstuk 2**. Dit hoofdstuk laat zien dat buffers de overpotentiaal verlagen van een Pt-gebaseerde kathode. Echter, dit effect blijkt sterk pH afhankelijk. Bovendien lieten experimentele data en een massa transport vergelijking zien dat een toename in buffer concentratie of pompsnelheid, of een afname in stroomdichtheid (i) de overpotentiaal verlaagt en (ii) de minimum overpotentiaal wordt bereikt bij een pH die de buffer dissociatie constante (pK_a) benadert. Dus om de kathode overpotentiaal te verlagen van een MEC, de buffer ($\text{m.a.w. } pK_a$), buffer concentratie, pompsnelheid en stroomdichtheid moeten goed worden afgestemd op de gewenste operationele pH.

In **Hoofdstuk 3** is de H_2 producerende microbiële biokathode bestudeerd als goedkoop alternatief voor de Pt-gebaseerde kathode. De werking van een microbiële biokathode was eerder al aangetoond. Echter, deze was nog niet toegepast in een MEC. Dit hoofdstuk toont de toepassing van een dergelijke kathode in een continu bedreven MEC aan. In deze MEC zijn zowel de anode als de kathode reacties dus gekatalyseerd door micro-organismen. Twee van deze MECs werden gelijktijdig bedreven bij een aangelegde spanning van 0.5 V en produceerden, na een lange opstartperiode, $0.04 \text{ m}^3 \text{ H}_2 \text{ m}^{-3} \text{ MEC dag}^{-1}$ (bij STP; maximale stroomdichtheid: 1.4 A m^{-2}). Na een bedrijfstijd van 1600 uur was

de stroomdichtheid van beide MECs gezakt tot 0.6 A m^{-2} . Dit werd waarschijnlijk veroorzaakt door neerslag van calcium fosfaat op de biokathode.

De microbiële biokathode is dus een goedkope kandidaat om de Pt-gebaseerde kathode in een MEC te vervangen. Echter, de MEC met microbiële biokathode had een lange opstartperiode en lage volumetrische waterstofproductie. Deze beperkingen moeten eerst worden verholpen voordat de microbiële biokathode een serieus alternatief kan zijn voor metaal gebaseerde kathodes. In **Hoofdstuk 4** veronderstelden we dat de opstarttijd van de microbiële biokathode kan worden verkort door het aanleggen van een meer negatieve kathodepotentiaal (m.a.w. een grotere overpotentiala) en/of door het voeden van een organische (acetaat) in plaats van een autotrofe (bicarbonaat) koolstofbron. Experimenten lieten echter zien dat een meer negatieve kathode potentiaal de opstarttijd van de microbiële biokathode niet verkortte. Het voeden met een lage concentratie acetaat (1 mM) verkortte de opstarttijd met meer dan een factor 2. De verkorte opstarttijd was waarschijnlijk veroorzaakt door een hogere biomassa opbrengst in het geval van acetaat in plaats van bicarbonaat. Dit werd ook ondersteund door thermodynamische berekeningen. In dit hoofdstuk wordt bovendien de doorstroom biokathode gevoed met acetaat beschreven. Deze biokathode produceerde $2.2 \text{ m}^3 \text{ H}_2 \text{ m}^{-3} \text{ reactor dag}^{-1}$ (bij STP; maximale stroomdichtheid: 2.7 A m^{-2}) bij een overpotentiala van -0.28 V. De volumetrische waterstofproductie van deze biokathode was 7 keer hoger dan van de niet doorstroomde biokathode die eerder was gebruikt.

Naast de microbiële biokathode zijn kathodes op basis van niet-edelmetalen onderzocht als alternatief voor de Pt gebaseerde kathode. Niet-edel metalen (bijv. Ni) hebben een hoge overpotentiala voor H_2 productie vergeleken met Pt, zelfs bij de lage stroomdichtheden van MECs. Om de overpotentiala te verlagen werden 2 strategieën onderzocht: 1) een toename van specifiek oppervlak van het niet-edel metaal en 2) het gebruik van niet-edel metaal legeringen. Beide strategieën zijn uitgebreid getest voor H_2 productie in sterk basische media. Echter, er is weinig bekend over H_2 productie in neutrale of mild basische media.

In **Hoofdstuk 5** is de toepassing van een Ni schuim kathode met hoog specifiek oppervlak ($128 \text{ m}^2 \text{ m}^{-2}$ geprojecteerd oppervlak) bestudeerd in een continu bedreven MEC met anion uitwisselend membraan en doorstroom bioanode. Deze MEC produceerde $50 \text{ m}^3 \text{ H}_2 \text{ m}^{-3} \text{ MEC dag}^{-1}$ (bij STP; $22.8 \pm 0.1 \text{ A m}^2$) bij een elektrische energie-input van $2.6 \text{ kWh m}^{-3} \text{ H}_2$ (aangelegde celspanning: 1.00 V). De hoge volumetrische waterstofproductie was het gevolg van de combinatie van MEC ontwerp, doorstroom anode en Ni schuim kathode. De Ni schuim kathode had een overpotentiaal van -0.23 V bij 22.8 A m^{-2} . Echter, de MEC prestaties namen af gedurende 32 dagen van functioneren vanwege een toename in anode en kathode overpotentiaal. Neerslagvorming veroorzaakte waarschijnlijk de toename in anode overpotentiaal, maar het is nog onduidelijk wat de toename in kathode overpotentiaal veroorzaakte.

Hoofdstuk 6 laat zien dat, rond neutrale pH, een koperen plaat gecoat met legeringen van nikkel-molybdeen, nikkel-ijzer-molybdeen of kobalt-molybdeen een lagere overpotentiaal voor waterstofproductie heeft dan een koperen plaat gecoat met nikkel. Echter, de katalytische activiteit van deze legeringen kan niet volledig worden benut rondom neutrale pH vanwege massa transport limitatie. De katalytische activiteit kan worden benut bij basische pH waar massa transport niet limiterend is. Dit was aangetoond met een vergelijkbare MEC als in Hoofdstuk 5, maar met een kobalt-molybdeen gecoate Cu kathode. Deze MEC produceerde $50 \text{ m}^3 \text{ H}_2 \text{ m}^{-3} \text{ MEC dag}^{-1}$ (bij STP) bij een elektriciteitsinput van $2.5 \text{ kWh m}^{-3} \text{ H}_2$. De overpotentiaal van de kobalt-molybdeen gecoate Cu kathode was -0.1 V bij 23 A m^{-2} .

Tenslotte zijn de bestudeerde kathodes met elkaar vergeleken in **Hoofdstuk 7**. Deze vergelijking maakt duidelijk dat de H_2 productiesnelheid van de microbiële biokathode omhoog moet en tegelijkertijd haar overpotentiaal omlaag moet om een serieus alternatief voor metaal gebaseerde kathodes te zijn. Daarnaast is de kathodische H_2 efficiëntie van de microbiële biokathode ($< 50 \%$) veel lager dan die van metaal gebaseerde kathodes ($> 90 \%$) en moet dus nog omhoog. Kathodes gebaseerd op legeringen van nikkel-molybdeen of kobalt-molybdeen behoren tot de beste niet-edelmetaal gebaseerde kathodes die tot nu toe onderzocht zijn voor een MEC.

Het lijkt erop dat deze kathodes het beste toegepast kunnen worden in een MEC met membraan, omdat een MEC met membraan een hoge kathode pH heeft waar de concentratie overpotential geen rol speelt. Daarnaast is het niet nodig om het katholiet te bufferen of te recirculeren en kan pure H_2 worden geproduceerd omdat methaanproductie wordt voorkomen en er geen menging optreedt met CO_2 afkomstig van de anode. Hoofdstukken 5 en 6 laten echter zien dat het gebruik van een membraan tot een substantieel spanningsverlies leidt. Toekomstige studies zouden zich dus moeten richten op het verlagen van dit spanningsverlies.

Hoofdstuk 7 laat verder zien dat een MEC zou kunnen worden opgeschaald als een monopolaire of bipolaire stack. Een schatting van de kapitaalskosten en operationele kosten van een MEC stack laat zien dat het mogelijk lijkt om een MEC te ontwerpen die qua kosten kan concurreren met waterstof van decentrale biomassa vergassing en water elektrolyse.

Appendices

Appendix - Chapter 2

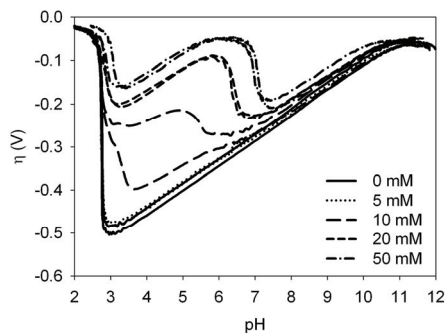


Figure S1 The HER overpotential (η) between pH 2.5 and 11.5 for catholytes containing different concentrations of phosphate buffer, with 1 M KCl background electrolyte, at a linear low speed of 2.8 cm/s and a current density of 15 A/m². All concentrations were tested in duplicate.

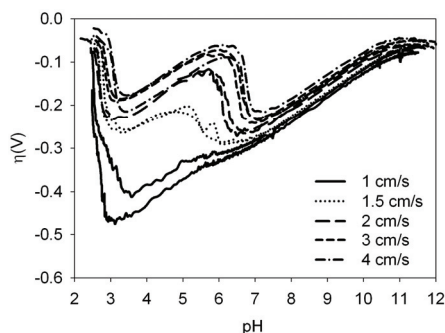


Figure S2 The HER overpotential (η) between pH 2.5 and 11.5 for 20 mM phosphate buffer with 1 M KCl background electrolyte, at a current density of 15 A/m² and different linear flow speeds. All linear flow speeds were tested in duplicate.

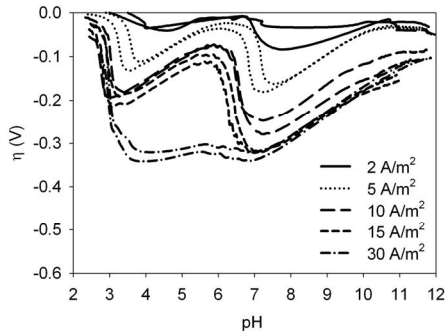


Figure S3 The HER overpotential (η) between pH 2.5 and 11.5 for 20 mM phosphate buffer with 1 M KCl background electrolyte, at a linear flow speed of 2.8 cm/s and different current densities. All current densities were tested in duplicate.

Appendix - Chapter 4

The methodology of Kleerebezem and Van Loosdrecht (2010) was followed to identify the catabolic and anabolic reaction, to calculate the Gibbs energy of anabolic reaction, catabolic reaction and dissipation, and to estimate the biomass yield.

First, the anabolic and catabolic reactions were identified, and their stoichiometries were calculated by solving the C, H, O, N and charge balances (Table S1 and S2).

Table S1 Values to calculate the stoichiometry of the metabolic reaction with bicarbonate as carbon source. Gibbs energy of formation (ΔG_f^0) at 298 K [1], experimental activities (a), elemental composition (C, H, O, N), charge (Ch) and stoichiometry of substances in anabolic (An), and catabolic reaction (Cat). The activities of dissolved species were assumed equal to the molar concentrations, and H_2 is represented by the partial pressure in atmosphere.

Substance	ΔG_f^0 (kJ mol ⁻¹)	a	C	H	O	N	Ch	An	Cat
HCO ₃ ⁻	-586.9	$5 \cdot 10^{-3}$	1	1	3	0	-1	-1	0
NH ₄ ⁺	-79.4	$5 \cdot 10^{-3}$	0	4	0	1	1	-0.2	0
CH _{1.8} O _{0.5} N _{0.2}	-67	1	1	1.8	0.5	0.2	0	1	0
H ₂ O	-237.2	1	0	2	1	0	0	2.5	0
Cathode-e ⁻ *	48.2-77.2**	1	0	0	0	0	-1	-4.2	-1
H ⁺	0	10^{-7}	0	1	0	0	1	-5	-1
H ₂	0	1	0	2	0	0	0	0	0.5

* Cathode electrons

**Variable with cathode potential from 48.2 kJ mol⁻¹ at -0.5 V to 77.2 kJ mol⁻¹ at -0.8 V.

Table S2 Values to calculate the stoichiometry of the metabolic reaction with acetate as carbon source. Gibbs energy of formation (ΔG_f^0) at 298 K [1], experimental activities (a), elemental composition (C, H, O, N), charge (Ch) and stoichiometry of substances in anabolic (An), and catabolic reaction (Cat). The activities of dissolved species were assumed equal to the molar concentrations, and H_2 is represented by the partial pressure in atmosphere.

Substance	ΔG_f^0 (kJ mol ⁻¹)	a	C	H	O	N	Ch	An	Cat
CH ₃ COO ⁻	-369.4	$6 \cdot 10^{-4}$	2	3	2	0	-1	-0.5	0
NH ₄ ⁺	-79.4	$5 \cdot 10^{-3}$	0	4	0	1	1	-0.2	0
CH _{1.8} O _{0.5} N _{0.2}	-67	1	1	1.8	0.5	0.2	0	1	0
H ₂ O	-237.2	1	0	2	1	0	0	0.5	0
Cathode-e ⁻ *	48.2-77.2**	1	0	0	0	0	-1	-0.2	-1
H ⁺	0	10^{-7}	0	1	0	0	1	-0.5	-1
H ₂	0	1	0	2	0	0	0	0	0.5

* Cathode electrons

**Variable with cathode potential from 48.2 kJ mol⁻¹ at -0.5 V to 77.2 kJ mol⁻¹ at -0.8 V.

Second, the Gibbs energies of the anabolic and catabolic reaction were calculated from their reaction stoichiometries and Gibbs energies of formation of the involved substances (Table S1 and S2). The cathode delivers electrons for the anabolic and catabolic reaction. These cathode-electrons have an energy level (determined by the cathode potential), which has to be taken into account in calculations of the Gibbs energies of the reactions. The Gibbs energies were calculated for standard conditions (ΔG^0 , 1M of all reactants and products), and for experimental conditions (ΔG^1) using equation 25 of [2] (Table S3 and S4).

Table S3 Gibbs energies at standard conditions (ΔG^0) and at experimental conditions (ΔG^1) for the catabolic and anabolic reaction at different cathode potentials (vs NHE), and with bicarbonate as carbon source (298 K).

	-0.5 V	-0.6 V	-0.7 V	-0.8 V
Catabolic reaction				
ΔG^0 (kJ reaction ⁻¹)	-48.2	-57.9	-67.5	-77.2
ΔG^1 (kJ reaction ⁻¹)	-8.3	-18.0	-27.6	-37.3
Anabolic reaction				
ΔG^0 (kJ reaction ⁻¹)	-259.9	-300.4	-340.9	-381.5
ΔG^1 (kJ reaction ⁻¹)	-44.5	-85.0	-125.5	-166.0

Table S4 Gibbs energies at standard conditions (ΔG^0), and at experimental conditions (ΔG^1) for the catabolic and anabolic reaction at different cathode potentials (vs NHE), and with acetate as carbon source (298 K).

	-0.5	-0.6	-0.7	-0.8
Catabolic reaction				
ΔG^0 (kJ reaction ⁻¹)	-48.2	-57.9	-67.5	-77.2
ΔG^1 (kJ reaction ⁻¹)	-8.3	-18.0	-27.6	-37.3
Anabolic reaction				
ΔG^0 (kJ reaction ⁻¹)	5.3	3.4	1.5	-0.5
ΔG^1 (kJ reaction ⁻¹)	37.1	35.2	33.3	31.3

Third, the Gibbs energy dissipation (ΔG_{dis}) for bicarbonate and acetate as carbon sources were calculated using equation 34 of [2]. $\Delta G_{dis} = 1088$ kJ C-mol⁻¹ for bicarbonate ($\gamma=4$, $NoC = 1$, no reversed electron transfer), and $\Delta G_{dis} = 432$ kJ C-mol⁻¹ for acetate ($\gamma=0$, $NoC = 2$). These values are close to the values measured by Heijnen et al. [3].

Fourth, the overall metabolism for bicarbonate and acetate as carbon source, and at different cathode potentials was calculated using equation 32 of [2]. The biomass yield for bicarbonate and acetate as carbon source, and at different cathode potentials could then be derived from the overall metabolism (Table S5).

Table S5 Biomass yield on electrons (Y_{xe}) for bicarbonate and acetate as carbon source and for different cathode potentials vs NHE (298 K). The biomass yield on electrons (Y_{xe}) has a negative sign, because it expresses the amount of biomass formed per amount electrons consumed [2].

	Y_{xe} (mol X mol ⁻¹ e ⁻)		
	-0.5 V	-0.7 V	-0.8 V
bicarbonate	-0.008	-0.026	-0.035
acetate	-0.018	-0.059	-0.079

References

- [1] R.K. Thauer, K. Jungermann, K. Decker, Energy conservation in chemotrophic anaerobic bacteria, *Bacteriol. Rev.*, 41 (1977) 100-180.
- [2] R. Kleerebezem, M.C.M. Van Loosdrecht, A Generalized Method for Thermodynamic State Analysis of Environmental Systems, *Crit. Rev. Env. Sci. Technol*, 40 (2010) 1 - 54.
- [3] J.J. Heijnen, M.C.M. Van Loosdrecht, L. Tijhuis, A black box mathematical model to calculate auto- and heterotrophic biomass yields based on Gibbs energy dissipation, *Biotechnol. Bioeng.*, 40 (1992) 1139-1154.

Appendix - Chapter 5

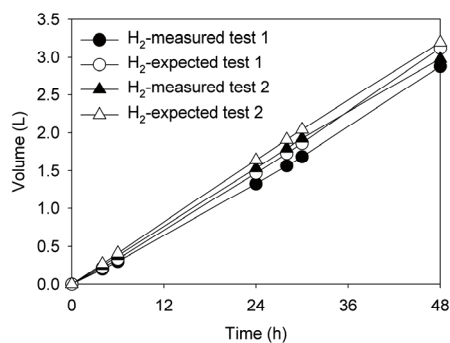


Figure S1 Measured and expected (based on charge, assuming 100% cathodic hydrogen recovery) hydrogen production of the MEC with Ni foam cathode at an applied voltage of 1.00 V. Volumes at standard temperature and pressure.

Appendix - Chapter 6

Equations 1 and 3 were combined using MathCad:

$$j = \frac{F \left(j - j_0 e^{-\frac{F\eta\beta}{RT}} \right) \left(D_{OH^-} \left(H_{bulk}^+ \right)^2 K_w j + D_{OH^-} K_{a2} K_w j + D_{OH^-} K_{a2}^2 K_w j_0 e^{-\frac{F\eta\beta}{RT}} + C_T D_A \left(H_{bulk}^+ \right)^2 K_{a2} j + D_{OH^-} \left(H_{bulk}^+ \right) K_{a2} K_w j + D_{OH^-} K_{a2} K_w j_0 e^{-\frac{F\eta\beta}{RT}} \right)}{\left(H_{bulk}^+ \right) j \delta \left(\left(H_{bulk}^+ \right) j + K_{a2} j_0 e^{-\frac{F\eta\beta}{RT}} \right) \left(\left(H_{bulk}^+ \right) + K_{a2} \right)}$$

This equation was analytically solved for η with MathCad.

Table S1 Approximate elemental composition (determined with EDX) of cathodes prepared with electrodeposition.

Bath composition	Deposit composition					
	Ni (%)	Co (%)	Fe (%)	Mo (%)	O (%)	C (%)
Ni ₁₀₀	82				5	13
Ni ₈₅ Mo ₁₅	34			18	33	15
Ni ₆₄ Fe ₁₈ Mo ₁₈	33		18	17	16	16
Ni ₇₆ Fe ₁₆ Mo ₈	32		15	16	26	11
Co ₇₅ Mo ₂₅		43		21	27	9

Publications

In peer-reviewed journals

- Rozendal R A, Jeremiasse A W, Hamelers H V M, Buisman C J N. Hydrogen production with a microbial biocathode. *Environ Sci Technol* 2008; 42: 629-34
- Logan B E, Call D, Cheng S, Hamelers H V M, Sleutels T H J A, Jeremiasse A W, Rozendal, R A. Microbial electrolysis cells for high yield hydrogen gas production from organic matter. *Environ Sci Technol* 2008; 42: 8630-40
- Jeremiasse A W, Hamelers H V M, Kleijn J M, Buisman C J N. Use of biocompatible buffers to reduce the concentration overpotential for hydrogen evolution. *Environ Sci Technol* 2009; 43: 6882-7
- Hamelers H V M, Ter Heijne A, Sleutels T H J A, Jeremiasse A W, Strik D P B T B, Buisman C J N. New applications and performance of bioelectrochemical systems. *Appl Microbiol Biotechnol* 2009; 85: 1673-85
- Jeremiasse A W, Hamelers H V M, Buisman C J N. Microbial electrolysis cell with a microbial biocathode. *Bioelectrochemistry* 2010; 78: 39-43
- Kleijn J M, l'Huillier Q, Jeremiasse A W, Monitoring the development of a bioanode using an electrochemical quartz crystal balance. *Bioelectrochemistry* 2010; 79: 272-5
- Jeremiasse A W, Hamelers H V M, Saakes M, Buisman C J N. Ni foam cathode enables high volumetric H₂ production in a microbial electrolysis cell. *Int J Hydrogen Energy* 2010; 35: 12716-23
- Jeremiasse A W, Bergsma J, Kleijn J M, Saakes M, Buisman C J N, Cohen Stuart M, Hamelers H V M. Performance of metal alloys as hydrogen evolution reaction catalysts in a microbial electrolysis cell. *Int J Hydrogen Energy* 2011: doi:10.1016/j.ijhydene.2011.06.013
- Jeremiasse A W, Hamelers H V M, Croese E, Buisman C J N, Acetate enhances development of a H₂-producing microbial biocathode. Submitted.

Contributions to book chapters

- Hamelers H V M, Sleutels T H J A, Jeremiasse A W, Post J W, Strik D P B T B, Rozendal R A, Technological factors affecting BES performance and bottlenecks towards scale up. In: Rabaey K, Angenent L T, Schröder U, Keller J (eds). *Bioelectrochemical systems: from extracellular electron transfer to biotechnological applications*. IWA Publishing, London, 2010.

Publications

- Rozendal R A, Harnisch F, Jeremiasse A W, Schröder U. Chemically catalyzed cathodes in bioelectrochemical systems, In: Rabaey K, Angenent L T, Schröder U, Keller J (eds). Bioelectrochemical systems: from extracellular electron transfer to biotechnological applications. IWA Publishing, London, 2010

Dankwoord

Gedurende het promotietraject heb ik veel mensen leren kennen die op wat voor manier dan ook betrokken zijn geweest en die ik op deze plaats wil bedanken.

Cees, dank voor je promotorschap. Zowel jouw inhoudelijke begeleiding en coaching, als het scheppen van de juiste randvoorwaarden hebben mij veel geholpen tijdens dit traject. Ik heb veel geleerd van jouw pragmatische aanpak en ik kan me geen betere leraar daarvoor indenken. Ook Martien Cohen Stuart wil ik graag bedanken voor zijn promotorschap. Dank voor je vertrouwen in mij en dit project.

Wat mij erg aantrekt in milieutechnologie is de multidisciplinaire en pragmatische aanpak. Bert, jij weet als geen ander verschillende disciplines je eigen te maken en aan elkaar te koppelen. Je bent een ideeënmachine waar geen rem op zit. Bovendien ben je gewoon een sympathieke vent. Ik kijk terug op een boeiende samenwerking. Mieke, jij complementeerde de fysisch chemische component van dit leertraject. Dank voor jouw verbeteringen van artikelen en proefschrift. Bovendien was het fijn dat ik altijd (telefonisch) terecht kon bij je voor een praktische of inhoudelijke vraag.

Mijn Wetsus tijd begon in december 2006 toen ik een afstudeervak op hetzelfde onderwerp bij René begon. René heeft me geïntroduceerd in de wereld van bioelektrochemische systemen. René, dank voor je sterke en plezierige begeleiding van mijn afstudeervak, alsmede je inspanningen die hebben geleid tot mijn eigen promotietraject! Vrij snel na mijn aanstelling kwam ik Michel als mijn begeleider bij Wetsus tegen. Michel, jouw enthousiasme werkt aanstekelijk. Ik heb veel met je gesproken over onderzoeksresultaten en nieuwe ideeën. Dit waren niet alleen vermakelijke gesprekken; het heeft ook geresulteerd in bijvoorbeeld hoofdstuk 5. Ik kijk uit naar onze samenwerking bij Magneto.

Onderzoek doe je niet alleen. Ik heb veel van gedachten kunnen wisselen met mijn lotgenoten Tom en Elsemiek. Ik wil Pieter Hack, Niels Groot, Henk Dijkman en Aad de Klerk danken voor de nuttige discussies tijdens de themavergaderingen. Er is mij veel werk uit handen genomen door studenten die mij gedurende de 4 jaren hebben bijgestaan in

het lab. Jixin, Sebastien, Adeline, Quentin, Johan, Oane, Agnes, Jerome and Suman, thanks for your help with the experiments and constructive discussions! Verder heb ik veel geleerd van Bob, Janneke, Jelmer, Pieter, Petra M, Ton, Mieke en Marianne: dank voor jullie analyses en uitleg van de diverse methoden. Gelukkig waren Wim, Harrie, Harm en Jan T altijd in de buurt voor de nodige handigheid om een opstelling te ontwerpen, installeren en lekkage vrij te houden. Daarnaast ben ik dankbaar voor de hulp van de secretariaten bij Wetsus (i.h.b. Trienke, Helena en Linda), Fysko (Josie) en ETE (Liesbeth).

Wetsus was de thuisbasis, maar ik kwam regelmatig in Wageningen waar ik altijd terecht kon bij Milieutechnologie of Fysko. Ik bewaar goede herinneringen aan de discussies met de leden van de “Renewable Energy” (David, Annemiek, Vinnie, Kirsten, Tom, Nienke, Jan P., Ruud, Tim, Marjolein, Mieke, Ralph, Alexandra, Doga, Bruno, Fei, Olivier and Michel) groep van Milieutechnologie. Hoewel de bezoeken aan Fysko minder frequent waren, heb ik ook daar regelmatig met anderen (m.n. Herman en Johan) van gedachten kunnen wisselen over mijn onderzoek.

Johannes, Cees en Gert-Jan, jullie inzet om ook de Wetsus waarde ‘joy’ na te streven is goed geslaagd. Mede dankzij alle collega’s voelde ik mij al gauw thuis bij Wetsus. Ik dank Petra O. in het bijzonder voor haar warme ontvangst, betrokkenheid en alle georganiseerde feestjes, avonden, weekenden etc. Natasja en Petra O, dank voor die keren dat ik niet thuis hoefde te koken. Natasja, mijn saxofoon ligt op dit moment wat te verstoffen, maar mooi dat we deze hobby nu delen! Wat me meteen brengt op de Wetsus band. Onze doorbaak bleef uit, maar het plezier niet. Tom, Elsemiek en Michel de waterstofentjes zal ik nooit vergeten. Gezien dit “subthema” doorgaat, lijkt me dat we deze traditie, onder het genot van een andere energiedrager, voort moeten zetten. Mijn kantoorgenoten (Astrid, Bruno, Bob, Tom, Jan P, Joost V., Piotr, Alexandra, Claudia), dank voor de leuke gesprekken en aansluiting bij de “Nespresso club” (incl. Elmar, Luewton). Speciale dank aan mijn paranimfen, Piotr en Jos voor de hulp rondom deze ceremonie. Piotr, I enjoyed the motorbike trips (together with Luciaan and Pieter), parties, talks and your associated endless flow of words. Jos, de timing van het weekend in Steenwijk na inlevering van dit werk kon niet beter! Dank ook voor het checken van het concept van dit

proefschrift. Tenslotte eenieder bedankt die ik hier niet met naam en toenaam heb genoemd, maar die ook zeker hebben bijgedragen aan deze mooie tijd!

Buiten Wetsus waren de volleybalavonden een welkome afwisseling op het labwerk. Ik kijk dan ook terug op een mooie tijd bij Leevoc. Dank ook aan Reinie, waar ik altijd terecht kon als ik voor een langere periode in Wageningen moest zijn, en aan (oud!)-tante Pie en oom Niek, waar ik terecht kon als ik naar Rotterdam af moest reizen. Dėkoju mano Lietuviškai “šeimai” Viktorui, Irenai ir Paulinai už jsitraukimą ir malonius įspūdžius ne tik Lietuvoje.

Joris en Maartje, van jongs af aan kom ik bij jullie over de vloer en fungeren jullie bovendien als inhoudelijke sparringpartners. Ik ben blij dat ik jullie hierbij kan betrekken.

Beste ouders, beste Dick en Betty, mijn stationering in Leeuwarden heeft de reis naar Terneuzen alleen maar langer gemaakt. Maar ongeacht de afstand, jullie staan altijd voor mij klaar en zijn erg betrokken. Jullie hebben me altijd gestimuleerd en gesteund in mijn keuzes, en ik ben jullie daarvoor zeer dankbaar. Ook mijn zus Wilma en broer Bart dank ik voor hun betrokkenheid. Onze verschillende werkvelden maken het des te leuker om ervaringen te delen.

And of course Justina, thanks a lot for your support in work *and* relaxation. I admire your perseverance, and continuous drive to do things. I think we make a nice team. I'm looking forward to many more activities we'll undertake.

Curriculum Vitae

Adriaan Jeremiasse was born on 13th of July, 1984 in Terneuzen, The Netherlands. After High School he moved to Wageningen to study Environmental Technology at Wageningen University. He performed his internship at Instituto de Biotecnología from the Universidad Nacional Autónoma de México in Cuernavaco, México. The internship focused on laccase-mediator systems to degrade polycyclic aromatic hydrocarbons. Subsequently, he carried out his thesis work on microbial electrolysis at Wetsus in Leeuwarden (The Netherlands), under the supervision of René Rozendal and Bert Hamelers. From 2007 to 2011 he was working on a PhD project. The results of this project are described in this thesis. From the 1st of September 2011, he started as Technologist at Magneto Special Anodes BV in Schiedam, The Netherlands.





Netherlands Research School for the
Socio-Economic and Natural Sciences of the Environment

C E R T I F I C A T E

The Netherlands Research School for the
Socio-Economic and Natural Sciences of the Environment
(SENSE), declares that

Adriaan Jeremiasse

born on 13 July 1984 in Terneuzen, The Netherlands

has successfully fulfilled all requirements of the
Educational Programme of SENSE.

Leeuwarden, 30 September 2011

the Chairman of the SENSE board

Prof. dr. Rik Leemans

the SENSE Director of Education

Dr. Ad van Dommelen

The SENSE Research School has been accredited by the Royal Netherlands Academy of Arts and Sciences (KNAW)



KONINKLIJKE NEDERLANDSE
AKADEMIE VAN WETENSCHAPPEN



The SENSE Research School declares that **Mr. Adriaan Jeremiasse** has successfully fulfilled all requirements of the Educational PhD Programme of SENSE with a work load of 41 ECTS, including the following activities:

SENSE PhD courses

- o Environmental Research in Context
- o Research Context Activity: Co-organization of the Wetsus Water Challenge (28 – 30 May 2008).
- o Sustainable Bio-energy and Innovation

Other PhD courses

- o Bath Electrochemistry Summer School
- o Catalysis, an integrated approach
- o Techniques for Writing and Presenting Scientific Papers
- o PhD Competence assessment
- o Project and Time Management
- o Career Perspectives
- o ETE department trip Turkey: Attending and giving presentations at Bogazici University, Istanbul Technical University, Marmara University, Tubitak, Thames drinking water plant, Omerli wastewater treatment plant.

Management skills

- o Co-organization of the 3rd MFC Conference since February 2010

Oral Presentations

- o H₂ production with Microbial Electrolysis, Novel Cost Effective Technologies for Wastewater Treatment and Bio-energy Production, Sense symposium, 4 – 5 September 2008, Wageningen, The Netherlands
- o High H₂ production with Microbial Electrolysis Cells, 3rd International MFC Conference, 5 – 8 June 2011, Leeuwarden, The Netherlands
- o Presentations at Bioenergy theme meetings, Wetsus colloquia and ETE/PCC colloquia, 2007 and 2011, Leeuwarden – Wageningen, The Netherlands

SENSE Coordinator PhD Education and Research



Mr. Johan Feenstra